AD-A132 174 OCEAN MIXING AND CIRCULATION RESPONSE IN THE MARGINAL ICE ZONE(U) NAVAL POSTGRADUATE SCHOOL MONTEREY CA D G MARKHAM JUN 83 1/1

UNCLASSIFIED F/G 8/3 NL

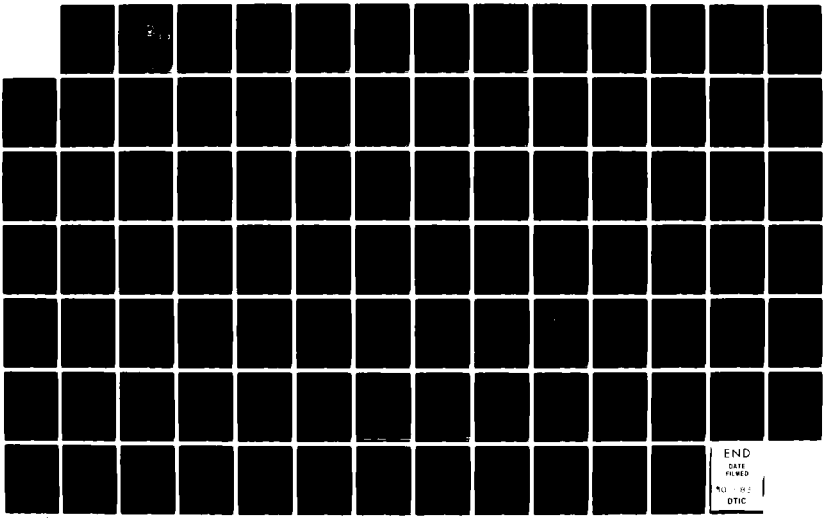

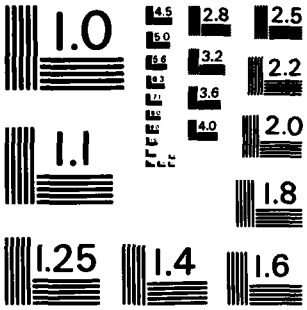


MICROCOPY RESOLUTION TEST CHART

NATIONAL BUREAU OF STANDARDS-1963-A

ADA132174

(2)

# NAVAL POSTGRADUATE SCHOOL
## Monterey, California

DTIC
ELECTE
SEP 6 1983
S D
B

# THESIS

OCEAN MIXING AND CIRCULATION RESPONSE

IN THE MARGINAL ICE ZONE

by

David Gregory Markham

June 1983

Thesis Advisor: Roland W. Garwood

DTIC FILE COPY

Approved for public release, distribution unlimited

83 09 01 039

SECURITY CLASSIFICATION OF THIS PAGE (When Data Entered)

# REPORT DOCUMENTATION PAGE

READ INSTRUCTIONS BEFORE COMPLETING FORM

1. REPORT NUMBER

2. GOVT ACCESSION NO. AD-A132 174

3. RECIPIENT'S CATALOG NUMBER

4. TITLE (and Subtitle)

Ocean Mixing and Circulation Response in the Marginal Ice Zone

5. TYPE OF REPORT & PERIOD COVERED

Master's Thesis
June 1983

6. PERFORMING ORG. REPORT NUMBER

7. AUTHOR(s)

David Gregory Markham

8. CONTRACT OR GRANT NUMBER(s)

9. PERFORMING ORGANIZATION NAME AND ADDRESS

Naval Postgraduate School
Monterey, California 93940

10. PROGRAM ELEMENT, PROJECT, TASK AREA & WORK UNIT NUMBERS

11. CONTROLLING OFFICE NAME AND ADDRESS

Naval Postgraduate School
Monterey, California 93940

12. REPORT DATE

June 1983

13. NUMBER OF PAGES

93

14. MONITORING AGENCY NAME & ADDRESS(if different from Controlling Office)

15. SECURITY CLASS. (of this report)

15a. DECLASSIFICATION/DOWNGRADING SCHEDULE

16. DISTRIBUTION STATEMENT (of this Report)

Approved for public release; distribution unlimited

17. DISTRIBUTION STATEMENT (of the abstract entered in Block 20, if different from Report)

18. SUPPLEMENTARY NOTES

19. KEY WORDS (Continue on reverse side if necessary and identify by block number)

ice edge upwelling, marginal ice zone, upwelling, upper ocean dynamics, numerical model, coupled sea ice--ocean model, mixed layer dynamics, mixing, ocean circulation, sea ice

20. ABSTRACT (Continue on reverse side if necessary and identify by block number)

The purpose of this research was to develop a coupled sea ice-ocean model capable of simulating the upper ocean circulation features of the Marginal Ice Zone (MIZ). A sea ice model using the Rossby-similarity method was added to a two-dimensional, embedded ocean general circulation--mixed layer model. Advection, diffusion, and mixing of buoyancy and momentum were included in the model to determine their effects on the ocean response. In particular, the case of Northern Hemisphere ice edge

DD FORM 1 JAN 73 1473 EDITION OF 1 NOV 65 IS OBSOLETE
S/N 0102-LF-014-6601



SECURITY CLASSIFICATION OF THIS PAGE (When Data Entered)

upwelling was investigated. Ice edge upwelling was created for a down-ice geostrophic wind and varying surface buoyancy flux forcing. It appeared in model solutions for both stationary and moving ice covers and is driven by a divergence in the oceanic surface transport across the ice edge. These results are supported by the observations of the NORSEX group in the Greenland Sea MIZ (Johannessen et al, 1983). For an up-ice geostrophic wind, the upper ocean response was modified by the buoyancy forcing and ice motion. The combined effects of the wind forcing and ice motion due to a nonstationary ice cover caused weak downwelling at the ice edge. Application of a downward surface buoyancy flux (simulating ice melting) resulted in a 8 m elevation of the mixed layer depth at the ice edge, or upwelling, next to the downwelling. The existence of this dual (upwelling and downwelling) feature at the ice edge differs from the weak downwelling predicted by Roed and O'Brien (1983). Adding the effects of mixing had a significant impact on the upper ocean response and should be incorporated in future models of dynamical MIZ processes.

DTIC COPY INSPECTED 2

Accession For
NTIS GRA&I ✓
DTIC TAB
Unannounced
Justification
By
Distribution/
Availability Codes
Dist | Avail and/or Special
A

Approved for public release; distribution unlimited

# Ocean Mixing and Circulation Response in the Marginal Ice Zone

by

David G. Markham
Lieutenant, United States Navy
B.S., United States Naval Academy, 1976

Submitted in partial fulfillment of the
requirements for the degree of

MASTER OF SCIENCE IN METEOROLOGY AND OCEANOGRAPHY

from the

NAVAL POSTGRADUATE SCHOOL
June 1983

Author: David G. Markham

Approved by: Roland W. Garwood Jr
Thesis Advisor

Co-Advisor

Chairman, Department of Oceanography

Dean of Science and Engineering

## ABSTRACT

The purpose of this research was to develop a coupled sea ice-ocean model capable of simulating the upper ocean circulation features of the Marginal Ice Zone (MIZ). A sea ice model using the Rossby-similarity method was added to a two-dimensional, embedded ocean general circulation--mixed layer model. Advection, diffusion, and mixing of buoyancy and momentum were included in the model to determine their effects on the ocean response. In particular, the case of Northern Hemisphere ice edge upwelling was investigated. Ice edge upwelling was created for a down-ice geostrophic wind and varying surface buoyancy flux forcing. It appeared in model solutions for both stationary and moving ice covers and is driven by a divergence in the oceanic surface transport across the ice edge. These results are supported by the observations of the NORSEX group in the Greenland Sea MIZ (Johannessen et al, 1983). For an up-ice geostrophic wind, the upper ocean response was modified by the buoyancy forcing and ice motion. The combined effects of the wind forcing and ice motion due to a nonstationary ice cover caused weak downwelling at the ice edge. Application of a downward surface buoyancy flux (simulating ice melting) resulted in a 8 m elevation of the mixed layer depth at the ice edge, or upwelling, next to the downwelling. The existence of this dual (upwelling and downwelling) feature at the ice edge differs from the weak downwelling predicted by Roed and O'Brien (1983). Adding the effects of mixing had a significant impact on the upper ocean circulation response and should be incorporated in future models of dynamical MIZ processes.

TABLE OF CONTENTS

I. INTRODUCTION ---------- 10

A. BACKGROUND AND MOTIVATION ---------- 10

B. PREVIOUS MODELS AND OBSERVATIONS ---------- 14

C. THE PROBLEM ---------- 15

II. THEORETICAL FORMULATION ---------- 17

A. GENERAL ---------- 17

B. SEA ICE MODEL ---------- 23

C. OCEAN MODEL ---------- 26

III. THE MODEL EXPERIMENT ---------- 33

A. THE MODEL RESPONSE TO BUOYANCY FLUX FORCING ---------- 37

1. Null Surface Buoyancy Flux Condition (Case IA) -------- 37

2. Downward Surface Buoyancy Flux Condition (Case IB) ---- 38

3. Upward Surface Buoyancy Flux Condition (Case IC) ------ 40

B. THE MODEL RESPONSE TO WIND FORCING ---------- 41

1. Down-Ice Wind Forcing (Case IIA) ---------- 42

2. On-Ice Wind Forcing (Case IIB) ---------- 42

3. Up-Ice Wind Forcing (Case IIC) ---------- 43

4. Off-Ice Wind Forcing (Case IID) ---------- 44

C. THE MODEL RESPONSE TO A MOVING ICE COVER ---------- 44

1. Down-Ice Wind Forcing (Case IIIA) ---------- 45

2. On-Ice Wind Forcing (Case IIIB) ---------- 45

3. Up-Ice Wind Forcing (Case IIIC) ---------- 46

4. Off-Ice Wind Forcing (Case IIID) ---------- 47

IV. SUMMARY AND CONCLUSIONS ---------- 49

FIGURES 5 THROUGH 40 ---------- 52

LIST OF REFERENCES ---------- 88

INITIAL DISTRIBUTION LIST ---------- 91

LIST OF FIGURES


1. MIZEX 1984 Experimental Area ---------- 12

2. The Coupled Sea Ice--Ocean Model Coordinate System ---------- 20

3. Balance of Forces on Sea Ice in the MIZ ---------- 25

4. Buoyancy Field Used for Model Initialization ---------- 35

5. Case IA - Along Edge Velocity (U) at Hour 6 ---------- 52

6. Case IA - Along Edge Velocity (U) at Hour 24 ---------- 53

7. Case IA - Across Edge Velocity (V) at Hour 24 ---------- 54

8. Case IA - Buoyancy (B) at Hour 24 ---------- 55

9. Case IA - Mixed Layer Depth (h) at Hour 24 ---------- 56

10. Case IA - Mixed Layer Depth (h) at Hour 42 ---------- 57

11. Case IB - Along Edge Velocity (U) at Hour 24 ---------- 58

12. Case IB - Across Edge Velocity (V) at Hour 24 ---------- 59

13. Case IB - Buoyancy (B) at Hour 24 ---------- 60

14. Case IB - Mixed Layer Depth (h) at Hour 24 ---------- 61

15. Case IC - Along Edge Velocity (U) at Hour 24 ---------- 62

16. Case IC - Across Edge Velocity (V) at Hour 24 ---------- 63

17. Case IC - Buoyancy (B) at Hour 24 ---------- 64

18. Case IC - Mixed Layer Depth (h) at Hour 24 ---------- 65

19. Case IIB - Along Edge Velocity (U) at Hour 24 ---------- 66

20. Case IIB - Across Edge Velocity (V) at Hour 24 ---------- 67

21. Case IIB - Buoyancy (B) at Hour 24 ---------- 68

22. Case IIB - Mixed Layer Depth (h) at Hour 24 ---------- 69

23. Case IIC - Along Edge Velocity (U) at Hour 36 ---------- 70

24. Case IIC - Across Edge Velocity (V) at Hour 36 ---------- 71

25. Case IIC - Buoyancy (B) at Hour 36 ---------- 72

26. Case IIC - Mixed Layer Depth (h) at Hour 36 ---------- 73

27. Case IIIA - Along Edge Velocity (U) at Hour 24 ---------- 74

28. Case IIIA - Across Edge Velocity (V) at Hour 24 ---------- 75

29. Case IIIA - Buoyancy (B) at Hour 24 ---------- 76

30. Case IIIA - Mixed Layer Depth (h) at Hour 24 ---------- 77

31. Case IIIB - Buoyancy (B) at Hour 24 ---------- 78

32. Case IIIB - Mixed Layer Depth (h) at Hour 24 ---------- 79

33. Case IIIC - Along Edge Velocity (U) at Hour 42 ---------- 80

34. Case IIIC - Across Edge Velocity (V) at Hour 42 ---------- 81

35. Case IIIC - Buoyancy (B) at Hour 42 ---------- 82

36. Case IIIC - Mixed Layer Depth (h) at Hour 42 ---------- 83

37. Case IIID - Along Edge Velocity (U) at Hour 36 ---------- 84

38. Case IIID - Across Edge Velocity (V) at Hour 36 ---------- 85

39. Case IIID - Buoyancy (B) at Hour 36 ---------- 86

40. Case IIID - Mixed Layer Depth (h) at Hour 36 ---------- 87

ACKNOWLEDGEMENT

This research was part of an Office of Naval Research sponsored project. A majority of the work in this thesis was accomplished using the facilities of the W. R. Church Computer Center. The author wishes to thank Dr. Miles G. McPhee whose expert counsel in adapting the model was invaluable, and who provided the bulk of the theoretical development for the sea ice model. Appreciation is expressed to Mr. David Adamec for his patient assistance with debugging problems and for a computer graphics routine that greatly enhanced the presentation of the results. To Dr. Roland W. Garwood, a very special thanks for his inspiration, encouragement, and dedication to the work and to this student. His time and effort were a positive influence on the author's desire for further graduate education and his guidance in the completion of the thesis is greatly appreciated.

# I. INTRODUCTION

## A. BACKGROUND AND MOTIVATION

Global climate and weather variability have been linked to large-scale interactions between the atmosphere, sea ice, and ocean. Recent investigations (e.g., Walsh and Johnson, 1979; Niebauer, 1980; Walsh and Sater, 1981; and, Overland and Pease, 1982) have associated an[illegible] and seasonal fluctuations in the extent of polar ice cover with atm[illegible]eric variability. The position and movement of the ice edge has an [illegible]tant effect on synoptic weather patterns. During the winter in the [illegible]ing Sea, extreme horizontal temperature gradients at the polar margins are well correlated with the development of cyclones (Overland and Pease, 1982). On the other hand, the seasonal advance and retreat of the sea ice is strongly influenced by the large-scale atmopheric circulation. Thus, dynamical interactions between the atmosphere, sea ice, and ocean develop a very complex system in which the growth, decay, and movement of the ice edge is both a cause and effect of variability.

The boundary between open water and ice-covered ocean, referred to as the Marginal Ice Zone (MIZ). serves as an important dynamical transition region. Over the past two decades, field experiments such as the Arctic Ice Dynamics Joint Experiment (AIDJEX) and theoretical modeling of sea ice and the adjacent atmospheric and oceanic boundary layers have added considerably to the understanding of the behavior or ice-covered oceans. The problem of understanding the nature of the MIZ was addressed in 1981 by the Joint Scientific Committee of the World Meteorological

Organization in a statement calling for an integrated research program (Johannessen et al, 1982). In response to this recommendation and as a result of workshops and meetings, a long-range experimental and modeling strategy was formulated from which emerged MIZEX (Marginal Ice Zone Experiment). MIZEX is an interdisciplinary project aimed at studying specific mesoscale processes in the MIZ as part of a larger, more comprehensive experimental and modeling effort relating the large-scale atmospheric and oceanic circulation to variability of the polar ice margins (Untersteiner, 1982). The first major experiment is sheduled to take place during the summer of 1984 in the Greenland Sea ice-edge zone north and west of Svalbard (see Figure 1).

A major goal of MIZEX will be to develop credible numerical models of MIZ processes, to be used prior to an experiment and in the field to optimize sampling strategies and as theoretical end products (McPhee, 1983b). The first coupled sea ice-ocean numerical model applied to problems in the MIZ was developed by Roed and O'Brien (1983). Their study of ice edge upwelling revealed the important hydrodynamic and ice rheology effects of the upper ocean in response to wind forcing. However, an important consideration was ignored; the sea ice in the MIZ is embedded in a turbulent, rotating oceanic planetary boundary layer (OPBL). The purpose of this investigation is to further the earlier work of Roed and O'Brien (1983) by including thermodynamic, advective, and mixing effects in numerical simulations of ice edge upwelling. This would seem to be the next logical step in the progression toward a complete, coupled model of MIZ processes.

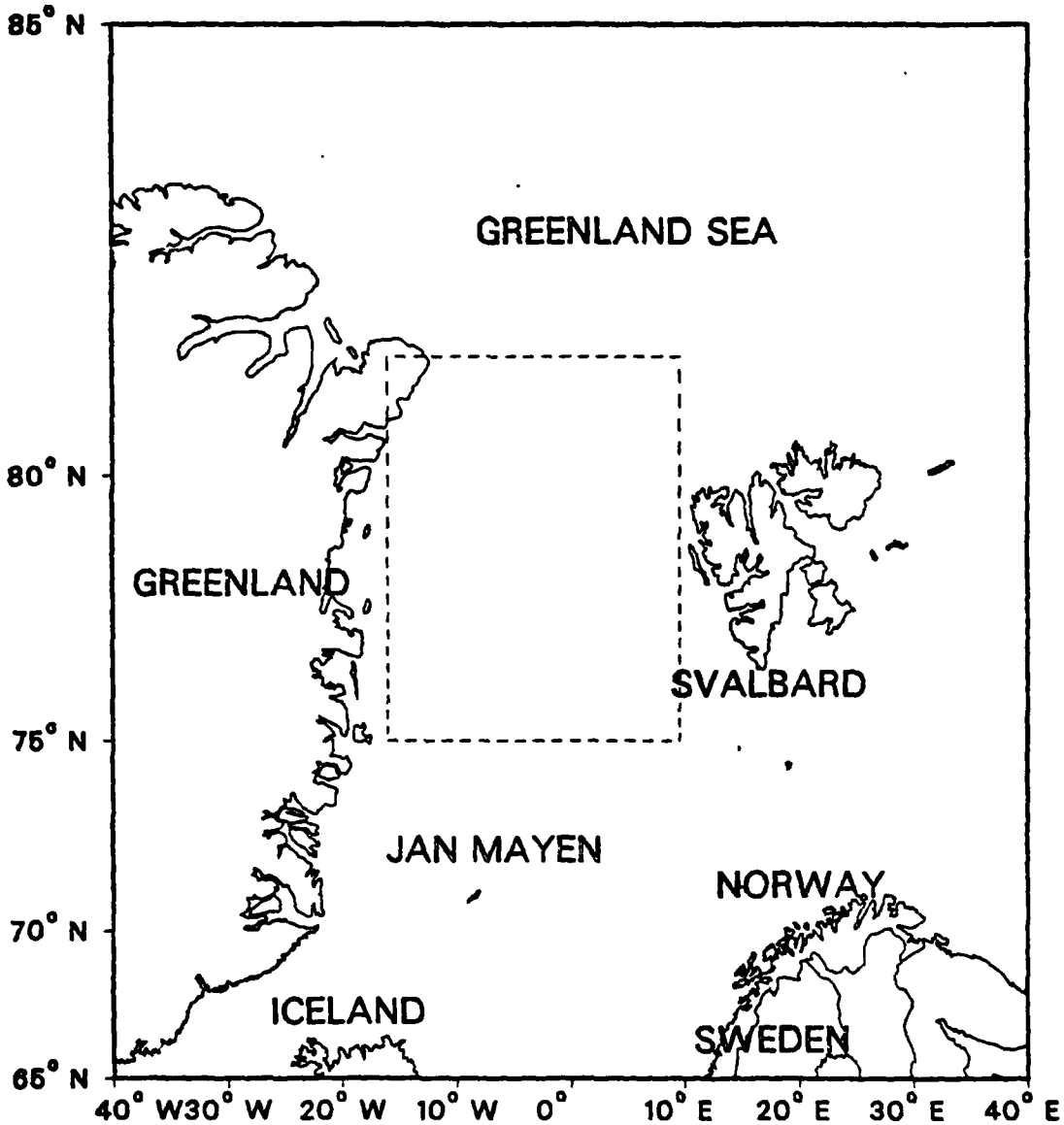


Figure 1. MIZEX 1984 Experimental Area. The dashed box represents the approximate operating area for the experimental phase.

Sea ice modifies the transfer of momentum from the atmosphere to the ocean; it acts as a thermal insulator; it significantly reduces the surface albedo; it dampens and reflects surface wave motion; and, by freezing and melting, it substantially alters the density structure of the upper ocean (McPhee, 1983b). The sensible heat flux at the ocean surface strongly influences ice growth and sea surface temperature. The associated surface buoyancy flux also influences mixing. Wind stress or momentum flux at the air-sea interface contributes to ice drift, wave and current generation, and mixing. As a result of wave action, the sea ice in the MIZ is broken into discrete floes. The combination of a greater exposed surface area and reduced ridging (brought about by erosion) produces drag coefficients in the atmospheric surface layer which are radically different than for the air flow over the interior ice pack (Johannessen et al, 1982). The surface wind stress is therefore a function of the surface roughness. The size and distribution of floes also affects the thermodynamics of the upper ocean. Melting of the ice in summer may be enhanced along the floe edges, while in winter, the growth rate is increased by the closing of open water areas (Johannessen et al, 1982).

Modification of the upper ocean across the ice edge can be extreme, with large horizontal gradients in temperature, salinity, and velocity caused by the horizontal differences in the surface momentum and buoyancy fluxes. The MIZ may at times coincide with manifestations of permanent oceanic fronts (e.g., the East Greenland Polar Front) and eddies; or, the ice edge itself may form a migrating, oceanic frontal zone. Near the ice edge these changes become more pronounced and may be

enhanced by advection. As the ice edge drifts in response to the surface wind and encounters warmer water, perhaps only slightly above the melting point, rapid ablation begins. The input of relatively fresh water at the top of the OPBL has the effect of stabilizing the water column and results in significant changes to both the momentum and buoyancy fluxes. Thus, the rate at which the sea ice grows or decays is indicative of the thermodynamic state of the oceanic surface mixed layer. (McPhee, 1983b).

## B. PREVIOUS MODELS AND OBSERVATIONS

Ice edge upwelling and other mesoscale oceanic circulations in the MIZ are believed to be caused by the surface gradients of wind stress and buoyancy flux. The possibility of upwelling was first studied by Gammelsrod et al (1975) using a linear, homogeneous, analytical model and invoking a stationary ice cover. They showed that the change in wind stress at the ice edge produced a divergence in the surface circulation, resulting in upwelling. Clarke (1978) extended the work by considering the effects of stratification. He modeled fast-ice edges using quasi-geostrophic theory and found similarity between the results and the ocean response near coasts. He also showed that a discontinuity in stress at the ice edge and the resultant infinite wind-stress curl caused the divergence of the surface flow, and hence upwelling. Buckley et al (1979) first observed upwelling along the ice edge north of Svalbard in winter during an experiment inspired by the earlier theoretical results. Niebauer (1982) developed a numerical model of the response of a shallow stratified ocean to wind forcing near an ice edge.

For computational stability, he assumed a stationary ice cover, and he included a meltwater front close to the ice edge. The presence of a stationary ice sheet has the effect of insulating the water from the surface wind stress, and it is dynamically analogous to coastal upwelling. The observations of Buckley et al (1979), and later by Alexander and Niebauer (1981), appear to justify this assumption.

A model recently developed by Roed and O'Brien (1983) coupled a dynamic sea ice cover with a two-layered ocean. The ice was allowed to move and to yield an internal ice stress. They demonstrated the importance of a moving ice cover. Although they assumed wind forcing conditions similar to those used in previous theoretical studies (e.g., Gammelsrod et al, 1975; Clarke, 1978; and, Niebauer, 1980), they found very different results concerning vertical motion. Roed and O'Brien's model predicted weak downwelling for the case of an along-ice edge wind stress vector with the ice to the left and open water to the right (the direction of this vector will be referred to as "up-ice"). In addition, they were able to show that the internal ice stress and nonlinear advection terms were not crucial for the prediction of upwelling. More recent observations by Johannessen et al (1983) support these results qualitatively.

## C. THE PROBLEM

The analytical study of Gammelsrod et al (1975) concluded that future models of the ocean response at an ice edge should include density stratification and diffusion. Clarke (1978) included stratification in his analytical model but found that the effects of nonlinearity

and mixing were potentially important and must be considered to completely understand the dynamics of oceanic features in the MIZ, such as ice edge upwelling. The present problem involves the development of a coupled sea ice-ocean model incorporating the recommendations of the previous analytical models and employing a nonstationary ice cover as suggested by the findings of Roed and O'Brien (1983). A model capable of simulating the upper ocean circulation response to wind and thermal forcing that includes the effects of advection, diffusion, and mixing is described below.

The application of the model to the case of ice edge upwelling and the effect of including advection and mixing on the upper ocean circulation will be shown in the sections to follow. Both stationary and moving ice cover cases are employed for comparison with the previous theoretical work. Also, the sensitivity of the model solutions to variations in wind forcing and surface buoyancy flux (thermal forcing) is determined. The model results are compared with observations in the MIZ and the other models of ice edge upwelling. The present model features a simple ice-ocean stress parameterization which is used to simulate an ice cover and to force the upper ocean under the ice, given the geostrophic wind. A key new feature is the inclusion of mixing which may be modulated by prescribing a surface buoyancy flux.

## II. THEORETICAL FORMULATION

### A. GENERAL

Designing a numerical model for the important processes of the MIZ is particularly difficult. Interactions between the atmosphere, sea ice, and ocean are physically and dynamically coupled. They involve feedbacks on all scales of motion and constitute a spatially complex and highly nonstationary system. In the polar seas, large-scale atmospheric forcing drives the ocean circulation for both the open and ice-covered areas. The resultant geometry of the MIZ may then affect climate and synoptic weather patterns by thermodynamic feedback mechanisms. Equally important are the intermediate and mesoscale atmosphere and ocean features which affect the temperature and salinity structure in the upper ocean and are a cause and effect of sea ice growth, decay, and movement.

Heat transfer from the ice to the ocean (and from the ocean to the ice) is an important factor in determining the position of the ice margin and how it evolves. Sea ice melting and freezing are thermodynamic processes which seasonally transform the MIZ. The melting of sea ice in contact with water above the melting temperature occurs by heat transfer across a turbulent OPBL (McPhee, 1983a). The resulting input of fresh meltwater into the upper ocean acts to stabilize the OPBL by producing an upward flux of surface salinity, or a downward surface buoyancy flux which consumes (damps) turbulence. The meltwater forms an insulating layer under the ice that also retards further heat transfer. The same effect can lessen the efficiency with which momentum is transferred by

effectively reducing the drag on the ice, with the result that the ocean beneath the ice cover is less accelerated (McPhee, 1983a). However, mixing of the OPBL will affect the transfer of momentum and virtually negates the insulating properties of the meltwater layer. When the water below the ice cover is colder, freezing takes place and there is a downward flux of salinity into the OPBL. Associated with the salinity flux is an upward surface buoyancy flux which produces turbulence in the OPBL.

The mixing response of the upper ocean to external forcing is complex. A continual input into the OPBL of wind energy maintains the turbulence and hence, acts to deepen the mixed layer through entrainment. Freezing or ice growth supports the effects of wind stirring through the buoyant production of turbulent energy which, when coupled with shear instability at the base of the mixed layer, causes rapid deepening of the mixed layer. The transfer of buoyancy into the OPBL by ice melting has the opposite effect on the mixed layer by reducing the amount of turbulent energy available for mixing. As a result, entrainment lessens and the mixed layer shallows. Shallowing will concentrate the momentum within the layer causing the ocean under the ice cover to accelerate. While the depth-integrated mass transport is the same regardless of changes to the mixed layer, the resultant vertical motion and upwelling are increased. Therefore, the evolution of the OPBL and its properties (e.g., well-mixed temperature, salinity, and density, and mixed layer depth) affect the ocean response to external forcing by concentrating the energy in a shallower layer (in the case of mixed layer shallowing) or by spreading the energy over a deeper layer (in the case of deepening).

This effect of mixing on the OPBL is a hypothesis for the observed ice edge upwelling with an up-ice wind.

The simulation of ice edge upwelling by a numerical model requires a system capable of resolving both small-scale motions and the large-scale horizontal variability of the upper ocean structure. The coupled sea ice-ocean model described below satisfies these requirements, and it incorporates thermodynamic and hydrodynamic processes in response to buoyancy flux and wind stress forcing. Advection, diffusion, and mixing, processes neglected in other models, were included in the ocean model. These processes may be as important as the wind stress in determining changes to the upper ocean circulation in the MIZ. By predicting mixed layer depth and comparing the results to the solutions for velocity and buoyancy, the importance of adding these effects can be seen and the applicability of the present model to MIZ problems demonstrated.

The motion will be described relative to a Cartesian coordinate system (x,y,z) in which the x-axis is parallel to the ice edge (along-ice) and the positive y-axis is taken to be in the off-ice direction. The model was applied to a two-dimensional (y,z) ocean region in the Northern Hemisphere, 100 km in horizontal extent and 500 m from the surface to the bottom (Figure 2).

Sea ice of varying thickness covers half of the surface (50 km) in the static ice cases. In cases simulating a nonstationary ice cover, the ice edge is advected away from the midpoint in the y-direction at a rate determined in the sea ice model.

The system is forced by a specified surface buoyancy flux, and a specified geostrophic wind field which is assumed to be constant over

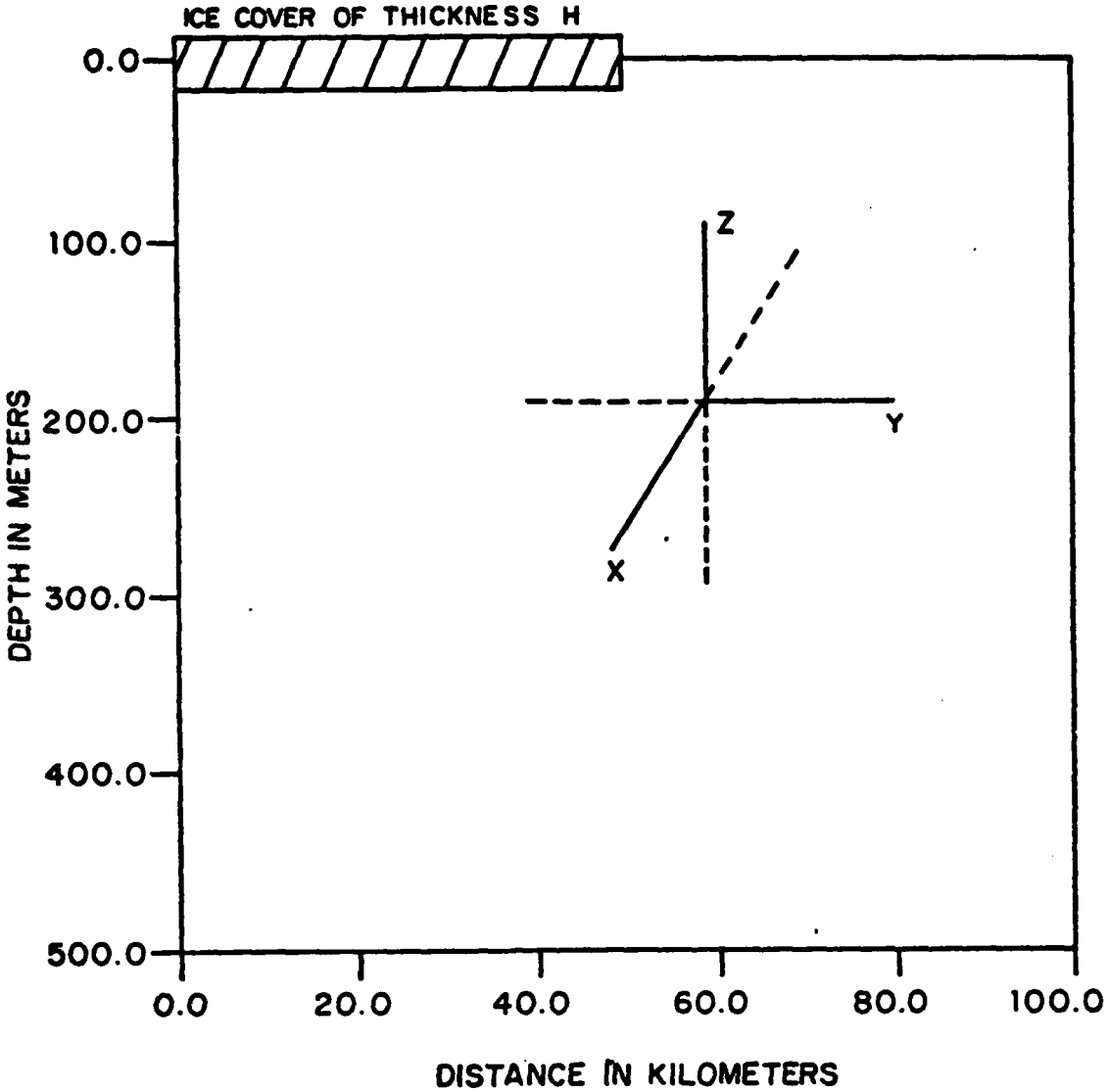


Figure 2. The Coupled Sea Ice--Ocean Model Coordinate System. The x-axis is parallel to the ice edge (along-ice) and the y-axis is perpendicular to the edge (across-ice).

the y-domain. The wind is input as a geostrophic wind vector which is given by

$$W_g = U_g + iV_g \tag{1}$$

where $U_g$ and $V_g$ are components of the geostrophic wind relative to the x and y axes respectively, and $i = \sqrt{-1}$ . The wind vector is then reduced to an equivalent wind stress vector in the sea ice model by a method to be described in the following section. In all cases, the geostrophic wind speed is assumed to be 10 m/sec. This value was selected as representative of the Greenland Sea MIZ during the summer melt season. Typical values of constants and parameters used in the model are given in Table I.

The conservation of buoyancy is employed as a generalization of the conservation of heat and salt after Garwood (1977). Buoyancy is the sole thermodynamic variable in the ocean model and contains the contributions due to salinity as well as temperature. Thus, the linearized equation of state for the ocean becomes

$$B = g\ \{\alpha(T - T_0) - \beta(S - S_0)\}$$

where B is buoyancy; T and S are the ambient temperature and salinity respectively; $T_0$ and $S_0$ are reference values of temperature and salinity; $\alpha$ and $\beta$ are the expansion and contraction coefficients for heat and salt respectively; and, g is gravity. The surface buoyancy flux, $\overline{B'w'}(0)$, is parameterized by

$$\overline{B'w'}(0) = \alpha g \frac{Q_0}{\rho c_p} - \beta g\ \overline{S'w'}(0) \tag{2}$$

Here, $Q_0/\rho c_p$ is the surface temperature (heat) flux and $\overline{S'w'}(0)$ is the surface salinity flux given by

$$\overline{S'w'}(0) = - \langle S \rangle\ d \tag{3}$$

TABLE I

Model Constants and Parameters

| SYMBOL | PARAMETER | VALUE | UNITS |
|---|---|---|---|
| $D$ | Maximum Depth | 500.0 | m |
| $\Delta y$ | Grid Length | 500.0 | m |
| $\Delta t$ | Timestep | 90.0 | sec |
| $H$ | Ice Thickness | 1.0 | m |
| $h$ | Mixed Layer Depth | 19.0 | m |
| $d$ | Sea Ice Melt Rate | 0.1 | m/day |
| $\rho_a$ | Density of Air | 1.3 | $kg/m^3$ |
| $\rho_w$ | Density of Seawater | 1027.6 | $kg/m^3$ |
| $\rho_i$ | Density of Sea Ice | 910.0 | $kg/m^3$ |
| $z_{0a}$ | Roughness Length over the Sea Ice | 0.005 | m |
| $z_{0w}$ | Roughness Length over the Seawater | $1.0 \times 10^{-4}$ | m |
| $z_{0i}$ | Roughness Length under the Sea Ice | 0.1 | m |
| $A_{HM}$ | Horizontal Eddy Coefficient of Viscosity | $10^2$ | $m^2/sec$ |
| $A_{HB}$ | Horizontal Eddy Coefficient of Conductivity | $10^2$ | $m^2/sec$ |
| $K_{VM}$ | Vertical Eddy Coefficient of Viscosity | $5.0 \times 10^{-3}$ | $m^2/sec$ |
| $K_{VB}$ | Vertical Eddy Coefficient of Diffusivity | $5.0 \times 10^{-3}$ | $m^2/sec$ |
| $c_{aw}$ | Drag Coefficient at the Air-Ocean Interface | $1.3 \times 10^{-3}$ | - |
| $\alpha$ | Expansion Coefficient for Heat | $0.2 \times 10^{-3}$ | $(^oC)^{-1}$ |
| $\beta$ | Contraction Coefficient for Salt | $0.75 \times 10^{-3}$ | $(^o/oo)^{-1}$ |
| $f$ | Coriolis Parameter | $1.4 \times 10^{-4}$ | $sec^{-1}$ |
| $g$ | Gravity | 9.81 | $m/sec^2$ |
| $\kappa$ | von Karman Constant | 0.4 | - |
| $T_0$ | Reference Temperature | 10.0 | $^oC$ |
| $S_0$ | Reference Salinity | 35.0 | $^o/oo$ |

<S> is a mixed-layer average representative salinity and d is the ice melting rate. In the experiments to be described later, a surface salinity flux of -0.003 $^{o}$/oo-cm/sec was assumed; this equates to a melt rate of approximately 10 cm/day. Melt rates of the order of 1 to 10 cm/day are not uncommon and may occur when ice moves across a frontal zone, where the mixed-layer temperature may change by as much as 2 to 3 K within several kilometers (McPhee, 1982). The surface buoyancy flux is taken to be positive in the upward direction and represents heat transfer.

## B. SEA ICE MODEL

The sea ice model consists of parameterizations for the transfer of momentum at the air-ice, air-ocean, and ice-ocean interfaces. When taken together, they provide the wind forcing that stirs the boundary layer below the ice cover and in the open ocean. (In a personal communication from Miles G. McPhee, a procedure for treating the interfacial stresses was outlined.) Applying similarity theory (McPhee, 1981), the prescribed geostrophic wind vector, $W_g$, is used to determine an equivalent surface wind stress over the ice,

$$\hat{\tau}_{ai} = \rho_a u_{*ai} \hat{u}_{*ai}$$

an equivalent surface wind stress over the open ocean (referred to as the open water stress),

$$\hat{\tau}_{aw} = \rho_a u_{*aw} \hat{u}_{*aw}$$

and the stress acting upon the ocean at its interface with the ice (referred to as the interfacial stress),

$$\hat{\tau}_{iw} = \rho_w u_* \hat{u}_*$$

where $u_{*a}$ and $u_*$ are friction velocities in the atmospheric and oceanic boundary layers respectively.

The (vector) friction velocity in the direction of the (ice) surface wind stress, $\hat{u}_{*ai}$, is determined from $W_g$ according to a Rossby-similarity law:

$$\frac{\hat{W}_g}{\hat{u}_{*a}} = \{ \frac{1}{\kappa} (\ln Ro_* - A) - i \frac{B}{\kappa} \} \tag{4}$$

Here, $\kappa$ is von Karman's constant; A and B are empirical constants (A = 2, B = 4); and, $Ro_*$ is a surface friction Rossby number given by

$$Ro_* = \frac{u_{*ai}}{fz_{0a}}$$

where $z_{0a}$ is the roughness length parameter over the sea ice. $\hat{u}_*$ is the (vector) friction velocity in the direction of the (ice-ocean) interfacial stress with a magnitude of $u_* = (\tau_{iw}/\rho_w)^{\frac{1}{2}}$.

An equation of motion for the ice is

$$\rho_i H \left(\frac{\partial \hat{V}_i}{\partial t} + if\hat{V}_i\right) + \text{Advection Terms} = - \nabla p + \rho_a u_{*a}\hat{u}_{*a} - \rho_w u_* \hat{u}_* + \nabla\sigma \tag{5}$$

where *H is the ice thickness; $\nabla p$ is the pressure gradient* due to the sea surface tilt; $\nabla\sigma_i$ is the gradient of the internal ice stress; and, $\hat{V}_i$ is the (vector) velocity of the ice. $\hat{V}_i$ can be determined from $\hat{u}_*$ by another application of the Rossby-similarity law:

$$\frac{\hat{V}_i}{\hat{u}_*} = \{ \frac{1}{\kappa} (\ln Ro_{*i} - A_i) - i \frac{B_i}{\kappa} \} \tag{6}$$

where $A_i$ and $B_i$ are constants ($A_i = B_i = 2$) and $Ro_{*i}$ is the interfacial Rossby number given by

$$Ro_{*i} = \frac{u_*}{fz_{0i}}$$

Here, $z_{0i}$ is the roughness length parameter for the underside of the ice. Assuming (1) that the local time derivative of $\hat{V}_i$ is negligibly small (i.e., steady state, as in the ocean model), (2) that the (geostrophic) current due to the pressure gradient can be ignored, (3) that the

advective acceleration terms are negligible, and (4) that the internal ice stress gradient is also negligible (a similar assumption was made by Roed and O'Brien), (5) reduces to

$$i\rho_i H f \hat{V}_i = \rho_a u_{*a} \hat{u}_{*a} - \rho_w u_* \hat{u}_* \tag{7}$$

Figure 3 is a sketch of the balance of forces represented in (7). As the ice thickness (H) decreases, the balance approaches $\hat{u}_{*ai} = (\rho_w/\rho_a)\hat{u}_*$. Thus, in the present Rossby-similarity approach, using a constant geostrophic wind field is very different from the assumption of a constant surface wind made in previous models.

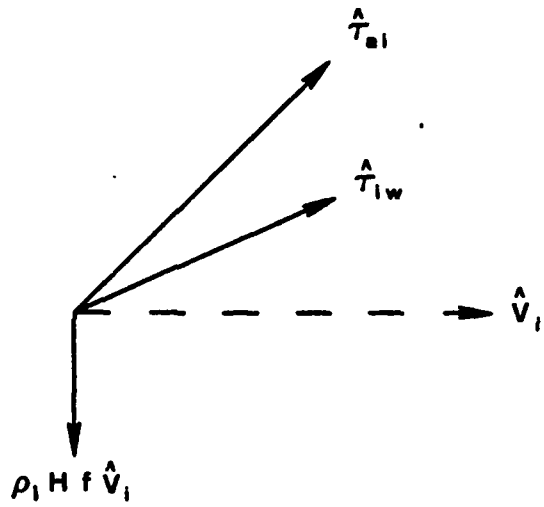


Figure 3. Balance of Forces on Sea Ice in the MIZ. $\hat{\tau}_{ai}$, $\hat{\tau}_{iw}$, and $\hat{V}_i$ are the air stress, the water stress, and the resultant ice velocity respectively.

Equations (4) and (6) are solved iteratively for $u_*$ and $u_{*ai}$, assuming an arbitrary initial value. These results are used to calculate stress components, relative to the model coordinate system, acting on the ocean under the ice cover. The open water stress components are determined by solving (4) for a (vector) friction velocity at the

air-ocean interface, assuming a different roughness length, $z_{0w}$ . The values for the roughness lengths over the ice and ocean were chosen such that the drag coefficient of the ice surface is about two times the drag coefficient over the open ocean. The ice velocity, determined by solving (6), is passed to the ocean model. The stress components provide the wind forcing in the ocean model while the ice velocity is used to advect the ice cover in the nonstationary cases.

## C. OCEAN MODEL

The embedded ocean general circulation--mixed layer model of Adamec et al (1981) was modified for the cartesian coordinate system described above. The wind forcing which is computed in the sea ice model is passed to the ocean model as an equivalent wind stress vector. The thermal and salinity forcing is prescribed as a total surface buoyancy flux. As mentioned before, buoyancy is the only thermodynamic variable in the ocean model and it includes the effects due to both temperature and salinity. The interfacial stress components and buoyancy forcing are applied to the ice-covered portion of the y-domain. Over the open ocean (assumed to be the remainder of the domain), the open ocean stress components and a zero buoyancy forcing are applied. Both the wind and buoyancy forcing are applied impulsively from the start time, and these values are maintained for the duration of the model run.

In the embedded ocean circulation--mixed layer model, hereafter called the ocean model, the ocean is assumed to be hydrostatic and incompressible, and density is taken to be a linear function of both temperature and salinity. In addition, the f-plane approximation is

made. The governing equations for the ocean model are

$$\frac{\partial u}{\partial t} = -\frac{\partial (uv)}{\partial y} - \frac{\partial (uw)}{\partial z} + fv + \frac{\partial}{\partial y}\left(A_{HM}\frac{\partial u}{\partial y}\right) - \frac{\partial \overline{(u'w')}}{\partial z} \tag{8}$$

$$\frac{\partial v}{\partial t} = -\frac{\partial (vv)}{\partial y} - \frac{\partial (vw)}{\partial z} - fu - \frac{1}{\rho_0}\frac{\partial p}{\partial y} + \frac{\partial}{\partial y}\left(A_{HM}\frac{\partial v}{\partial y}\right) - \frac{\partial \overline{(v'w')}}{\partial z} \tag{9}$$

$$\frac{\partial B}{\partial t} = -\frac{\partial (Bv)}{\partial y} - \frac{\partial (Bw)}{\partial z} + \frac{\partial}{\partial y}\left(A_{HB}\frac{\partial B}{\partial y}\right) - \frac{\partial \overline{(B'w')}}{\partial z} \tag{10}$$

$$\frac{\partial v}{\partial y} + \frac{\partial w}{\partial z} = 0 \tag{11}$$

$$\frac{\partial p}{\partial z} = -\rho_0 \, (g - B) \tag{12}$$

where u, v, and w are the components of velocity parallel to the ice edge, normal to the ice edge, and in the vertical, respectively; p is pressure; $\rho$ is density; $A_{HM}$ and $A_{HB}$ are the coefficients of horizontal eddy viscosity and conductivity, respectively; and, $\rho_0$ is the density of seawater at the reference temperature, $T_0$, and salinity, $S_0$.

In the ocean model, fluxes of momentum and buoyancy are computed across the air-ocean interface and across the y-axis boundaries where cyclic continuity is maintained. The specific boundary conditions are

$$w = 0 \quad \text{at } z = 0, -D \tag{13}$$

$$\left.\begin{aligned} -\overline{(u'w')} &= \tau_x / \rho_0 \\ -\overline{(v'w')} &= \tau_y / \rho_0 \\ -\overline{(B'w')} &= \alpha g \, (Q_0/\rho c_p) - \beta g \, \overline{(S'w')} \end{aligned}\right\} \quad \text{at } z = 0 \tag{14}$$

$$\overline{(u'w')} = \overline{(v'w')} = \overline{(B'w')} = 0 \quad \text{at } z = -D \tag{15}$$

Setting $w = 0$ at the top of the ocean, as in (13), requires that the divergence of the vertically-averaged motion be zero; in the ocean model, the vertically-averaged horizontal motion is assumed to be identically zero. Taking the vertical average of the u and v momentum equations, and subtracting them from (8) and (9), gives the prediction equations for u and v.

$$\frac{\partial u}{\partial t} = -\frac{\partial (uv)}{\partial y} - \frac{\partial (uw)}{\partial z} + fv + \frac{\partial}{\partial y}\left(A_{HM}\frac{\partial u}{\partial y}\right) - \frac{\partial \overline{(u'w')}}{\partial z} - \left\{-\frac{\partial (\widetilde{uv})}{\partial y} + \frac{\tau_x}{\rho_0 D}\right\} \quad (16)$$

$$\frac{\partial v}{\partial t} = -\frac{\partial (vv)}{\partial y} - \frac{\partial (vw)}{\partial z} - fu - \frac{1}{\rho_0}\frac{\partial p}{\partial y} + \frac{\partial}{\partial y}\left(A_{HM}\frac{\partial v}{\partial y}\right) - \frac{\partial \overline{(v'w')}}{\partial z} - \left\{-\frac{\partial (\widetilde{vv})}{\partial y} + \frac{\tau_y}{\rho_0 D}\right\} \quad (17)$$

Here, $(\tilde{\ })$ denotes a vertical average over the total ocean depth, D, and $\langle p\rangle = p - \tilde{p}$ is the mixed-layer average pressure. Vertically integrating (12) gives $\langle p\rangle$ as a function of B alone, or

$$\langle p\rangle = p - \tilde{p} = -\int_z^0 \rho_0 (g - B)\, dz + \frac{1}{D}\int_{-D}^0 \left\{ \int_z^0 \rho_0 (g - B) dz\right\} dz \quad (18)$$

The final element in the ocean system is derived by integrating the continuity equation, (11), over the mixed layer and applying the rigid-lid approximation, (13). A prediction equation for the depth of the well-mixed layer, h, is given by

$$\frac{\partial h}{\partial t} + w(-h) = w_e \quad (19)$$

where $w_e$ is the entrainment velocity. The equations (10), (11), (16), (17), (18), and (19), along with the boundary conditions (13) - (15), represent a closed system of equations for the variables u, v, B, $\langle p\rangle$, w, and h.

The parameterization of the turbulence quantities (e.g., $\overline{u'w'}$, $\overline{v'w'}$, $w_e$, etc.) is dependent on the mixed layer depth (h). At depths greater

than h, i.e., below the ocean surface mixed layer, the classical eddy viscosity and eddy diffusivity formulation is used. The vertical turbulent fluxes of momentum and buoyancy become

$$\overline{u'w'} = - K_{VM} \frac{\partial u}{\partial z}$$

$$\overline{v'w'} = - K_{VM} \frac{\partial v}{\partial z} \tag{20}$$

$$\overline{B'w'} = - K_{VB} \frac{\partial B}{\partial z}$$

where $K_{VM}$ and $K_{VB}$ are the vertical eddy coefficients for viscosity and diffusivity respectively. In the upper ocean below the influence of atmospheric stirring, the values of $K_{VM}$ and $K_{VB}$ are approximately constant. However, between the ocean surface and the base of the mixed layer, in the region of intense turbulent mixing, their values are depth and time dependent. Here, a scheme based on the intensity of the turbulence and entrainment is appropriate.

Using equations derived from the turbulent kinetic energy budget, Garwood (1977) proposed a parameterization for the mixed-layer turbulence variables. These same bulk second-order closure methods are incorporated in the mixing part of the ocean model. The buoyancy flux at the base of the OPBL is given by

$$\overline{B'w'}(-h) = - \frac{\langle \overline{w'w'} \rangle^{\frac{1}{2}} \langle \overline{E} \rangle}{h} \tag{21}$$

where $\langle \overline{w'w'} \rangle$ and $\langle \overline{E} \rangle$ are mixed-layer average (bulk) values of the vertical component and total turbulent kinetic energies, respectively. In the entrainment zone, buoyant damping attributable to $\overline{B'w'}(-h)$ is assumed to be balanced by the convergence of turbulent kinetic energy flux. The prediction equations for the mixed layer turbulence quantities are

$$\frac{\partial}{\partial t}\left(\frac{h}{2}\langle\bar{E}\rangle\right) = mu_*^3 - \frac{h\,\overline{B'w'}(-h)}{2Ri^*} - \left(\langle\bar{E}\rangle^{1/2} + fh\right)\langle\bar{E}\rangle \tag{22}$$

$$\frac{\partial}{\partial t}\left(\frac{h}{2}\langle\overline{w'w'}\rangle\right) = \frac{h\{\overline{B'w'}(-h) - \overline{B'w'}(0)\}}{2} + \left(\langle\bar{E}\rangle - 3\langle\overline{w'w'}\rangle\right)\langle\bar{E}\rangle^{1/2} - \frac{\left(\langle\bar{E}\rangle^{1/2} + fh\right)\langle\bar{E}\rangle}{3} \tag{23}$$

Here, $u_* = (\tau/\rho_a)^{1/2}$ where $\tau$ is the magnitude of the surface wind stress, $\rho_a$ is the density of air, and $Ri^* = (h\Delta B/\Delta u^2 + \Delta v^2)$ is the bulk Richardson number.

The bulk turbulent kinetic energy equations, (22) and (23), are solved by assuming a quasi-steady state. For time scales of greater than a few hours, this assumption was found to be valid (Adamec et al, 1981) and permitted the use of longer time steps, improving the numerical efficiency of the model. The downward fluxes of momentum associated with entrainment at the base of the mixed layer are then computed from the entrainment buoyancy flux, (21), and are given by

$$-\overline{u'w'}(-h) = w_e\,\Delta u = -\overline{B'w'}(-h)\,\frac{\Delta u}{\Delta B} \tag{24}$$

$$-\overline{v'w'}(-h) = w_e\,\Delta v = -\overline{B'w'}(-h)\,\frac{\Delta v}{\Delta B} \tag{25}$$

The quantities $\Delta B$, $\Delta u$, and $\Delta v$ are the buoyancy and velocity differences (or "jumps") between the bulk values in the mixed layer and the water column below the mixed layer.

The amount of turbulent kinetic energy available for mixing at the base of the mixed layer is dependent upon the surface buoyancy flux and the friction velocity. The ocean model can treat both fundamental types of boundary layer evolution: (1) deepening by entrainment and (2) shallowing. Provided the computed values for h and the momentum and buoyancy profiles are unique, i.e., the mixed layer is homogeneous, heat

is conserved, and the new h is deeper than the previous value, there will be sufficient turbulent energy for entrainment and deepening. In the event that there is inadequate vertical turbulent kinetic energy to transport buoyancy down to the base of the existing mixed layer, shallowing will occur. Then (21) is not applicable and there will be new steady state forms of (22) and (23) which conserve potential energy. In general, the depth of the shallowing mixed layer is a function of the two nondimensional parameters, $h/L$ and $hf/u_*$, where L is the Obukhov length scale.

In the derivation of the bulk model, Garwood (1977) assumed that the mixed layer was dynamically unstable and the underlying water column was dynamically stable. Dynamic stability, as measured by the gradient Richardson number (Ri), is enforced throughout the water column below the mixed layer in the ocean model. This "dynamical adjustment", which is an improvement upon the convective parameterizations employed in ocean circulation models, is performed at each timestep.

The specific method of embedding the mixed layer model of Garwood (1977) into the ocean circulation model of Haney (1980) is described in Adamec et al (1981). To summarize how the model works, at the beginning of each timestep the tendencies due to advective and diffusive processes are calculated in the dynamic portion of the model for all layers and the predicted variables (u, v, B, and h) are stepped forward in time. Next, the changes due to the surface fluxes of momentum and buoyancy and entrainment mixing are calculated in the mixing part of the model. During this stage, the treatment depends on whether the layer is deepening or shallowing. The computed mixing tendencies are then applied to the variables and returned to the dynamic part for the next timestep.

All of the computations are done using a staggered grid for better resolution and improved computational stability.

The following section will describe a model experiment in which the coupled sea ice-ocean system described above is employed to determine the upper ocean circulation response to variations in wind and surface buoyancy flux forcing. The case of ice edge upwelling is examined to show the significance of the new features incorporated in the present model, and their effects on the ocean circulation.

## III. THE MODEL EXPERIMENT

In the previous theoretical studies, the importance of the magnitude and direction of the surface wind stress has been demonstrated in the occurrence of ice edge upwelling. According to Gammelsrod et al (1975) and Clarke (1978) an up-ice wind forcing causes an oceanic surface transport to the right of the wind, or off-ice. Since they assumed that the ice cover behaved like a coast, i.e., it was stationary, there would be no similar transport under the ice. This condition would lead to a divergence in the surface Ekman transport across the ice edge and upwelling. Conversely, using the previous analytical models (Gammelsrod et al, 1975; Clarke, 1978), a down-ice wind causes an oceanic surface transport convergence and downwelling at the ice edge.

A more recent study using a coupled sea ice-ocean numerical model with a moving ice cover (Roed and O'Brien, 1983) showed that an up-ice wind was actually conducive of weak downwelling at the ice edge. Roed and O'Brien attributed the disparity between their numerical result and the earlier analytical models to ice motion. Assuming a drag coefficient for the ice surface twice as large as for the open (ice-free) ocean, they compute an interfacial stress acting on the ocean under the sea ice cover. The atmospheric momentum transferred to the ocean via the interfacial stress is greater and, therefore, the surface transport is larger in magnitude than in the open water. The resultant convergence of the across-ice-edge surface Ekman transport drives the downwelling.

The intent of the model experiment is to determine the effects of surface forcing on the upper ocean dynamics in the MIZ. Of general interest is the effect of the addition of mixing upon the vertical motion and MIZ upper ocean circulation. Of special interest is the contention of Roed and O'Brien (1983) that a nonstationary ice cover is critical for the upwelling phenomenon. For the purpose of investigating these effects and testing the mixing hypothesis, several runs of the model were made. By varying the wind and surface buoyancy flux forcing, the relative effect of each on the upper ocean circulation response can be measured. Comparing these results using a stationary ice cover to the case where a moving ice cover is employed, the effect of ice motion is determined.

In each run, the coupled sea ice-ocean system described in the previous chapter is initialized with a buoyancy profile derived from observations of temperature and salinity structure in the MIZ (Paquette and Bourke, 1978; Buckley et al, 1979). Figure 4 depicts the initial buoyancy field to be used in the model runs. It was derived from temperature and salinity using the equation of state for the ocean. This particular field was used because it is typical of melting sea ice in the MIZ. The mixed layer at the initial time is assumed to have a uniform depth of 19 meters.

There are three model cases using this initialization: Case I includes runs with different surface buoyancy fluxes; Case II varies the wind forcing; and, Case III invokes a moving ice cover with varying wind forcing and a downward surface buoyancy flux (simulating ice melting). Each model run spans a period of two days and the output consists of fields of horizontal velocity, buoyancy, and mixed layer depth. All of

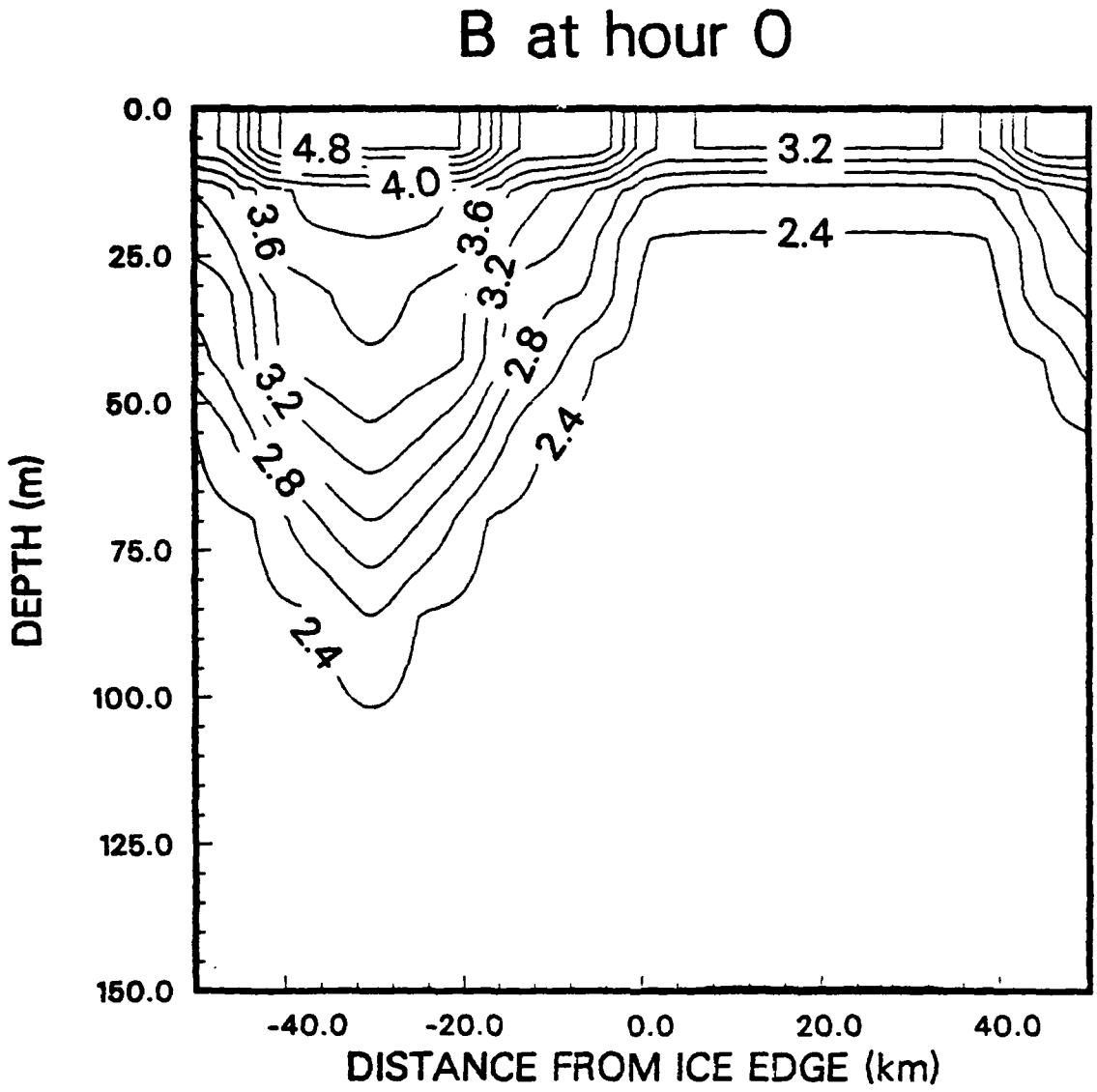


Figure 4. Buoyancy Field Used for Model Initialization. The units of buoyancy are cm/sec$^2$ and the contouring interval is 0.1 cm/sec$^2$.

the predicted variables are plotted every six hours. For runs in which a stationary ice cover is assumed (Cases I and II), the ice edge position is fixed at the midpoint of the model domain. A nonstationary ice cover is simulated by advecting the ice edge with the y-component of the ice velocity determined in the sea ice model. (In these runs, Case III, the zero label on the abscissa of the figures represents the initial and not the actual, time-dependent ice edge position.)

The following sections will describe the results of the case studies and offer some explanations for the predicted ocean response. In all cases the wind forcing is applied as components of the surface stress over the ice-free ocean and the interfacial stress under the ice cover. For a 10 m/sec geostrophic wind, the open (ice-free) ocean surface stress is approximately 0.78 dynes/cm$^2$; the surface stress on the ice cover is 1.12 dynes/cm$^2$; and, the interfacial stress under the ice is about 1.21 dynes/cm$^2$. The direction of the stresses depends upon the wind; the open water stress, ice surface stress, and interfacial stress are directed 6.7, 11.6, and 5.7 degrees to the left of the geostrophic wind in each case, respectively.

The figures which depict the model solutions have been placed together at the end for easy reference. Positive contours of a quantity are represented by solid lines in a field while dashed lines represent negative contours. Also, the depth scale on the ordinate is potentially misleading. Because of the coarse vertical resolution of the ocean model, the mixed layer is not accurately portrayed in the fields of velocity and buoyancy. Although this graphical distortion can be eliminated in future studies, the qualitative results will be very similar.

## A. THE MODEL RESPONSE TO BUOYANCY FLUX FORCING

The first case of the model experiment reveals the importance of buoyancy flux forcing and the nature of the contribution of buoyancy in predicting the response of the upper ocean circulation in the MIZ. The sensitivity of the model to such forcing was investigated by alternately prescribing null, downward, and upward surface buoyancy fluxes. An upward (positive in the model) surface buoyancy flux was chosen a priori to simulate ice growth or freezing, while the downward (negative) surface buoyancy flux was determined from (2) and (3) above. Solutions using 0, -0.002, and 0.001 $cm^2/sec^3$ for the surface buoyancy flux are described below.

The wind forcing for all three runs of this case is down-ice or (10.0,0.0) m/sec, where 10.0 m/sec is the x-component of the geostrophic wind ($U_g$) and 0.0 m/sec is the y-component of the geostrophic wind ($V_g$). According to Gammelsrod et al (1975) and Clarke (1978) this forcing is conducive of downwelling at the ice edge. Using the model of Roed and O'Brien (1983), a down-ice surface wind drives upwelling. In this case, like the previous analytical models, a stationary ice cover is assumed. Hence, the effects of ice motion have been omitted. However, because of the interfacial stress which results when momentum is transferred through the ice, the ocean under the ice is accelerated.

### 1. Null Surface Buoyancy Flux Condition (Case IA)

The condition of zero surface buoyancy flux is equivalent to forcing the system with the surface wind stress alone. In this run, the response of the model to wind forcing which by Gammelsrod et al (1975) is conducive of downwelling is considered. Here, the wind stress is in

the direction of the positive x-axis. The x-component of velocity, or the along-ice edge component of the upper ocean circulation, calculated by the model at hour 6 of the run (Figure 5) shows a strong geostrophic response to the imposed initial conditions under the ice cover with weak, positively-directed flow in the open ocean. A maximum current of 32 cm/sec is found at about 20 km from the ice edge. The open ocean near-surface current is only 1 cm/sec. At hour 24 (Figure 6), the magnitude of the under-ice current is less (22 cm/sec) while the open ocean response has intensified (2 cm/sec).

The convergence or divergence of the oceanic surface transport can best be visualized in the V-field, the y-component of the velocity (or across-ice edge component of the upper ocean circulation), since the transport for a down-ice wind is directed on-ice (in the negative y-direction). At hour 24 (Figure 7), the cluster of dashed contours under the ice indicates a divergence of the on-ice surface flow; the ocean under the ice cover is moving faster due to the larger stress acting on it. The corresponding buoyancy field (Figure 8) and mixed layer depth curve (Figure 9) have features which indicate upwelling at the ice edge. The mixed layer depth is displaced upward about 8 m at the ice edge.

The wind stirring of the mixed layer increases the level of turbulence and mixing which in turn deepens the mixed layer by entrainment. The model solution for mixed layer depth at hour 42 (Figure 10) shows that a deepening of about 6 - 8 m has occurred under the ice cover.

2. Downward Surface Buoyancy Flux Condition (Case IB)

The downward surface buoyancy flux of -0.002 $cm^2/sec^3$ corresponds to a melt rate of approximately 10 cm/day. The influx of fresh meltwater

under the ice cover acts to stabilize the mixed layer and should oppose the deepening influence of the wind forcing. That is, the effect of ice melting alone will be to shallow the mixed layer and concentrate the momentum transferred to the ocean under the ice by effectively increasing the current within the mixed layer.

The model solutions for this run were very similar to those for Case IA. The magnitude of the downward surface buoyancy flux was too small to influence perceptively the results. The velocity fields, U and V at hour 24 (Figures 11 and 12), are the same as in the previous run. Again, the orientation of the dashed contours under the ice in the V-field is indicative of a divergence of the flow from the slower moving open ocean. The buoyancy field at hour 24 (Figure 13) show a deformation of the 2.5 $cm/sec^2$ contour at the ice edge, an upward bending, that indicates an upward flux of buoyancy at that point. It corresponds to a similar feature in the mixed layer depth (Figure 14) which is indicative of upwelling. The upwelling is presumably occurring in response to the wind forcing. Since there is no appreciable difference between the curves of mixed layer depth at hour 24 for the null and downward surface buoyancy flux conditions, the wind forcing effect is considered dominant and probably masks the response due to the buoyancy flux forcing in this case. Forcing the model system with a larger buoyancy flux and/or a weaker wind should demonstrate the modifying effect of the buoyancy forcing. A run was made using such forcing and the results show a marked shallowing of the mixed layer under the ice with weak upwelling at the ice edge.

3. Upward Surface Buoyancy Flux Condition (Case IC)

In contrast to the previous conditions, an upward surface buoyancy flux of 0.001 $cm^2/sec^3$ produces instability within the mixed layer, enhancing entrainment at the base of the mixed layer. The upward transfer of buoyancy out of the OPBL occurs in the presence of ice growth by freezing. During the freezing process, salt is excluded from the surface causing a downward flux of salinity or an upward buoyancy flux. As a result, turbulence is increased and the mixed layer deepens by entrainment. This effect is superimposed on the deepening influence of the wind stirring of the mixed layer.

The model solutions after 24 hours are not very different from the two previous runs. The velocity fields (Figures 15 and 16) are nearly identical in all three runs of Case I. Buoyancy (Figure 17) and mixed layer depth (Figure 18) at hour 24 depict features which resemble the effect of upwelling at the ice edge. The mixed layer appears to be only slightly deeper under the ice than in the open ocean, a trend that continues for the remainder of this run.

Clearly, the down-ice wind forcing in this case contributes to an upwelling at the ice edge. This result is in qualitative agreement with the study by Roed and O'Brien (1983). It also shows the impracticality of assuming the ice cover acts like a coast, with no momentum transfer to the ocean beneath the ice. The interfacial stress and the surface Ekman transport it causes are critical for the oceanic response that drives the upwelling. Here, the imposed surface buoyancy fluxes have little effect on the upwelling phenomenon. In the run with a downward surface buoyancy flux, the mixed layer under the ice shallowed

indicating that any upwelling may be enhanced. With an upward surface buoyancy flux, mixing is increased and the upwelling is opposed by deepening of the mixed layer. The next step will be to vary the wind forcing direction and to look at cases in which downwelling might be predicted by the other models. Perhaps, then the effect of applying a downward surface buoyancy flux will be more evident.

## B. THE MODEL RESPONSE TO WIND FORCING

Next, the response of the model system to wind forcing is considered. The sensitivity of the model to wind forcing was investigated by prescribing a geostrophic wind of 10 m/sec of varying direction. The effect on the upper ocean circulation of down- and up-ice wind forcing is described above. An on-ice wind should act through surface friction to compact the ice floes, while an off-ice wind would disperse the ice floes that make up the edge zone. Observations by Bauer and Martin (1980) in the Bering Sea MIZ during March 1979 show that the leading floes at the ice edge accelerated away from the pack forming so-caller "ice-edge bands." McPhee (1983a) suggests that this divergence occurs when off-ice winds advect the edge over water that is above the melting point for the ice. The effect on the ocean circulation of off-ice or on-ice wind forcing has not been previously reported.

In this case, the model employs a stationary ice cover as before. The buoyancy flux forcing for all runs of this case was the same, -0.002 $cm^2/sec^3$. A downward surface buoyancy flux was chosen to determine the comparitive influence of the different wind forcing under simulated ice melting conditions. There are four runs in this case, with a down-ice,

on-ice, up-ice, and off-ice geostrophic wind prescribed. The results are described below.

1. Down-Ice Wind Forcing (Case IIA)

The results for a (10.0,0.0) m/sec or down-ice geostrophic wind are indistinguishable from those described above for Case IB. As before, the wind forcing drives the upwelling at the ice edge by creating a divergence in the oceanic surface transport across the ice edge. The ocean under the ice is accelerated more by the interfacial stress than is the open ocean by its surface stress. The buoyancy flux forcing in this case modifies the solutions by enhancing the upwelling at the ice edge and shallowing the mixed layer under the ice cover.

2. On-Ice Wind Forcing (Case IIB)

An on-ice wind, (0.0,-10.0) m/sec, applied to the model system with a stationary ice cover causes a surface Ekman transport in the along-ice direction. The transport is in the negative x-direction (or up-ice) and opposes the geostrophic current which is the result of the imposed buoyancy field. As expected, at hour 24, the U-field (Figure 19) shows a much weaker total current under the ice than in the previous runs with a down-ice wind (maximum current speed is about 16 cm/sec). The open ocean circulation is up-ice (dashed contours), in the direction of the net surface Ekman transport. Also as expected, the corresponding V-field (Figure 20) indicates that the on-ice flow is stronger under the ice cover due to the larger stress. From the buoyancy field for hour 24 (Figure 21), there appears to be a small downward pertubation in the 2.7 cm/sec$^2$ contour at the ice edge. The mixed layer curve (Figure 22) shows that in fact there is weak upwelling at the ice edge.

3. Up-Ice Wind Forcing (Case IIC)

In principle, the condition of a (-10.0,0.0) m/sec or up-ice geostrophic wind forcing the model is most similar to the treatment by the earlier analytical studies which also assumed a stationary ice cover. From the results described above for Case IIA (or Case IB), one would expect the model solutions to support downwelling at the ice edge which contradicts the findings of Gammelsrod et al (1975) and Clarke (1978). The initial response of the ocean in this run is for weak downwelling. Since the ocean under the ice is accelerated more than it is in the open ocean, there is a convergence of the off-ice directed oceanic surface transport across the ice edge which drives the downwelling.

Later, at hour 36, the downwelling is replaced by weak upwelling. The U-field (Figure 23) shows that the open ocean flow is in the negative x-direction (or up-ice) while the total current under the ice is reduced by the ocean response to the up-ice wind stress. The V-field at hour 36 (Figure 24) has no recognizable convergence or divergence pattern. The contours on both sides of the ice edge position are similar. However, in the buoyancy field (Figure 25) the contours near the ice edge are displaced upward indicating an upward vertical motion. The ocean circulation response is manifested by a decrease in the mixed layer depth at the ice edge of about 7 m (Figure 26), which is presumably attributable to weak upwelling.

In this case, the weak downwelling predicted by Roed and O'Brien (1983) is replaced by weak upwelling due to a shallowing of the mixed layer under the ice. The downward buoyancy flux simulating ice melting has the effect of opposing the ocean circulation response to wind forcing.

4. Off-Ice Wind Forcing (Case IID)

The wind forcing for this run is (0.0,10.0) m/sec or off-ice. Since ice motion has been neglected, the oceanic response is limited to the geostrophic current due to the buoyancy field under the ice and a surface Ekman transport in the positive x-direction (or down-ice). The model solutions indicate no upwelling or downwelling at the ice edge.

By varying the direction of the applied wind forcing with a consistent downward surface buoyancy flux, it is clear that the upper ocean circulation near the ice edge is not only dependent upon the wind forcing but also upon the thermodynamic state of the OPBL. For an up-ice geostrophic wind, the present model predicts weak upwelling at the ice edge. The upwelling occurs after about 36 hours into the run and is a result of mixed layer shallowing which, in this case, opposes the effect of the wind forcing. Although the ice cover in this case was stationary, the important forcing on the ocean under the ice by the interfacial stress was incorporated. Hence, with forcing similar to that employed by Roed and O'Brien (1983) in their numerical model, the ocean circulation response is opposite. The only remaining variable in the problem under consideration is the motion of the ice.

## C. THE MODEL RESPONSE TO A MOVING ICE COVER

In the present model simulation a moving ice cover is incorporated and the model is forced with a downward surface buoyancy flux and a 10 m/sec geostrophic wind in varying directions. As the ice edge advects across the model domain (in the y-direction), the ocean area under the ice that is affected by the ice melting and the interfacial stress

changes. As a result, the upper ocean circulation and mixing are modified from the earlier cases where a stationary ice cover is assumed. Solutions are described below for down-ice, on-ice, up-ice, and off-ice wind forcing.

1. Down-Ice Wind Forcing (Case IIIA)

The model solutions for this run are nearly identical to those for Cases IB and IIA, where similar forcing is applied. The y-component of the ice velocity is on-ice at approximately 1.4 cm/sec. In other words, the ice edge is moving to the left in the model domain and the ice cover is "shrinking." After 24 hours, the ice edge has moved about 1.2 km from the initial position (center or "U" in the figures).

The U-field at hour 24 (Figure 27) is nearly identical to the field in Case IB. The under-ice current and the open ocean circulation are both directed down-ice. A divergence of the faster under-ice flow from the near-surface flow in the open ocean is depicted in the V-field (Figure 28). At the same time, the buoyancy field (Figure 29) and mixed layer depth curve (Figure 30) show features that are indicative of upwelling at the ice edge. As before, the buoyancy forcing enhances the upwelling.

2. On-Ice Wind Forcing (Case IIIB)

The results for this run are similar to those for Case IIB, described above. Here, the ice velocity is on-ice at 14.4 cm/sec. In 24 hours the ice edge will have retreated about 12.4 km. The ocean response is modified due to the ice motion. The intensity of the upwelling feature described earlier is reduced (see Figures 31 and 32). The

depth of the mixed layer under the ice is somewhat reduced due to the stabilizing effect of the downward surface buoyancy flux.

3. Up-Ice Wind Forcing (Case IIIC)

The model solutions for this run are similar to those for Case IIC. The ice velocity determined in the sea ice model is off-ice at approximately 1.4 cm/sec. After 42 hours, the ice edge will have advected 2.1 km. In the modeling study by Roed and O'Brien (1983), an up-ice wind was conducive of weak downwelling at the ice edge. Accordingly, the wind forcing for this run is up-ice (as in Case IIC). The model solutions from Case IIC show that the downward surface buoyancy flux drives a vertical motion that opposes the effect of the wind stirring on the upper ocean circulation.

As expected, at hour 42 of this run, weak upwelling is replaced by weak downwelling at the ice edge and the mixed layer has shallowed under the ice due to the downward surface buoyancy flux. In the velocity fields (Figures 33 and 34) the influence of the growing ice cover over the domain is evident. The geostrophic current is wider and the open ocean circulation is very weak. The surface flow in the V-field indicates that there is weak convergence of the surface transport at a point just to the right of the initial ice edge position. An upward fluctuation in the 3.2 cm/sec$^2$ buoyancy contour (see Figure 35) is accompanied by a depression of the contours at the ice edge. From the mixed layer curve (Figure 36), it is evident that this feature is due to weak upwelling located to the left of the weak downwelling at the ice edge. Like in Case IIC, it is conjectured that the downwelling is a response to the wind forcing while the upwelling is caused by the buoyancy flux

forcing. To test this conjecture, another run of the model was made using the same wind forcing, but with an upward surface buoyancy flux. This test shows that the weak downwelling predicted by Roed and O'Brien is indeed a response of the upper ocean circulation to an up-ice wind forcing, and the upwelling is driven by the downward surface buoyancy flux.

Clearly, the addition of ice motion has had a dramatic effect on the upper ocean circulation. In Case IIC the downward surface buoyancy flux resulted in weak upwelling at the ice edge. Here (Case IIIC), the movement of the ice edge (off-ice) has the effect of enhancing the wind-forced response and results in weak downwelling at the ice edge. This downwelling is accompanied by weak upwelling caused by the buoyancy forcing. These results are very different from the earlier studies and indicate the complexity of the problem.

4. Off-Ice Wind Forcing (Case IIID)

The combination of wind and buoyancy forcing and ice motion cause weak upwelling at the ice edge. This differs from the response described earlier for Case IID. The ice velocity for this run was determined to be 14.4 cm/sec in the off-ice direction. At this speed, at hour 36 the ice edge will have moved 18.7 km off-ice from the initial position.

The total current in this case is increased due to the down-ice surface Ekman transport (see Figure 37). The upper ocean circulation in the ice-free region is also down-ice. At hour 36, the across-ice component of the circulation (Figure 38) is nearly uniform in the off-ice direction (positive contours). Buoyancy (Figure 39) and mixed layer

depth (Figure 40) show weak disturbances indicative of upwelling at the ice edge. The mixed layer under the ice has shallowed.

The observations of Buckley et al (1979) are inconsistent with the model results since they reported ice edge upwelling during the early winter with up-ice surface winds. It is difficult to justify making the assumption that the ice surface was melting, the condition for which the model predicts upwelling. However, more recent observations in the Greenland Sea MIZ (Johannessen et al, 1983) are in strong agreement with the model results. They describe ice edge upwelling during down-ice surface wind conditions in the early fall. The months of August and September are usually when melting occurs and it is reasonable to expect the model to predict strong upwelling at the ice edge.

## IV. SUMMARY AND CONCLUSIONS

The analysis of the ocean mixing and circulation response to the prescribed wind and surface buoyancy flux forcing shows that advection, diffusion, and mixing can be successfully introduced into this coupled sea ice-ocean model. This is an important development. It indicates that the important processes of ice melting and growth, and their effects on the OPBL can be simulated to study features of the upper ocean circulation in the MIZ, such as ice edge upwelling. This step is part of a larger goal in which numerical models of important MIZ processes may be developed and used to determine the position and evolution of the ice margin.

Using a coupled sea ice-ocean general circulation mixed layer model, the two-dimensional mixing and circulation response of the upper ocean with an ice cover to prescribed wind and buoyancy forcing was simulated. With an initial buoyancy field (from observations in the MIZ) and cyclic horizontal boundary conditions, ice edge upwelling was created for a down-ice geostrophic wind and varying surface buoyancy flux forcing. The upwelling feature appeared in model solutions for both stationary and moving ice covers and is due primarily to a divergence in the oceanic surface transport. This finding is supported by observations from the Greenland Sea MIZ in the early fall of 1979 (during NORSEX) as reported by Johannessen et al (1983). In the case of ice melting (downward surface buoyancy flux imposed), the upwelling is enhanced by mixed layer shallowing caused by the influx into the upper ocean of fresh meltwater

and an associated stabilizing effect on the layer. For an upward surface buoyancy flux caused by freezing, the mixed layer deepens and the upwelling is reduced somewhat.

The relationship between mixing processes and the wind-forced circulation of the upper ocean is particularly important in the case of an up-ice wind. This is clearly demonstrated in the numerical experiments in which both stationary and moving ice covers are employed and the forcing is varied. Here, the combined effect of the wind forcing and ice motion causes weak downwelling at the ice edge and the downward surface buoyancy flux drives weak upwelling nearby. This interaction between the effects of thermodynamics-mixing, wind stirring, and ice motion may, therefore, be an important mechanism for the generation of ice edge upwelling. Under similar wind conditions, observations in the MIZ north of Svalbard of ice edge upwelling were reported by Buckley et al (1979).

In the case of on-ice geostrophic wind forcing with a nonstationary ice cover, the imposition of a downward surface buoyancy flux caused a weak upwelling at the ice edge. Similarly, for an off-ice wind, the model solutions indicated no upwelling or downwelling.

Further study is required in this area. While the present sea ice model does a good job of calculating the ice-ocean interfacial stress using a Rossby-similarity approach, given the components of the geostrophic wind (relative to the axis system oriented to the ice edge), several important ice effects have been neglected (e.g., internal ice stress and ice concentration). A more complete sea ice model could be developed and coupled with the ocean model to produce more realistic ocean responses.

The ocean model should be tested with dual thermodynamic variables (temperature and salinity) and not just buoyancy.

Finally, the model results should be tested in the field by experiments such as those planned during MIZEX. Observations of the upper ocean properties near the ice edge and documenting of the conditions under which upwelling or downwelling occur will aid in the development of better models. Thermodynamic and mixing processes are important modifiers of the upper ocean circulation in the MIZ, and should be included in the future modeling of MIZ processes.

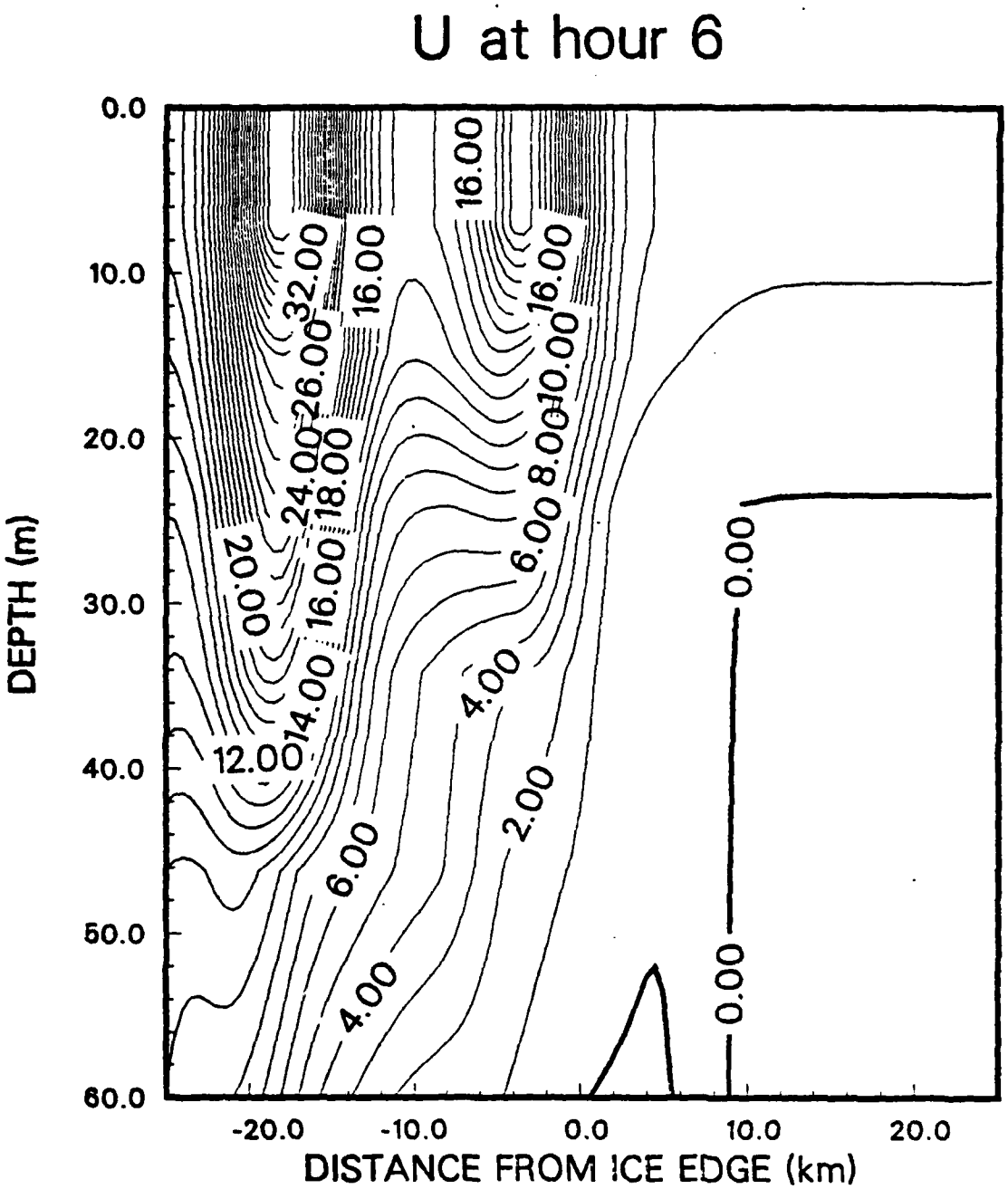


Figure 5. Case IA - Along Edge Velocity (U) at Hour 6. The units of velocity are cm/sec and the contouring interal is 1.0 cm/sec.

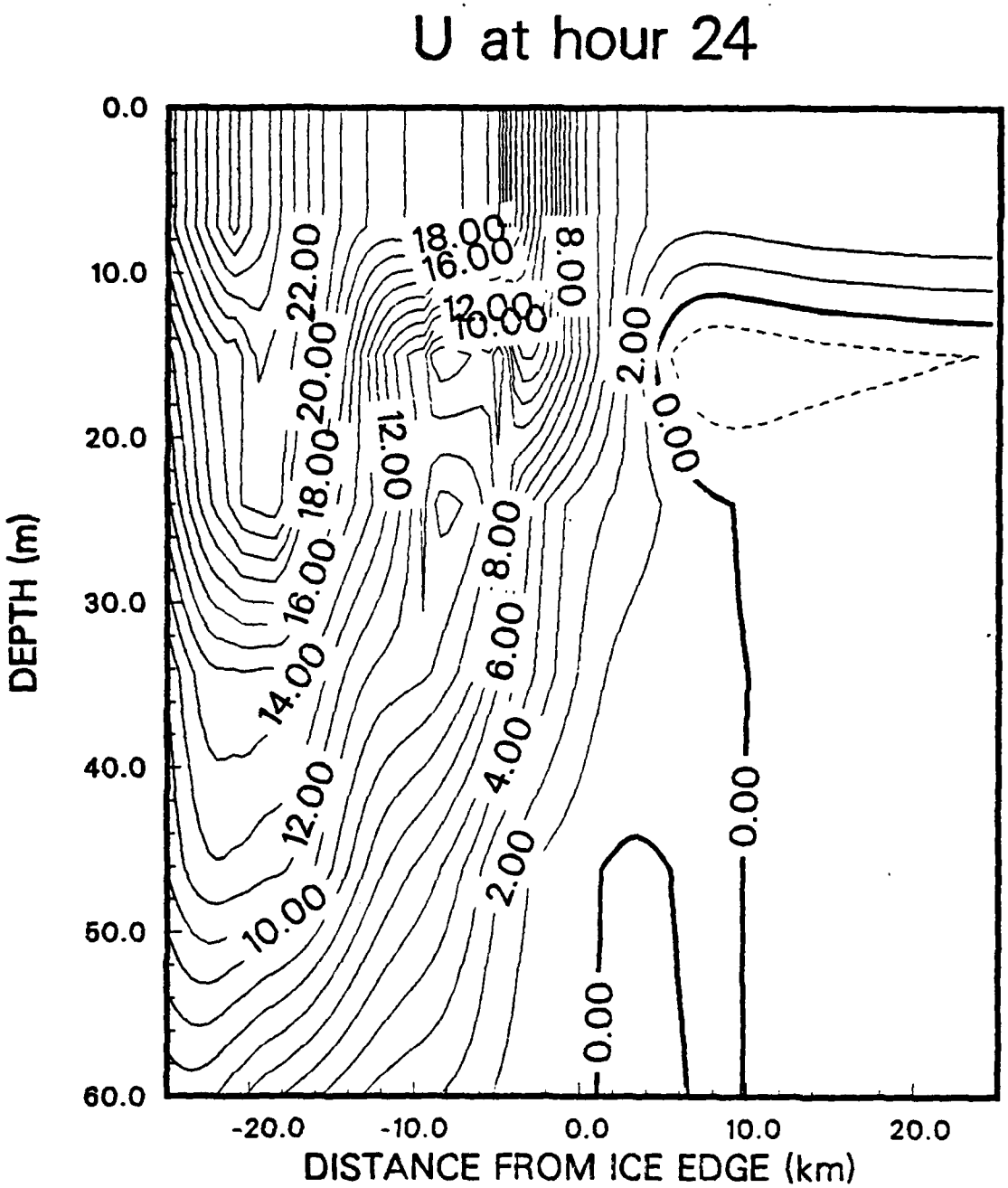


Figure 6. Case IA - Along Edge Velocity (U) at Hour 24. The units of velocity are cm/sec and the contouring interval is 1.0 cm/sec.

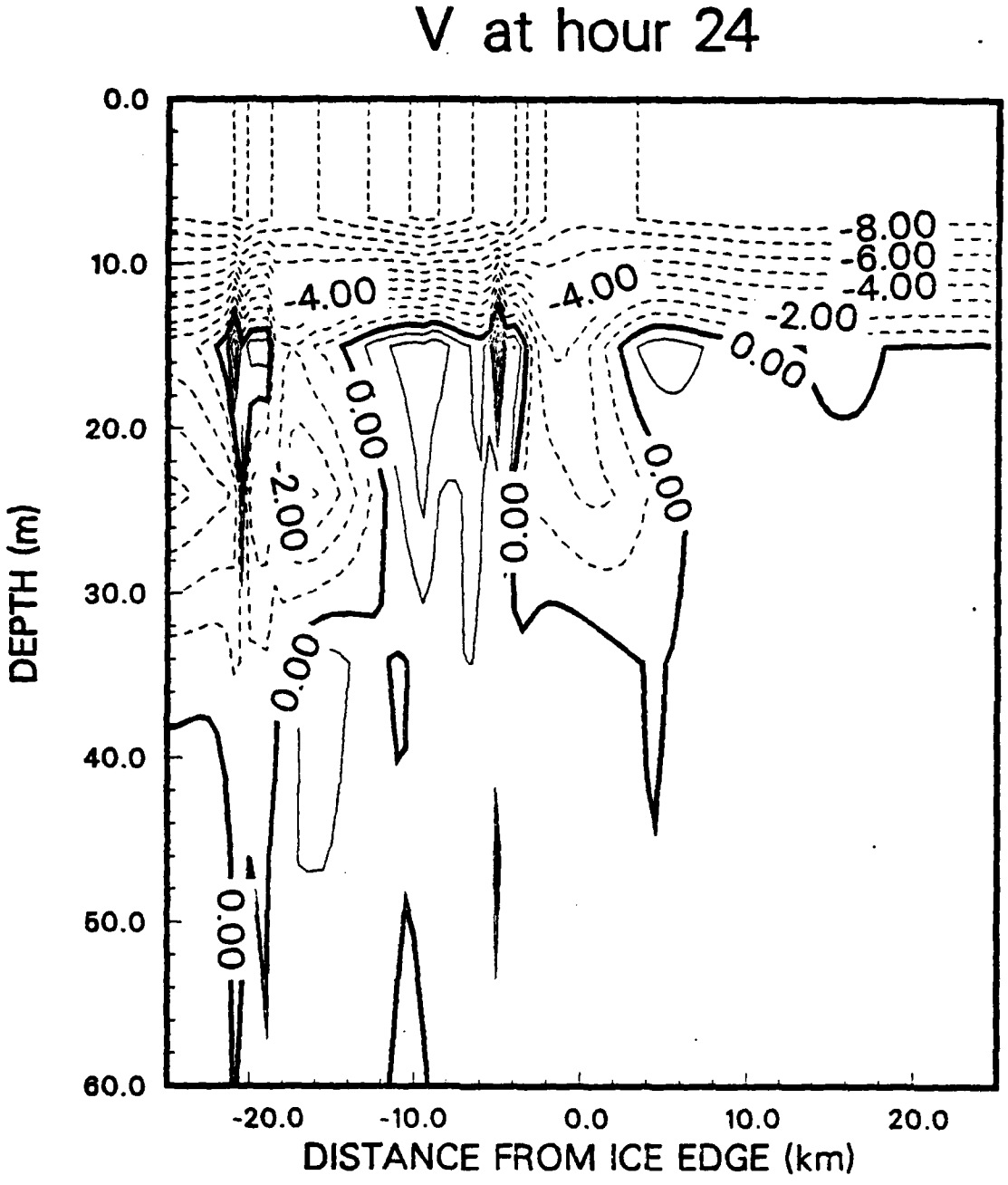


Figure 7. Case IA - Across Edge Velocity (V) at Hour 24. The units of velocity are cm/sec and the contouring interval is 1.0 cm/sec.

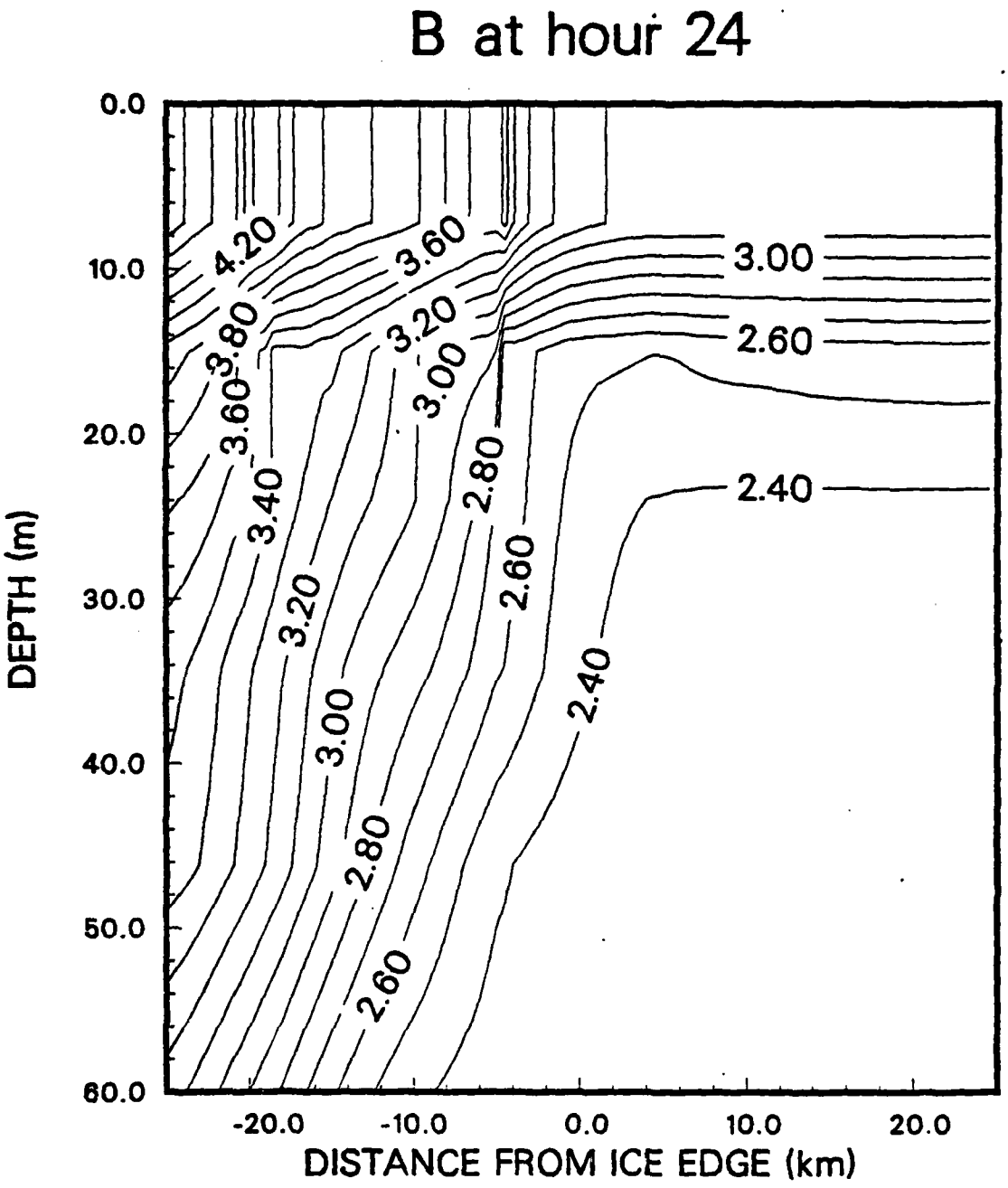


Figure 8. Case IA - Buoyancy (B) at Hour 24. The units of buoyancy are $cm/sec^2$ and the contouring interval is 0.1 $cm/sec^2$.

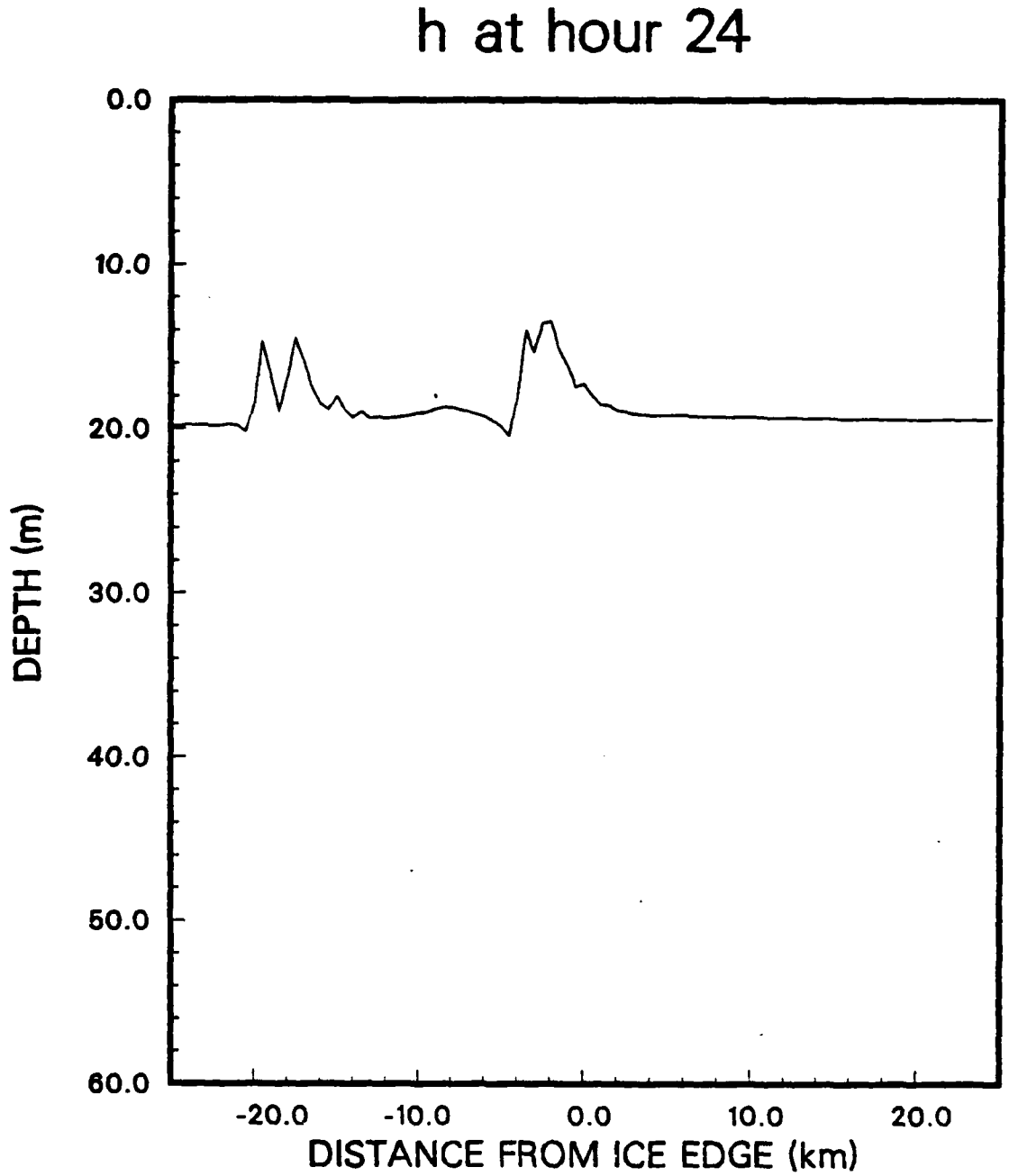


Figure 9. Case IA - Mixed Layer Depth (h) at Hour 24.

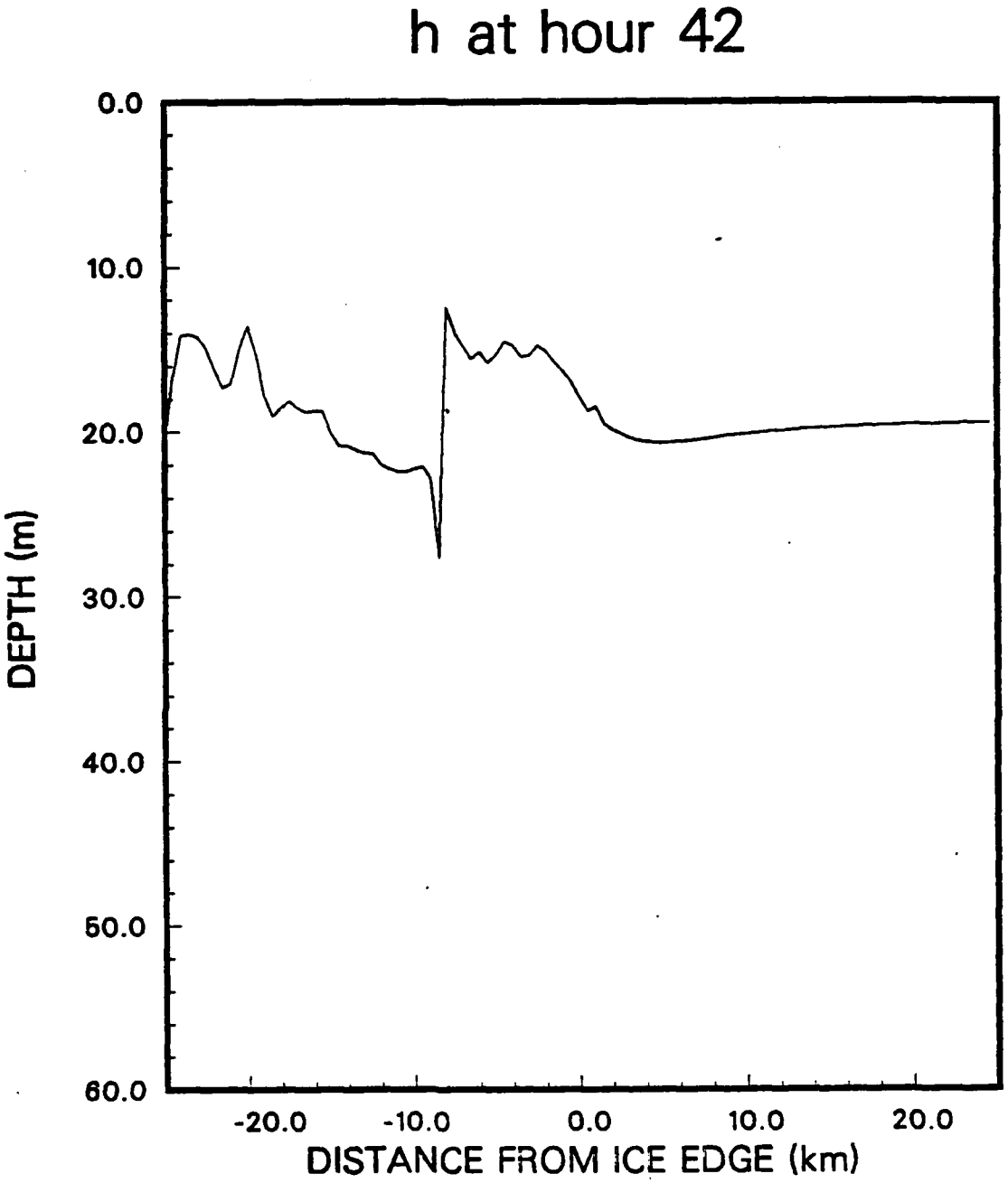


Figure 10. Case IA - Mixed Layer Depth (h) at Hour 42.

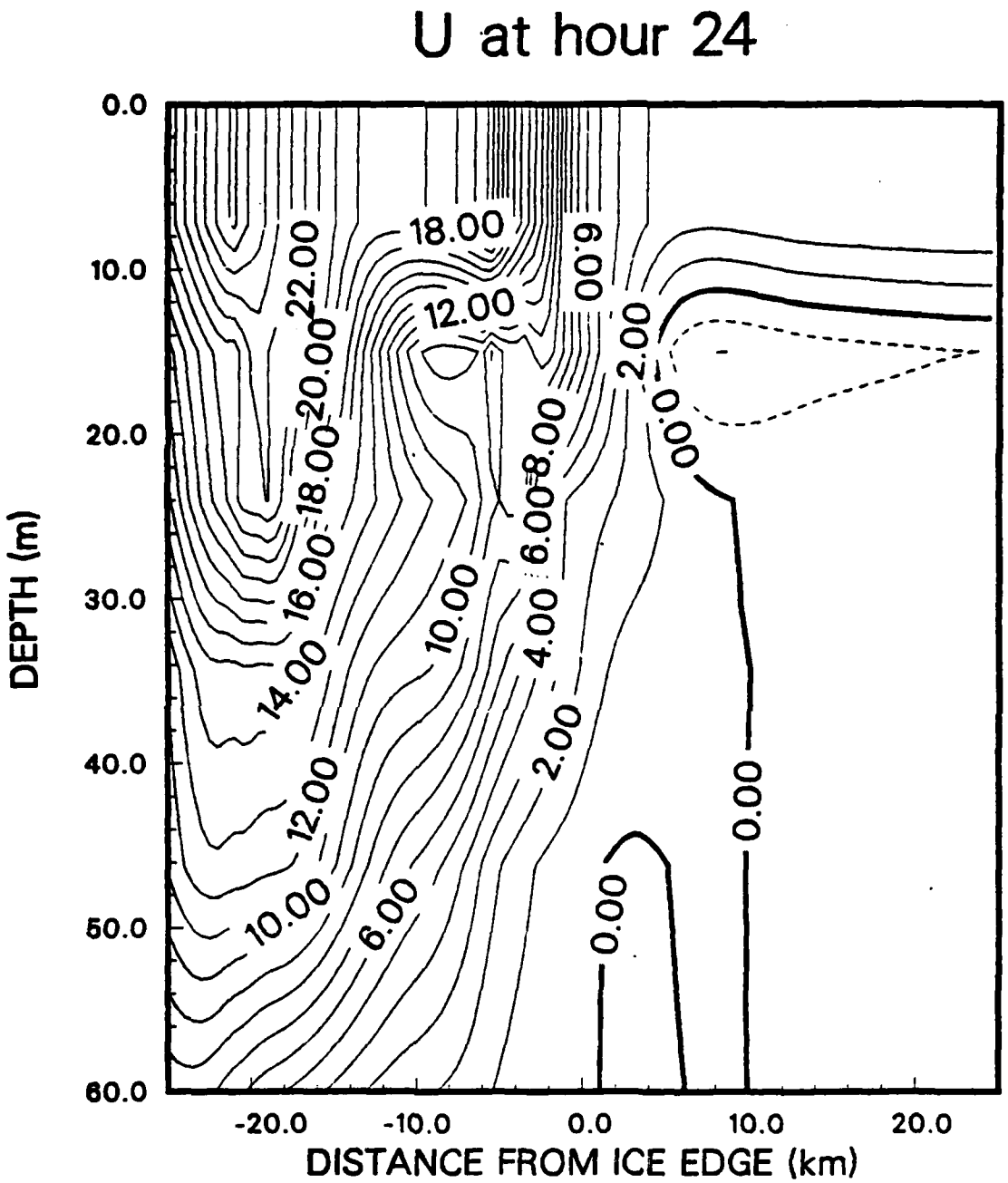


Figure 11. Case IB - Along Edge Velocity (U) at Hour 24. The units of velocity are cm/sec and the contouring interval is 1.0 cm/sec.

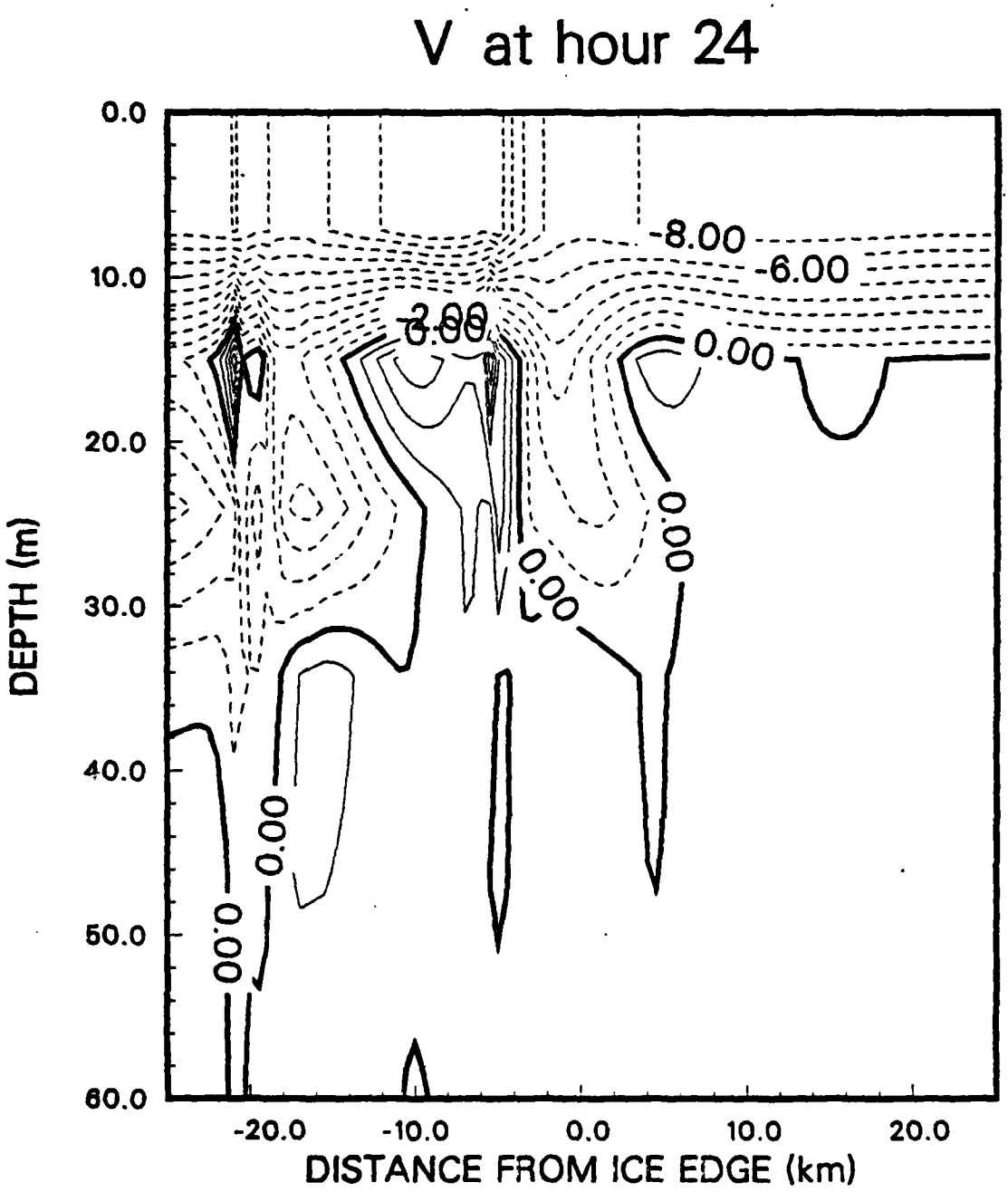


Figure 12. Case IB - Across Edge Velocity (V) at Hour 24. The units of velocity are cm/sec and the contouring interval is 1.0 cm/sec.

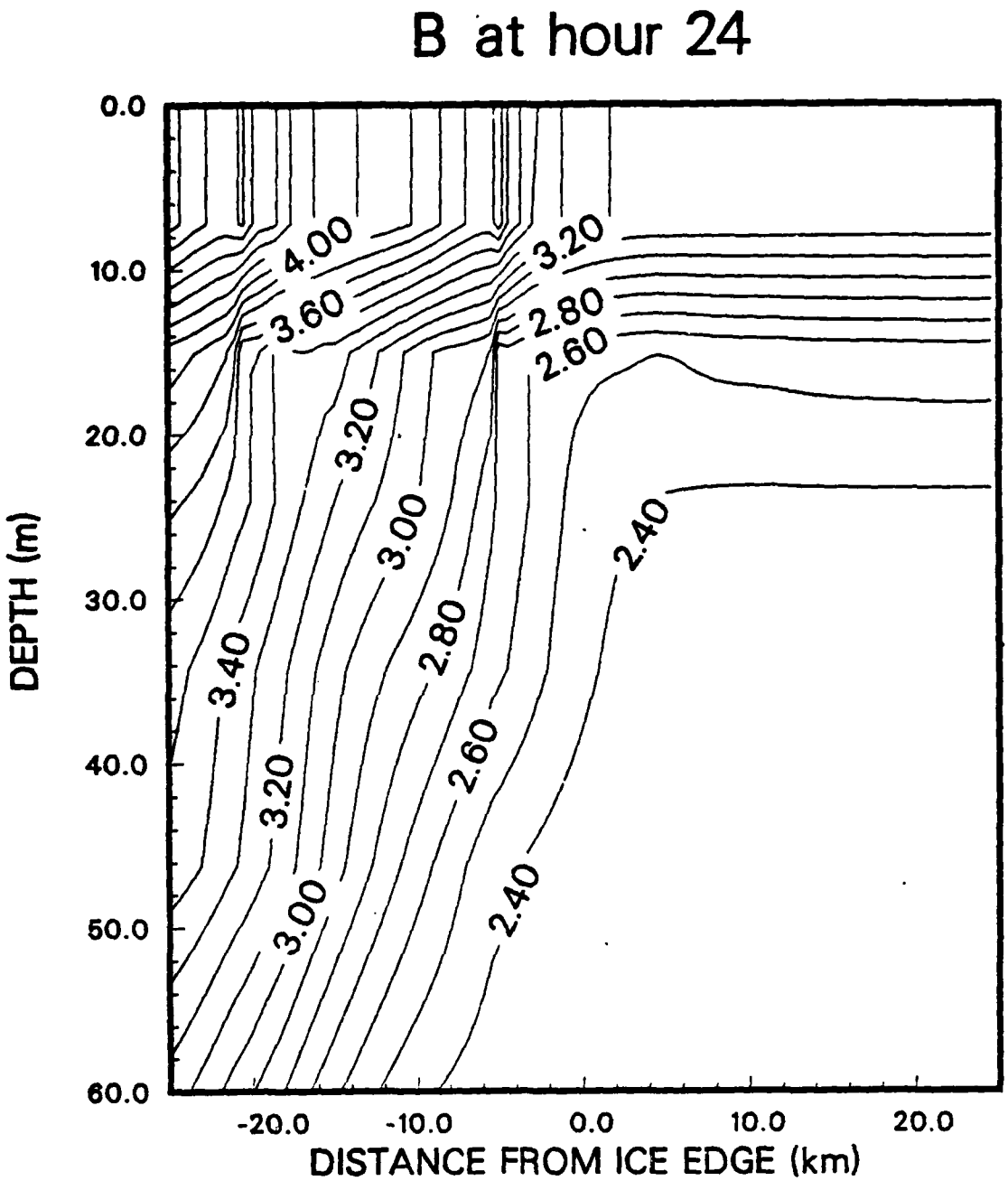


Figure 13. Case IB - Buoyancy (B) at Hour 24. The units of buoyancy are cm/sec$^2$ and the contouring interval is 0.1 cm/sec$^2$.

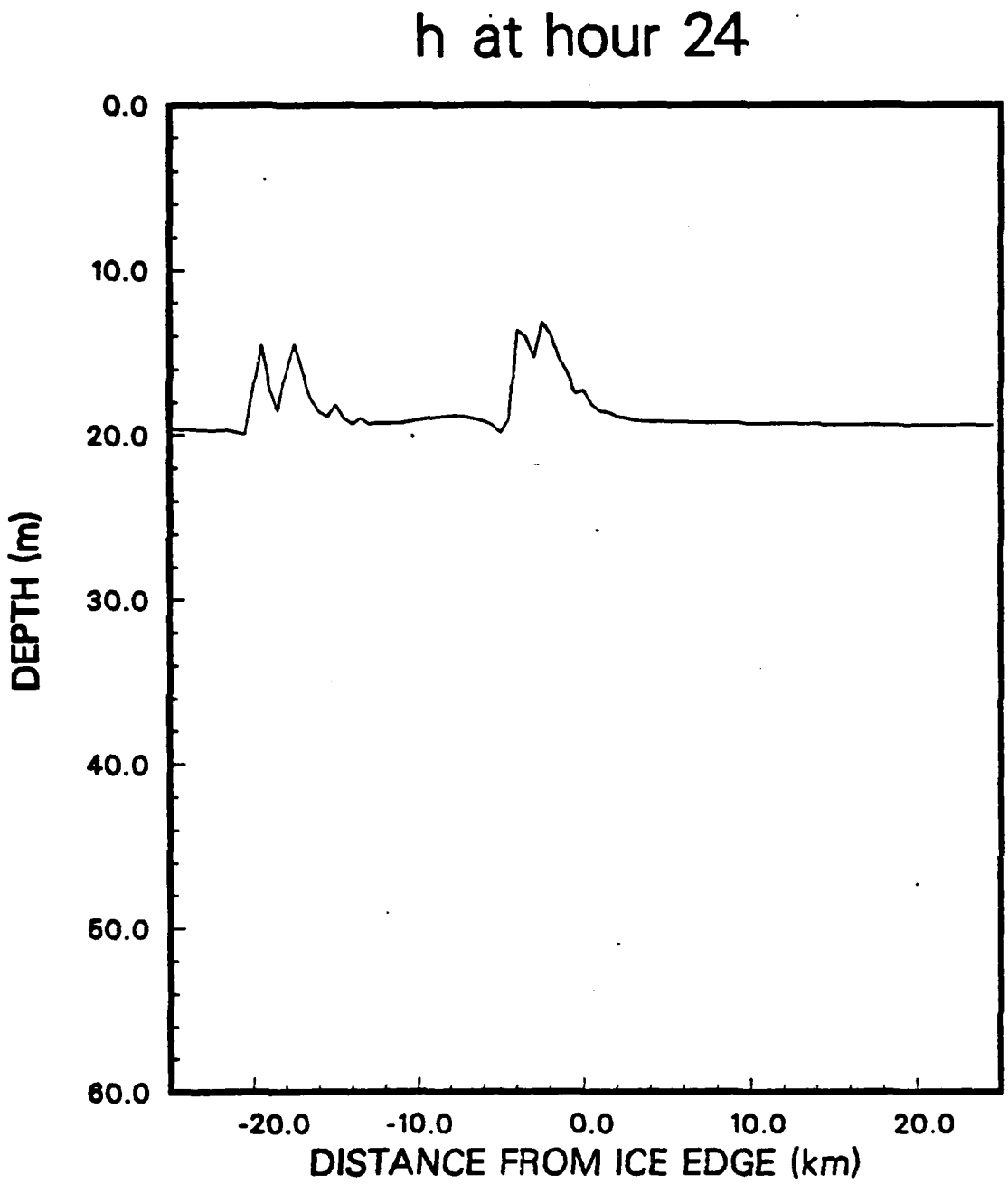


Figure 14. Case IB - Mixed Layer Depth (h) at Hour 24.

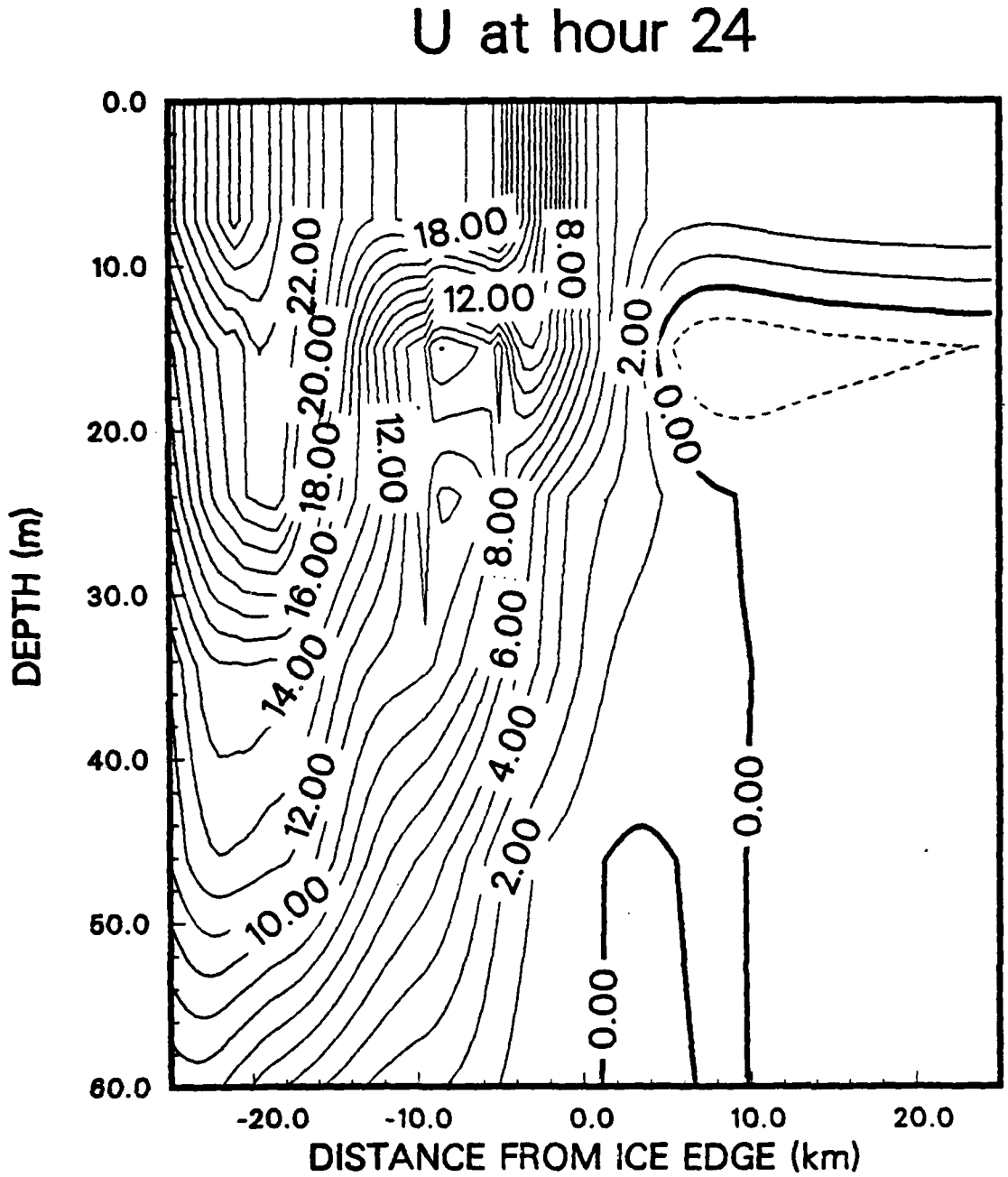


Figure 15. Case IC - Along Edge Velocity (U) at Hour 24. The units of velocity are cm/sec and the contouring interval is 1.0 cm/sec.

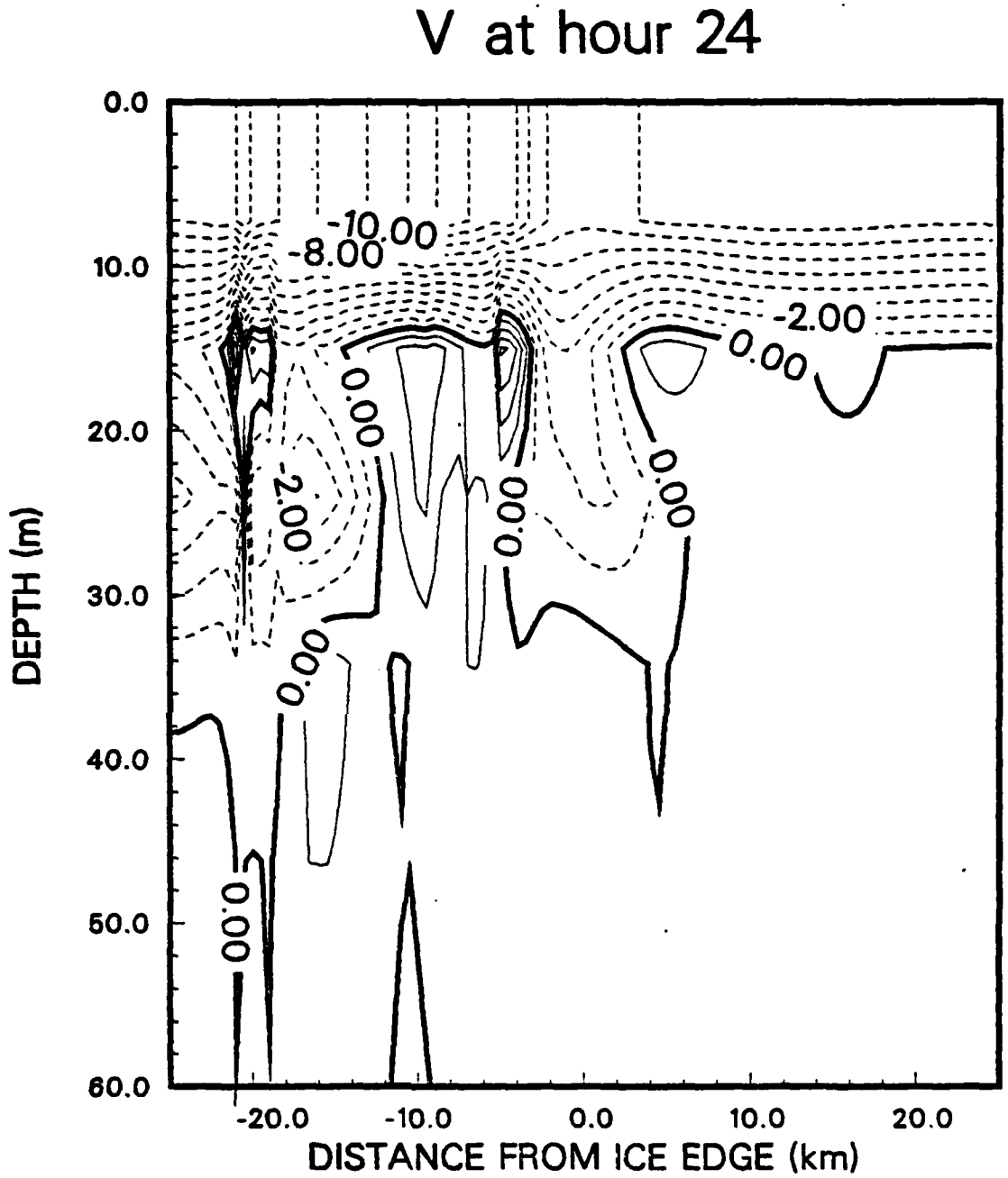


Figure 16. Case IC - Across Edge Velocity (V) at Hour 24. The units of velocity are cm/sec and the contouring interval is 1.0 cm/sec.

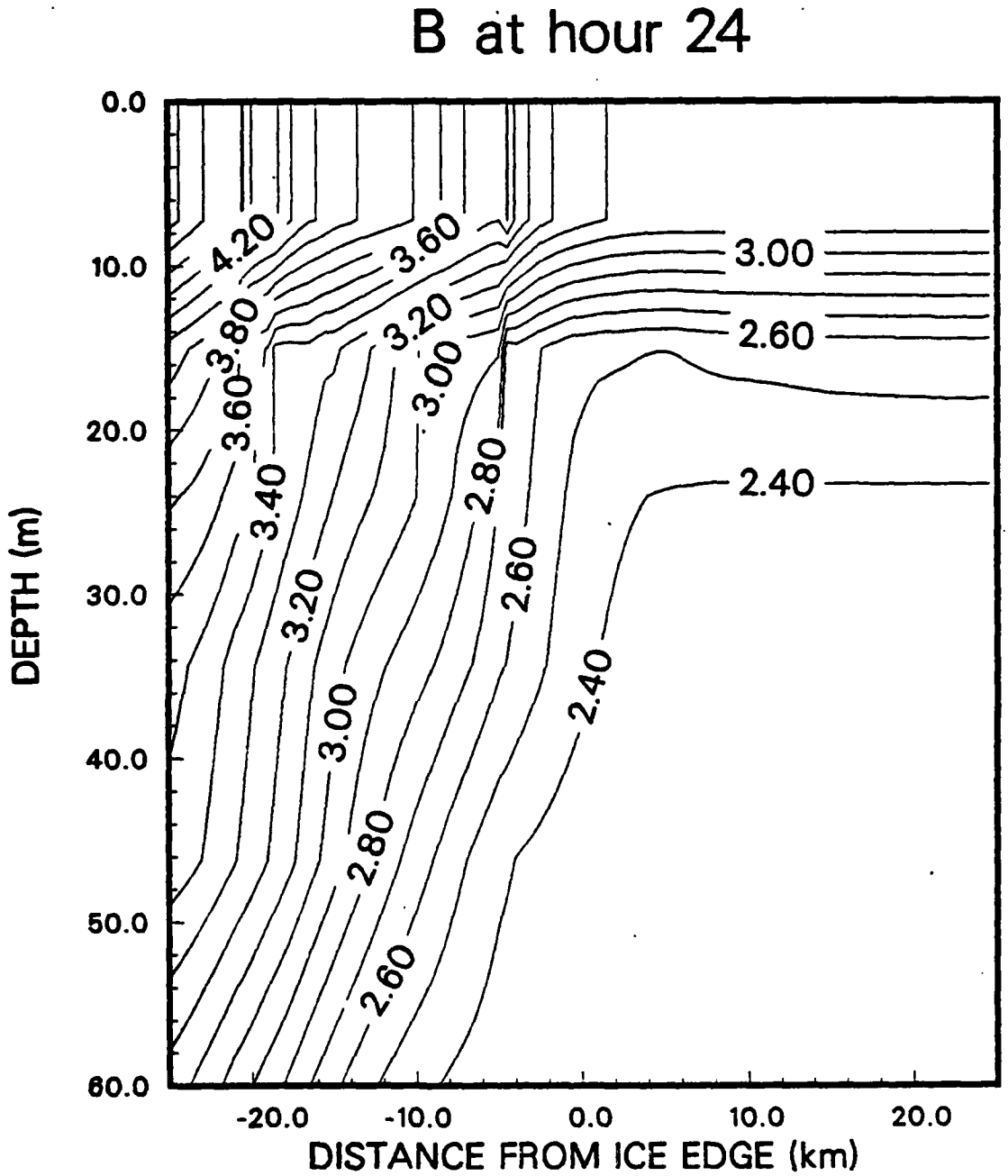


Figure 17. Case IC - Buoyancy (B) at Hour 24. The units of buoyancy are $cm/sec^2$ and the contouring interval is 0.1 $cm/sec^2$.

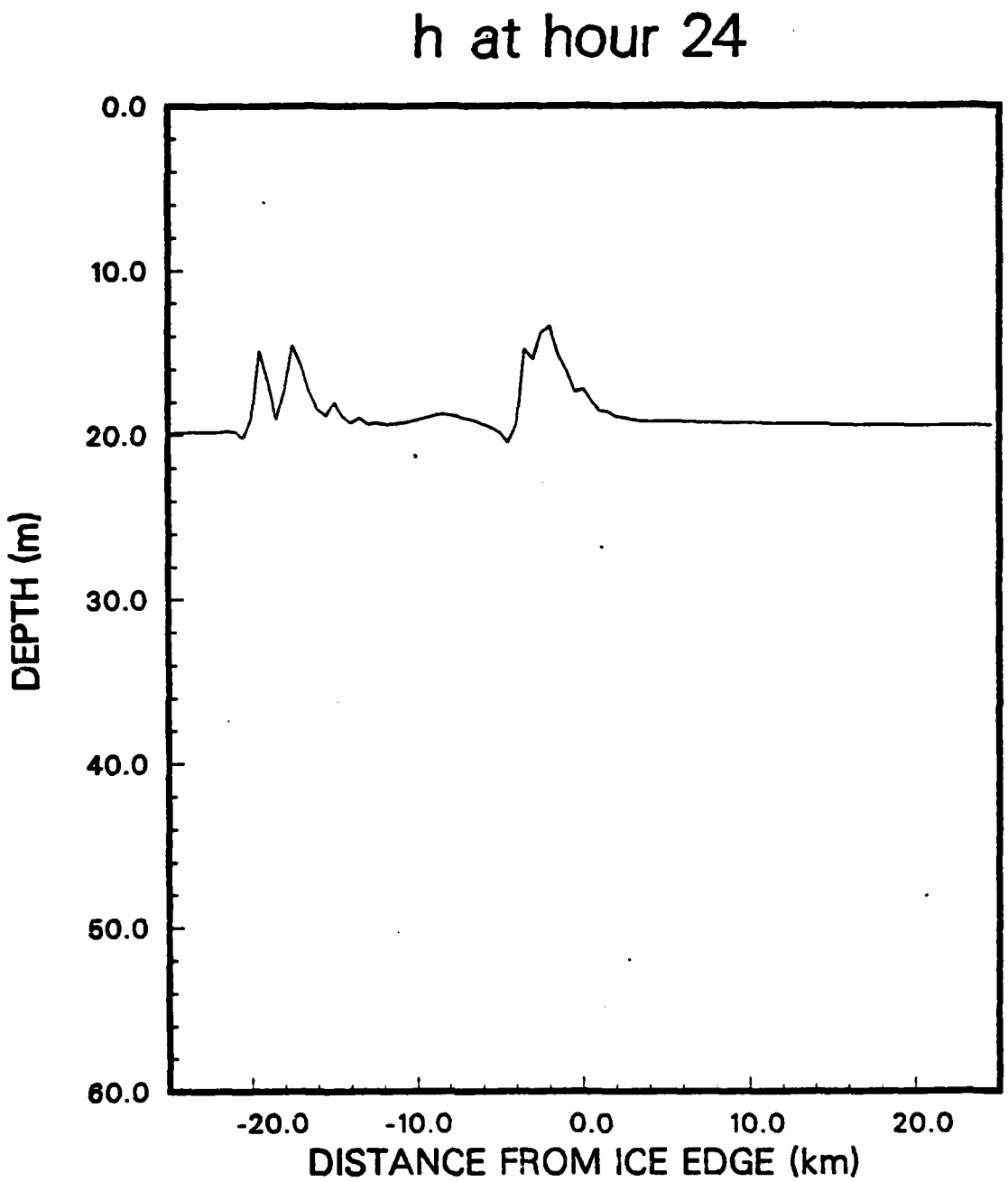


Figure 18. Case IC - Mixed Layer Depth (h) at Hour 24.

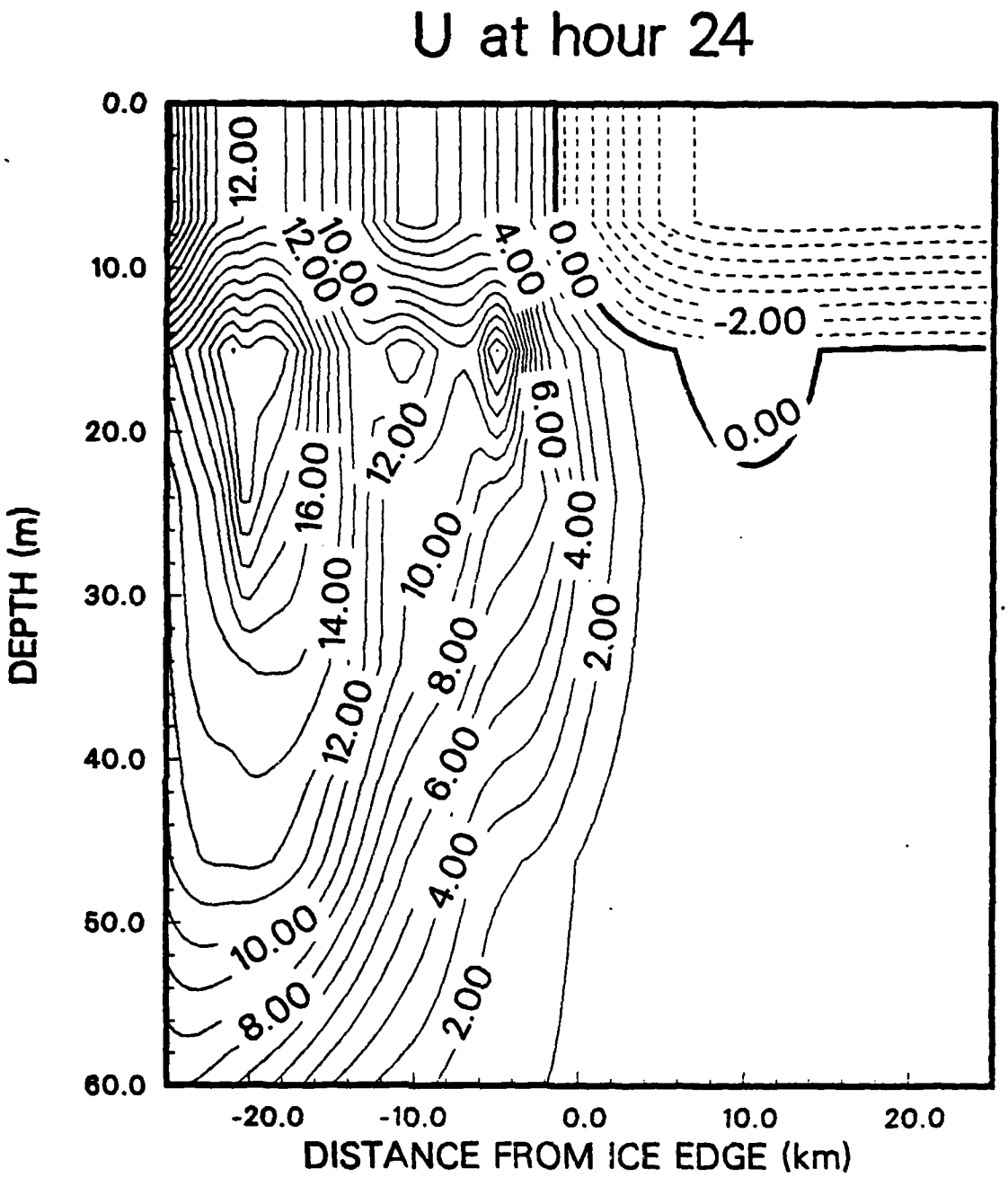


Figure 19. Case IIB - Along Edge Velocity (U) at Hour 24. The units of velocity are cm/sec and the contouring interval is 1.0 cm/sec.

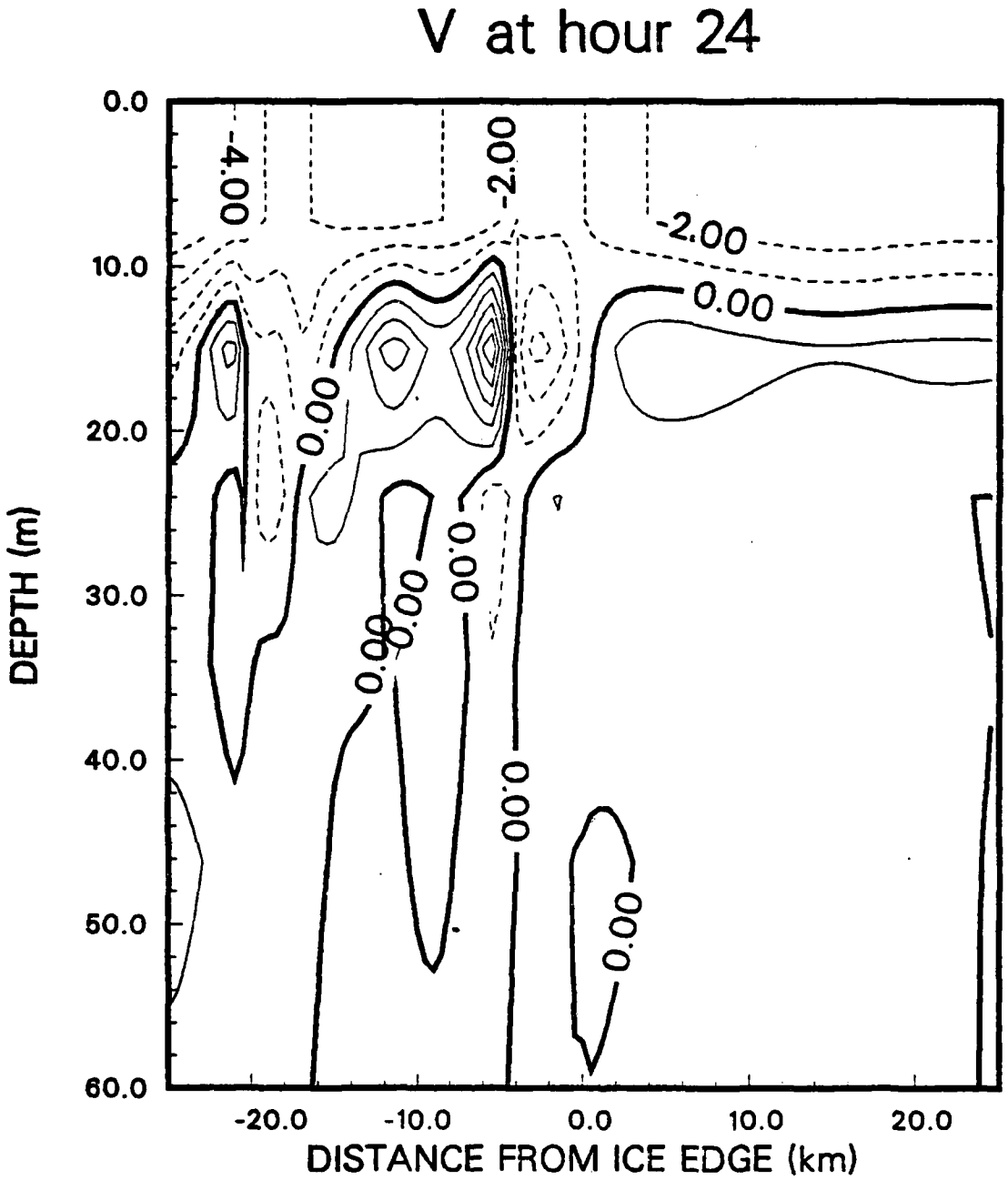


Figure 20. Case IIB - Across Edge Velocity (V) at Hour 24. The units of velocity are cm/sec and the contouring interval is 1.0 cm/sec.

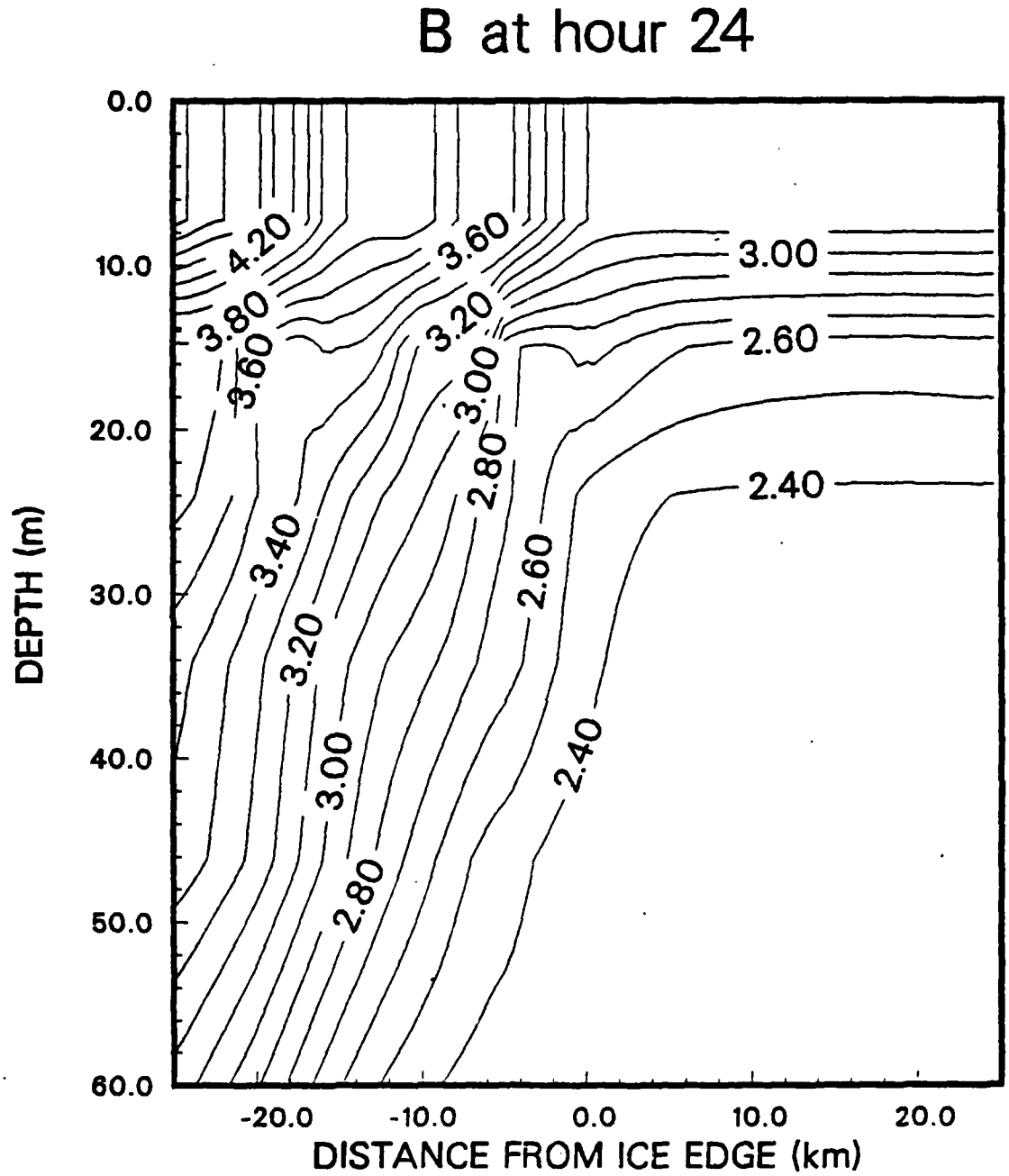


Figure 21. Case IIB - Buoyancy (B) at Hour 24. The units of buoyancy are $cm/sec^2$ and the contouring interval is 0.1 $cm/sec^2$.

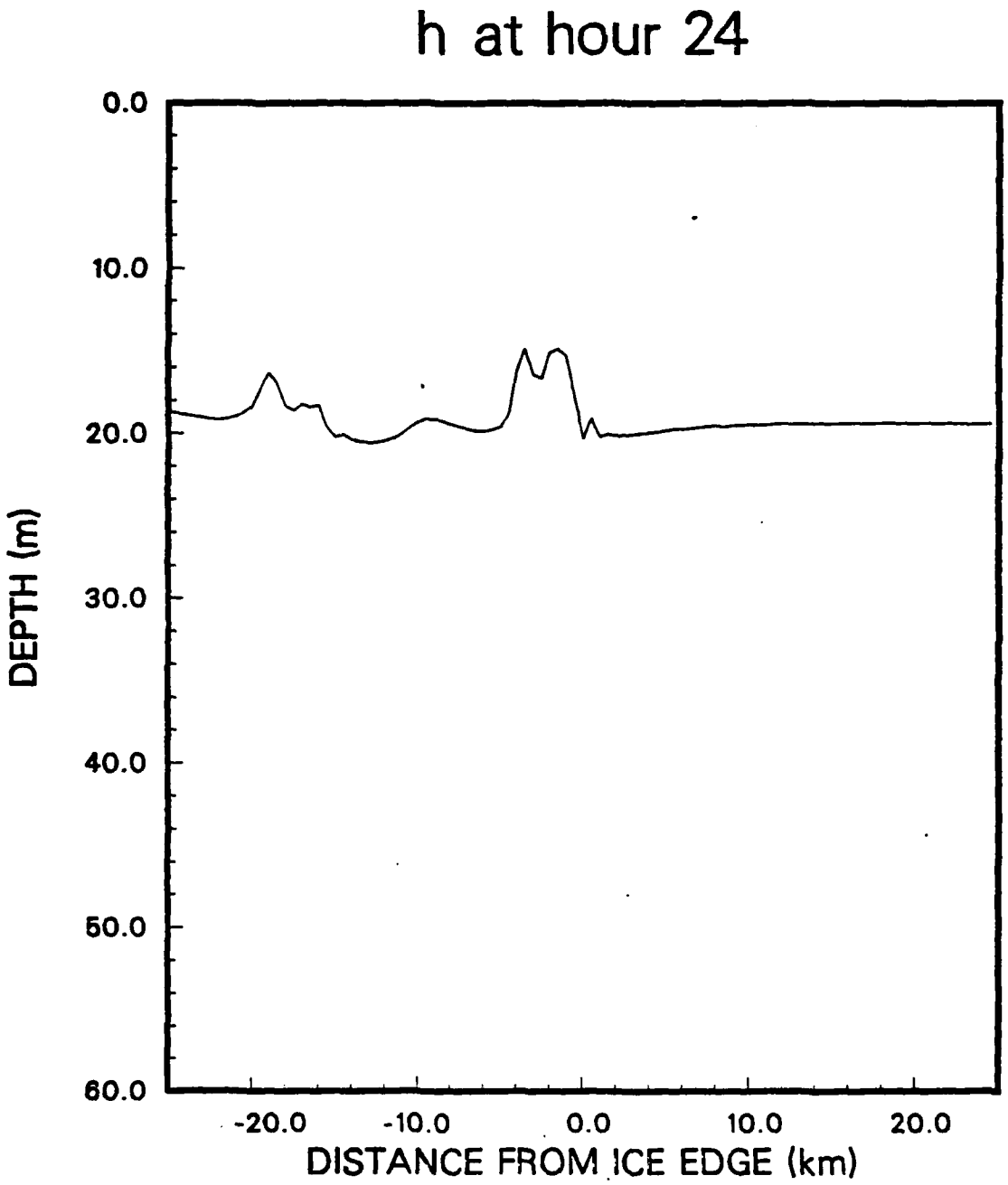


Figure 22. Case IIB - Mixed Layer Depth (h) at Hour 24.

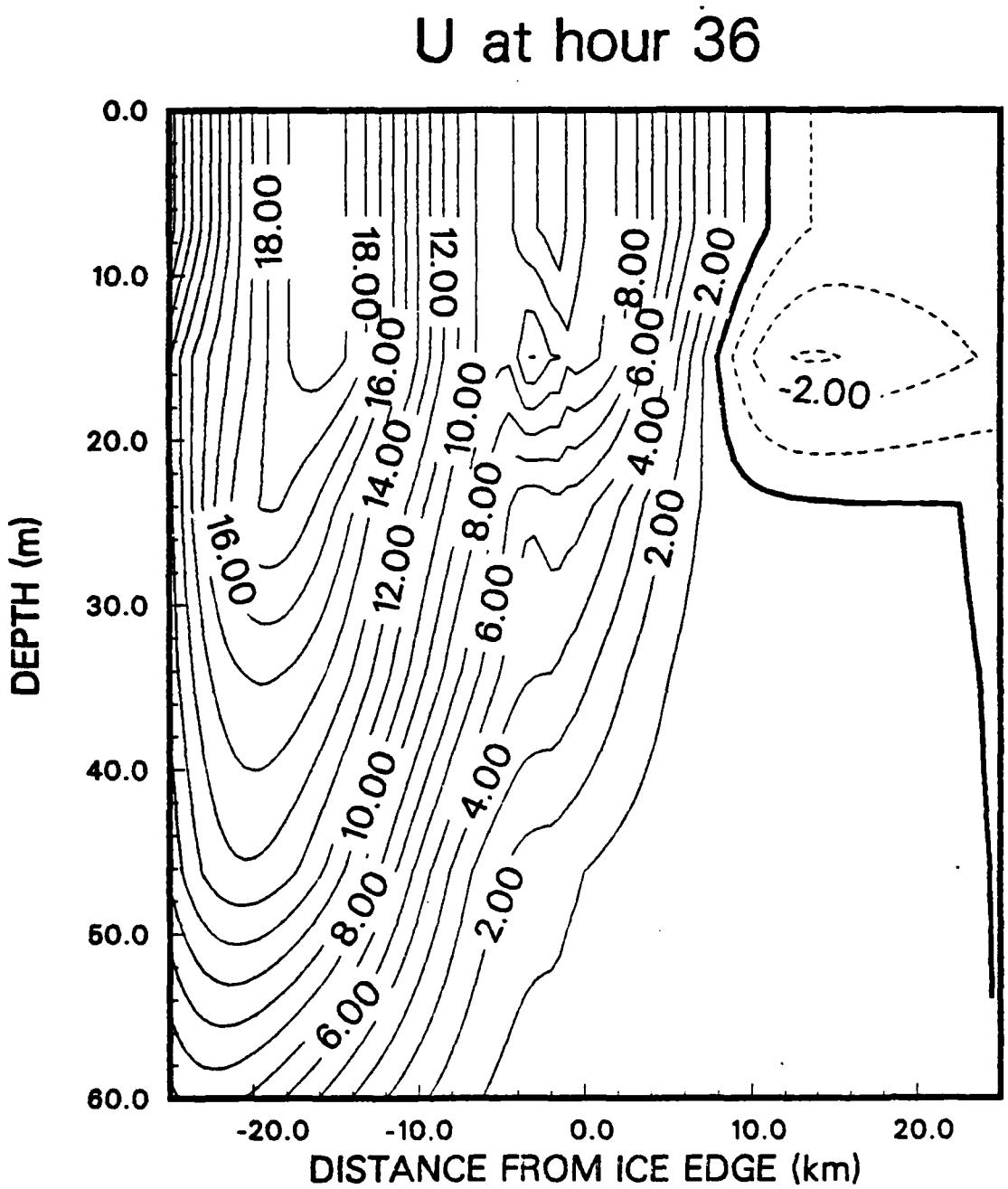


Figure 23. Case IIC - Along Edge Velocity (U) at Hour 36. The units of velocity are cm/sec and the contouring interval is 1.0 cm/sec.

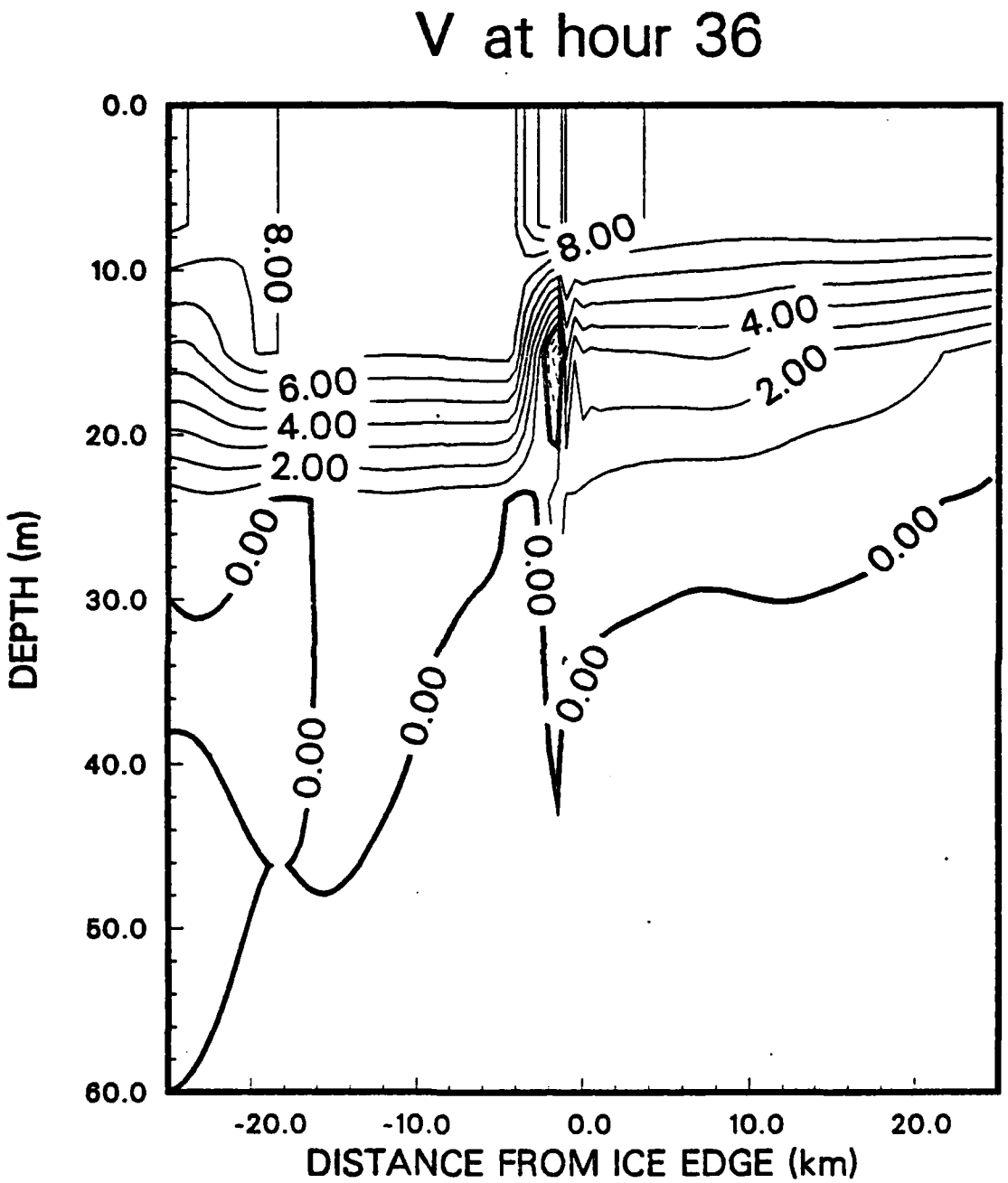


Figure 24. Case IIC - Across Edge Velocity (V) at Hour 36. The units of velocity are cm/sec and the contouring interval is 1.0 cm/sec.

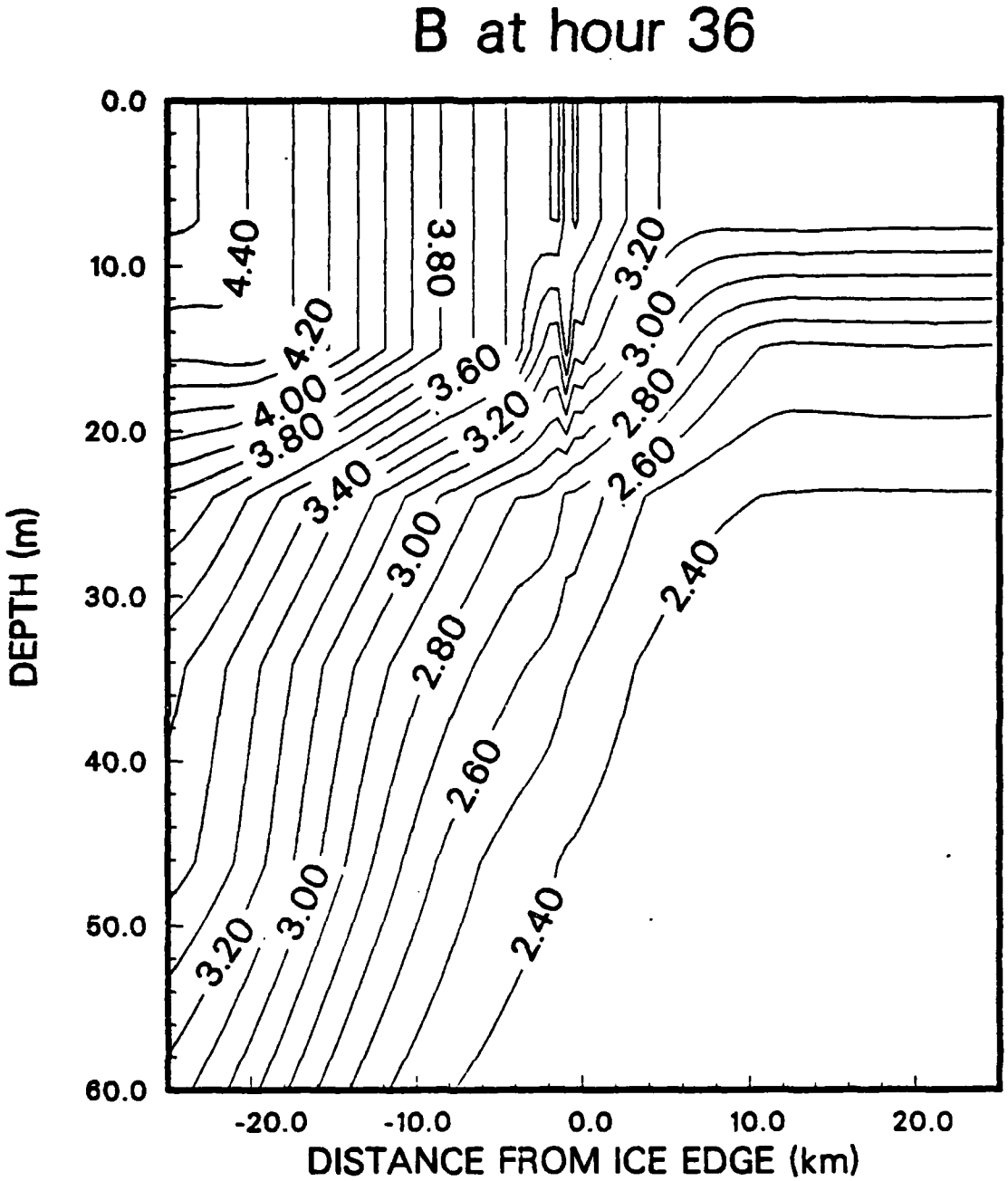


Figure 25. Case IIC - Buoyancy (B) at Hour 36. The units of buoyancy are cm/sec$^2$ and the contouring interval is 0.1 cm/sec$^2$.

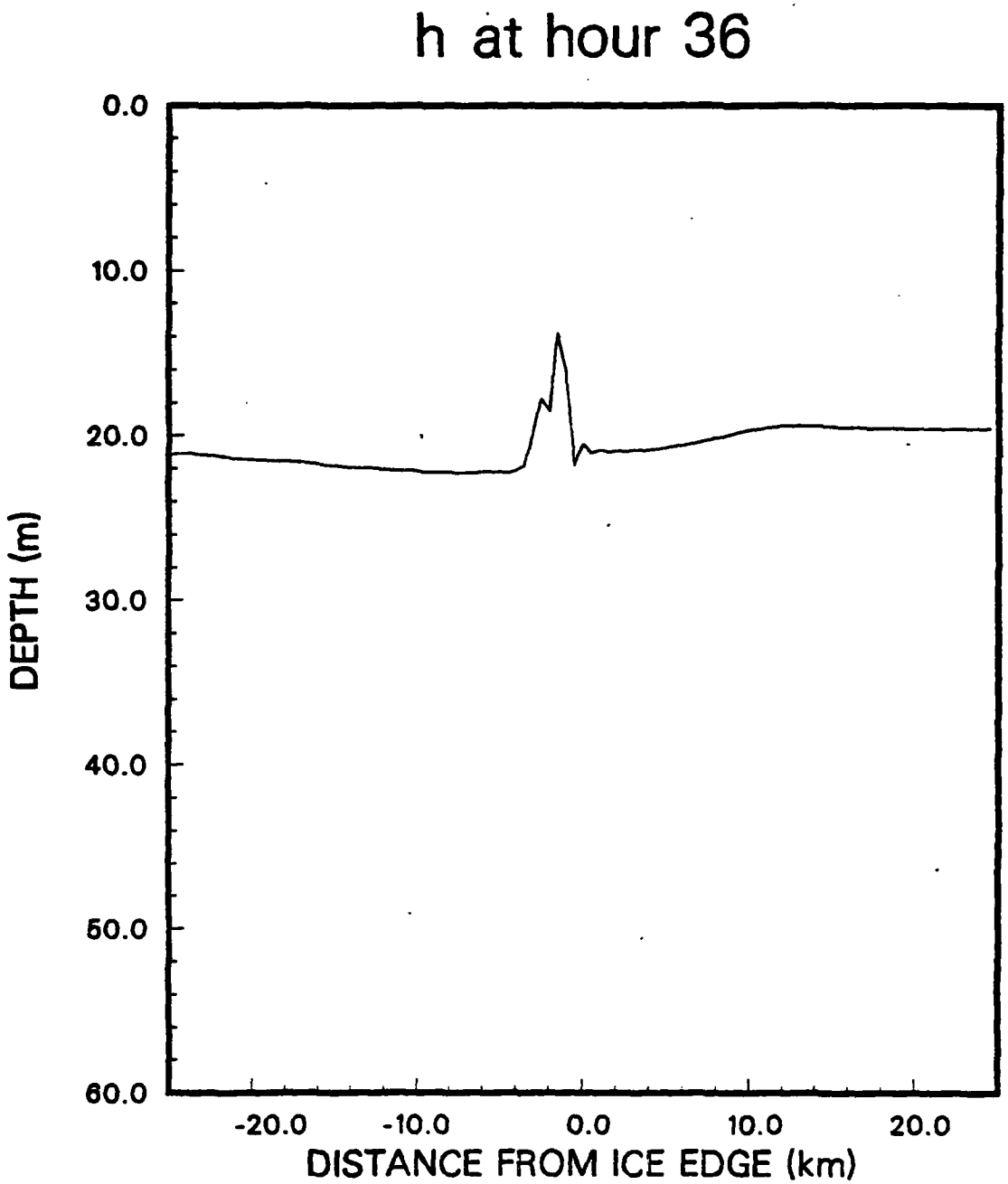


Figure 26. Case IIC - Mixed Layer Depth (h) at Hour 36.

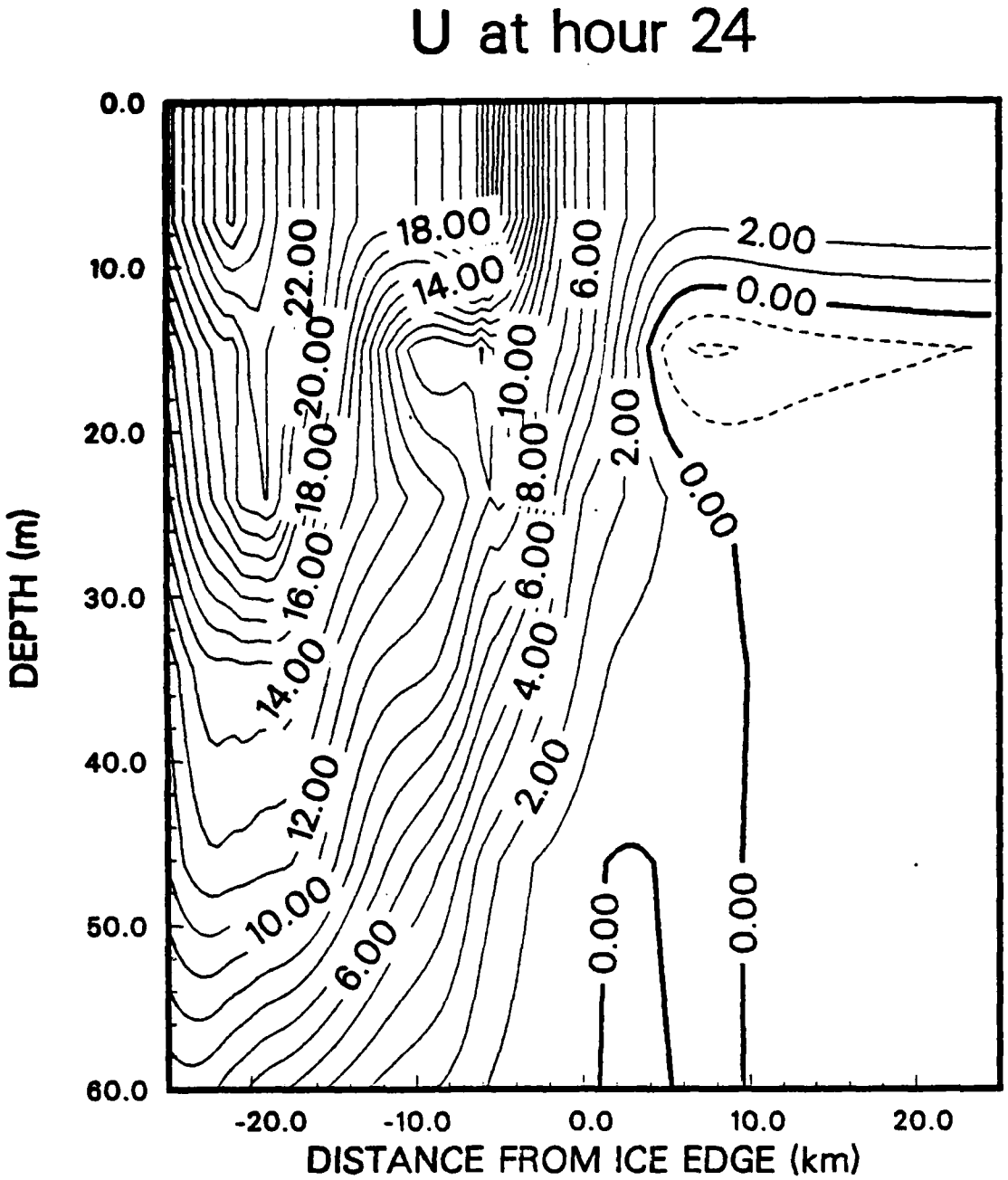


Figure 27. Case IIIA - Along Edge Velocity (U) at Hour 24. The units of velocity are cm/sec and the contouring interval is 1.0 cm/sec.

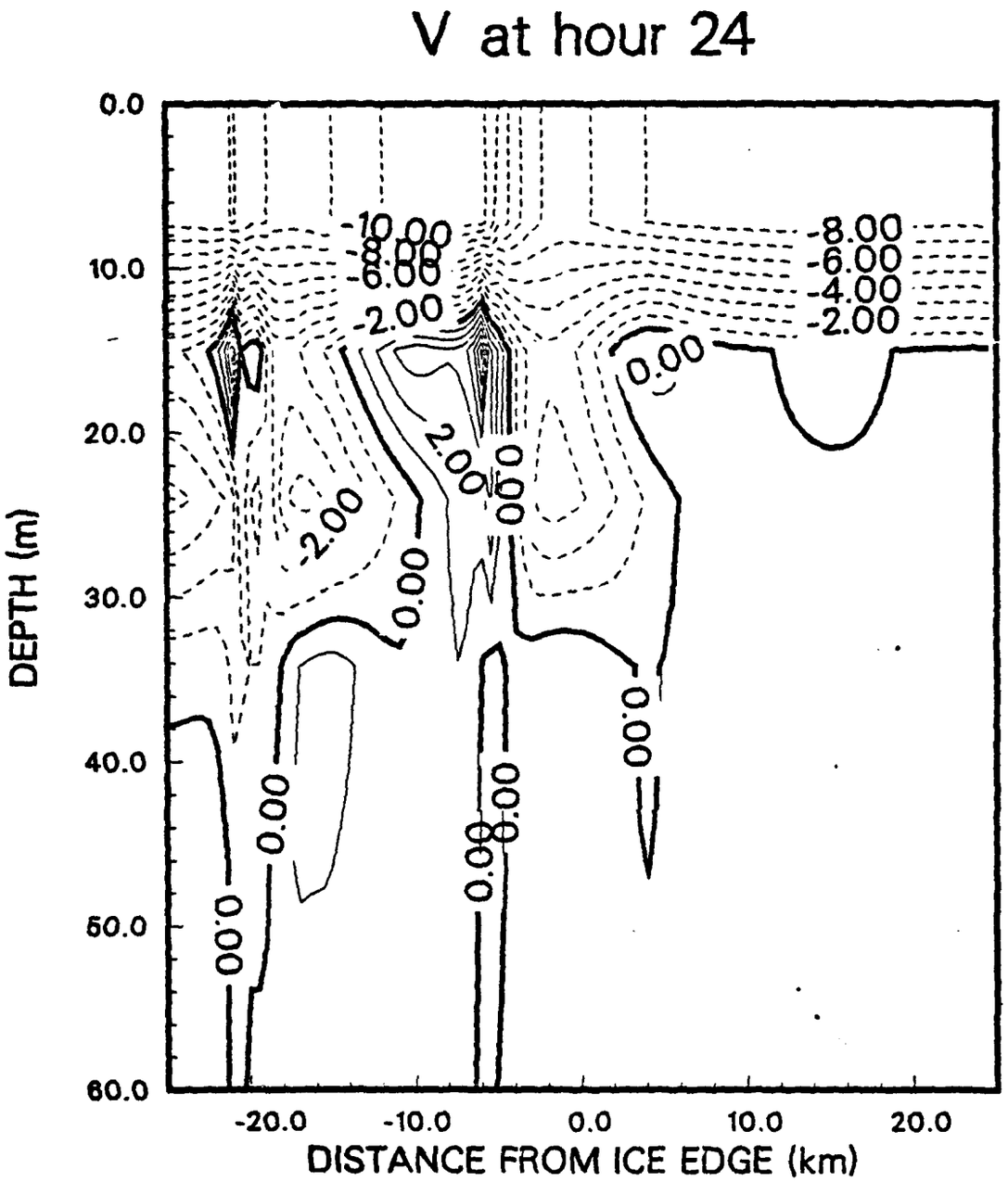


Figure 28. Case IIIA - Across Edge Velocity (V) at Hour 24. The units of velocity are cm/sec and the contouring interval is 1.0 cm/sec.

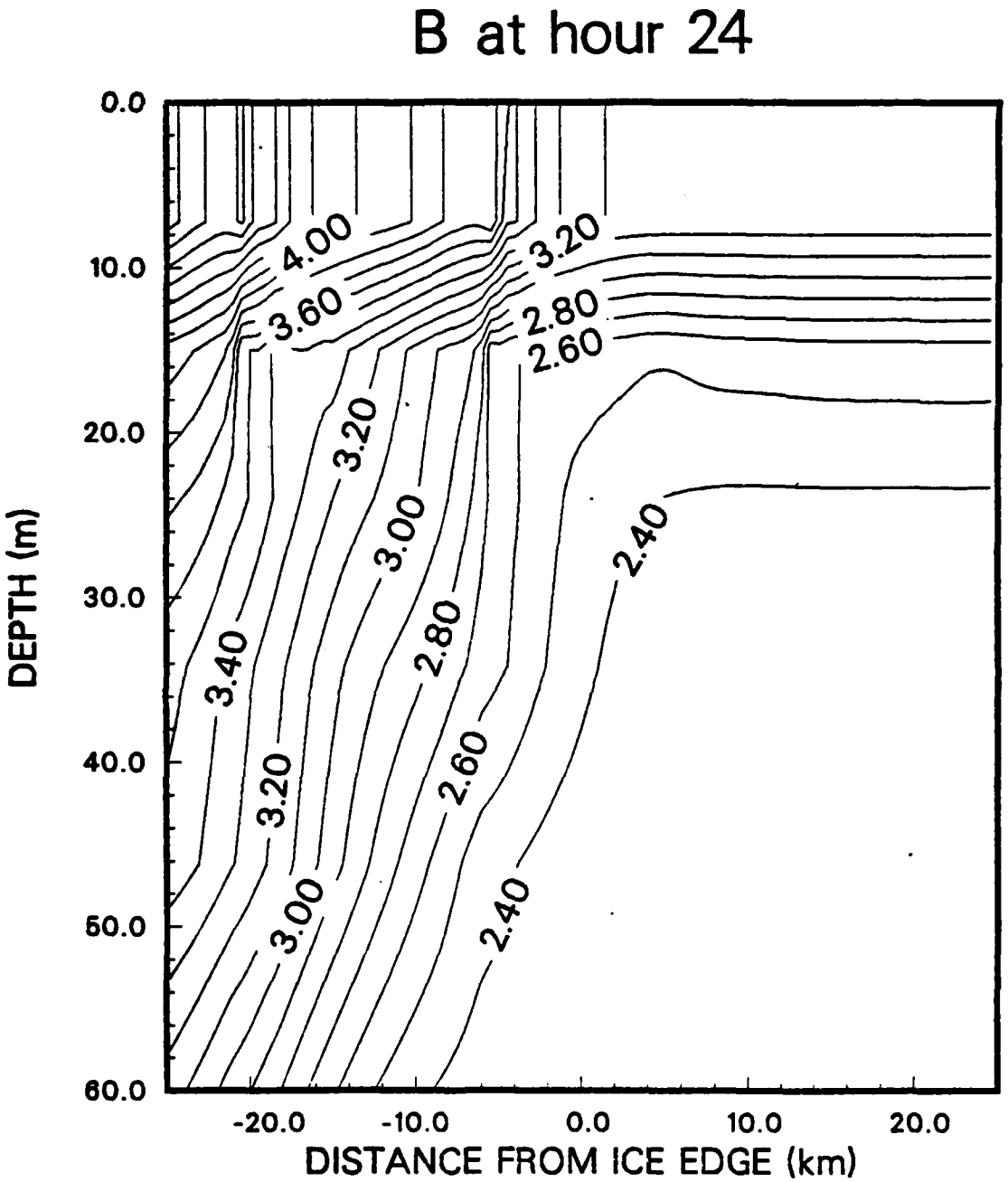


Figure 29. Case IIIA - Buoyancy (B) at Hour 24. The units of buoyancy are $cm/sec^2$ and the contouring interval is 0.1 $cm/sec^2$.

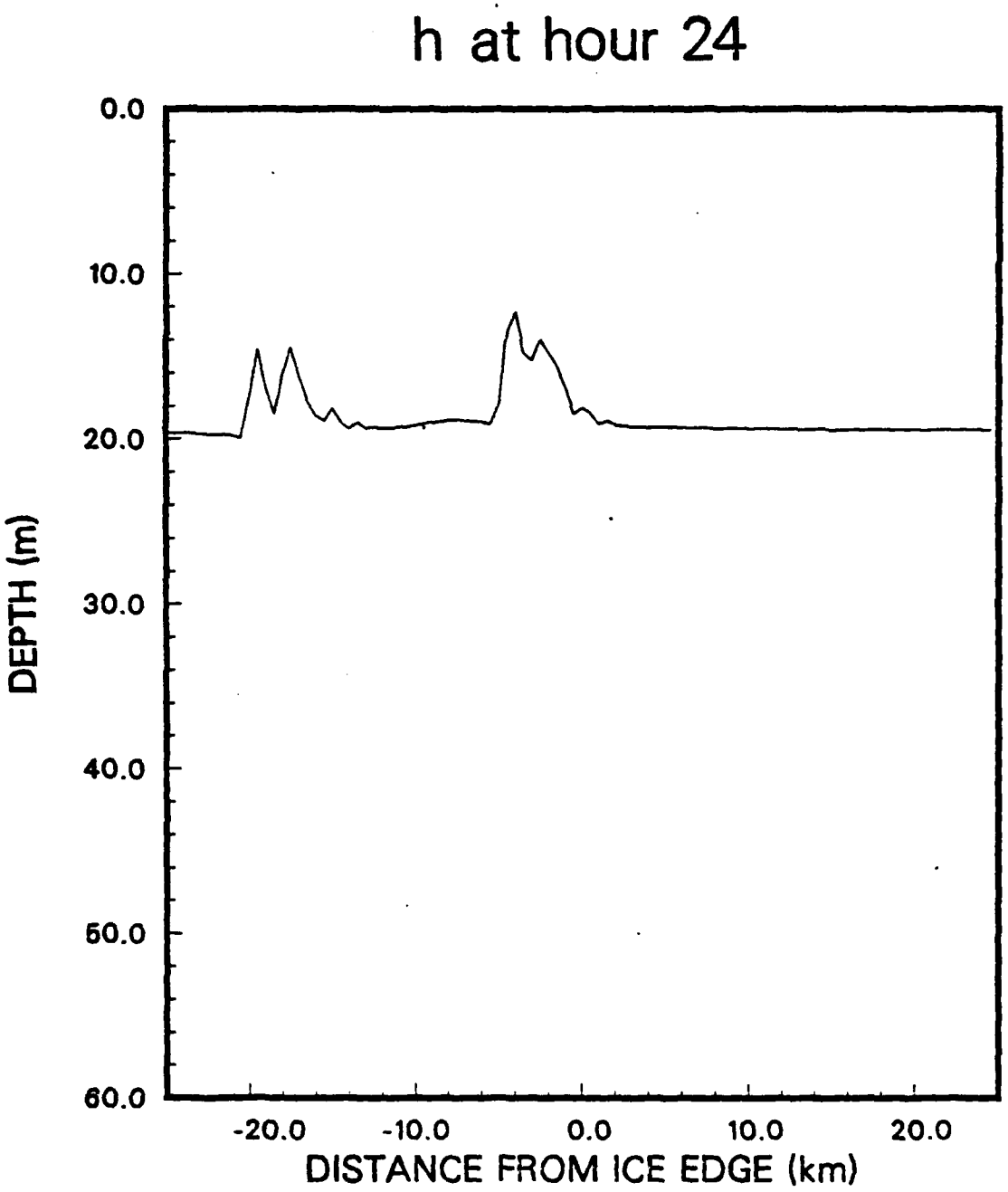


Figure 30. Case IIIA - Mixed Layer Depth (h) at Hour 24.

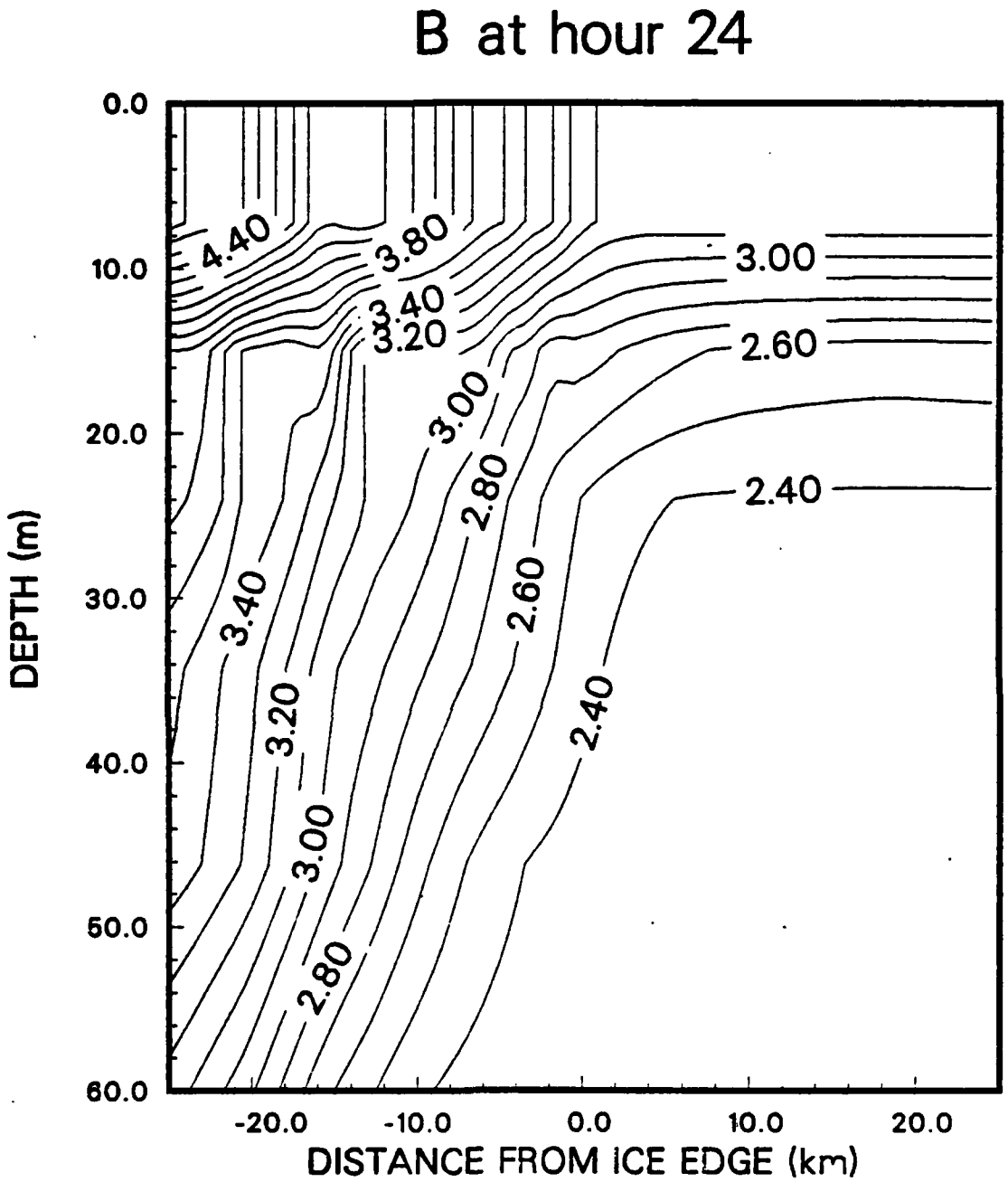


Figure 31. Case IIIB - Buoyancy (B) at Hour 24. The units of buoyancy are $cm/sec^2$ and the contouring interval is 0.1 $cm/sec^2$.

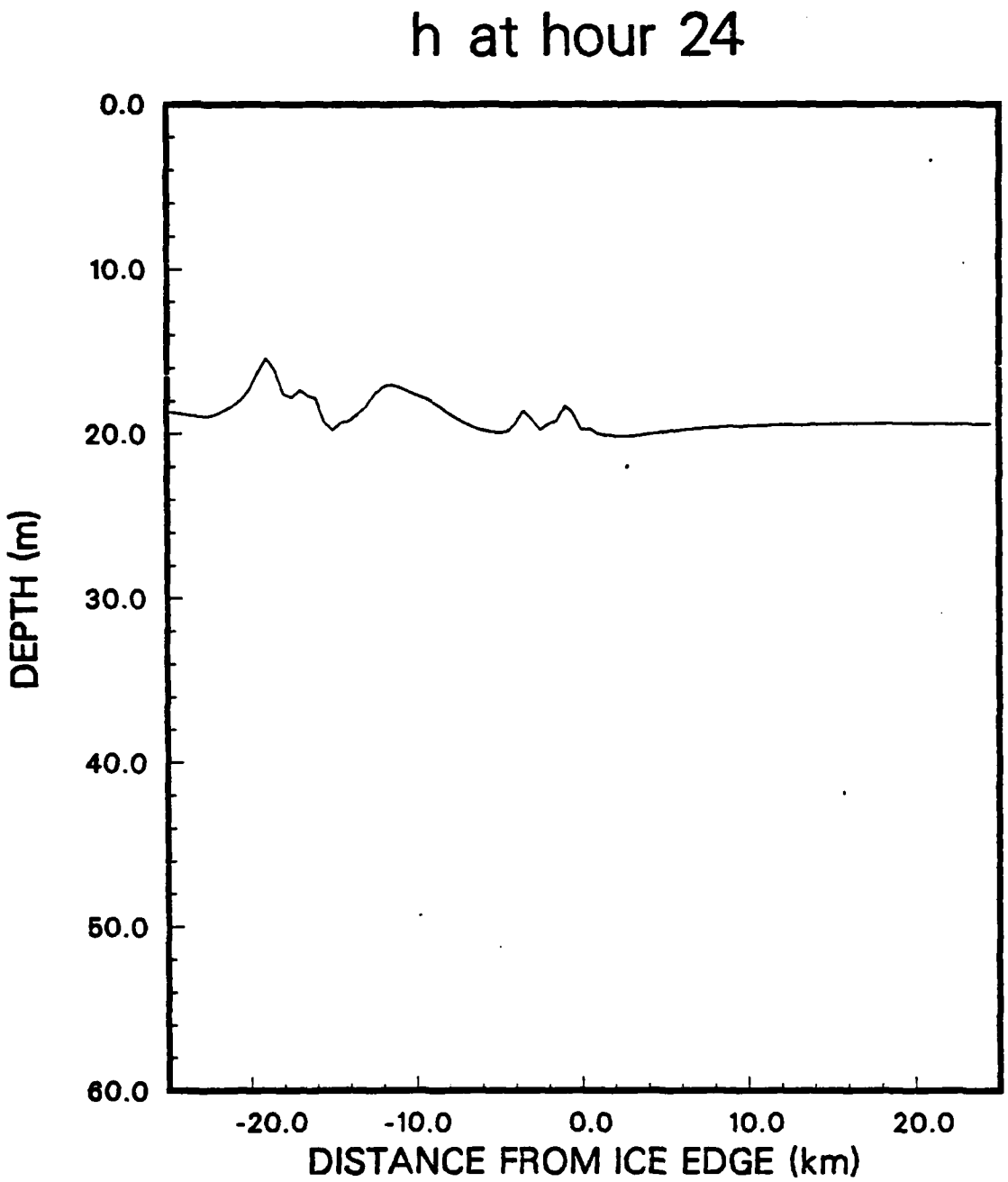


Figure 32. Case IIIB - Mixed Layer Depth (h) at Hour 24.

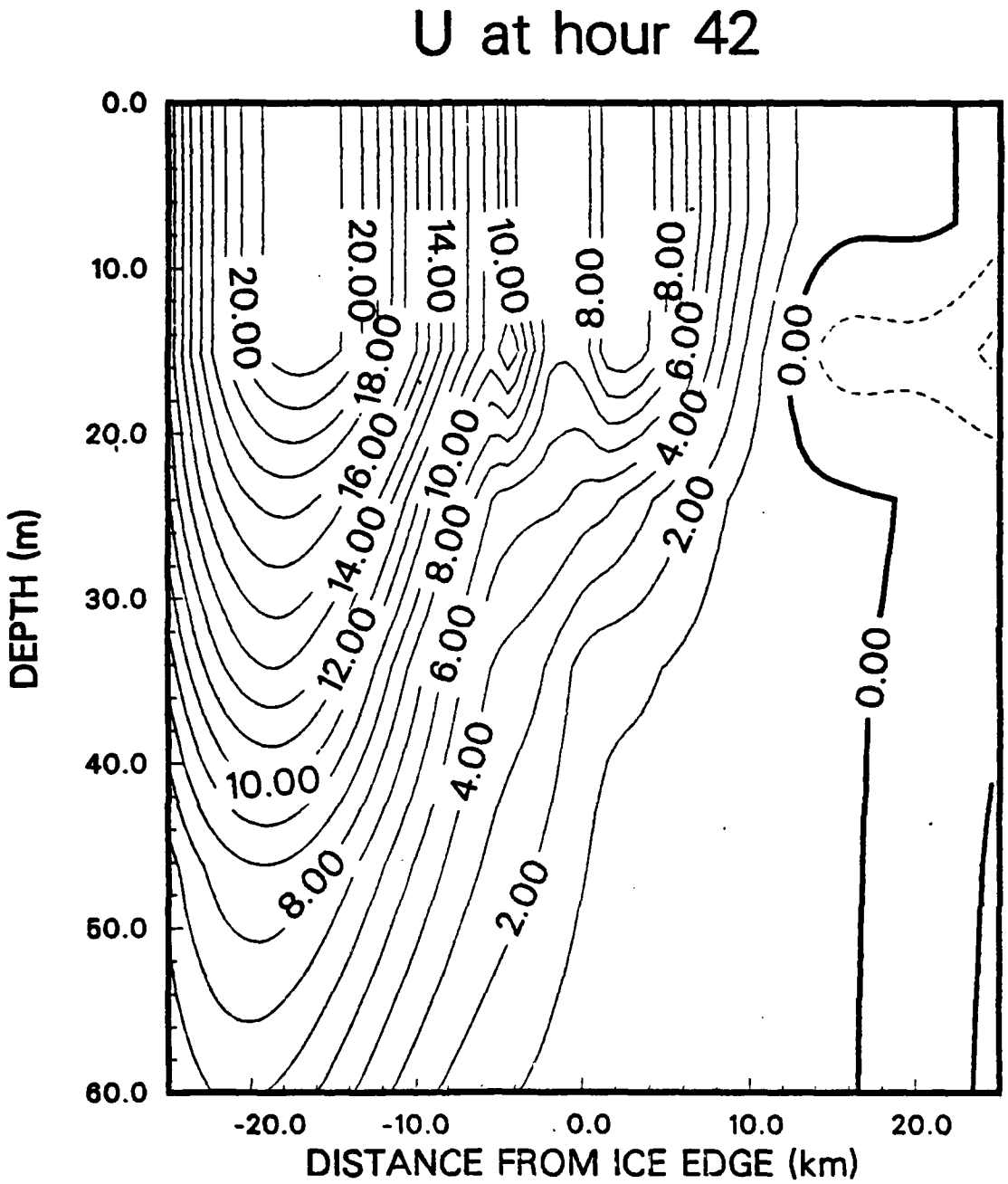


Figure 33. Case IIIC - Along Edge Velocity (U) at Hour 42. The units of velocity are cm/sec and the contouring interval is 1.0 cm/sec.

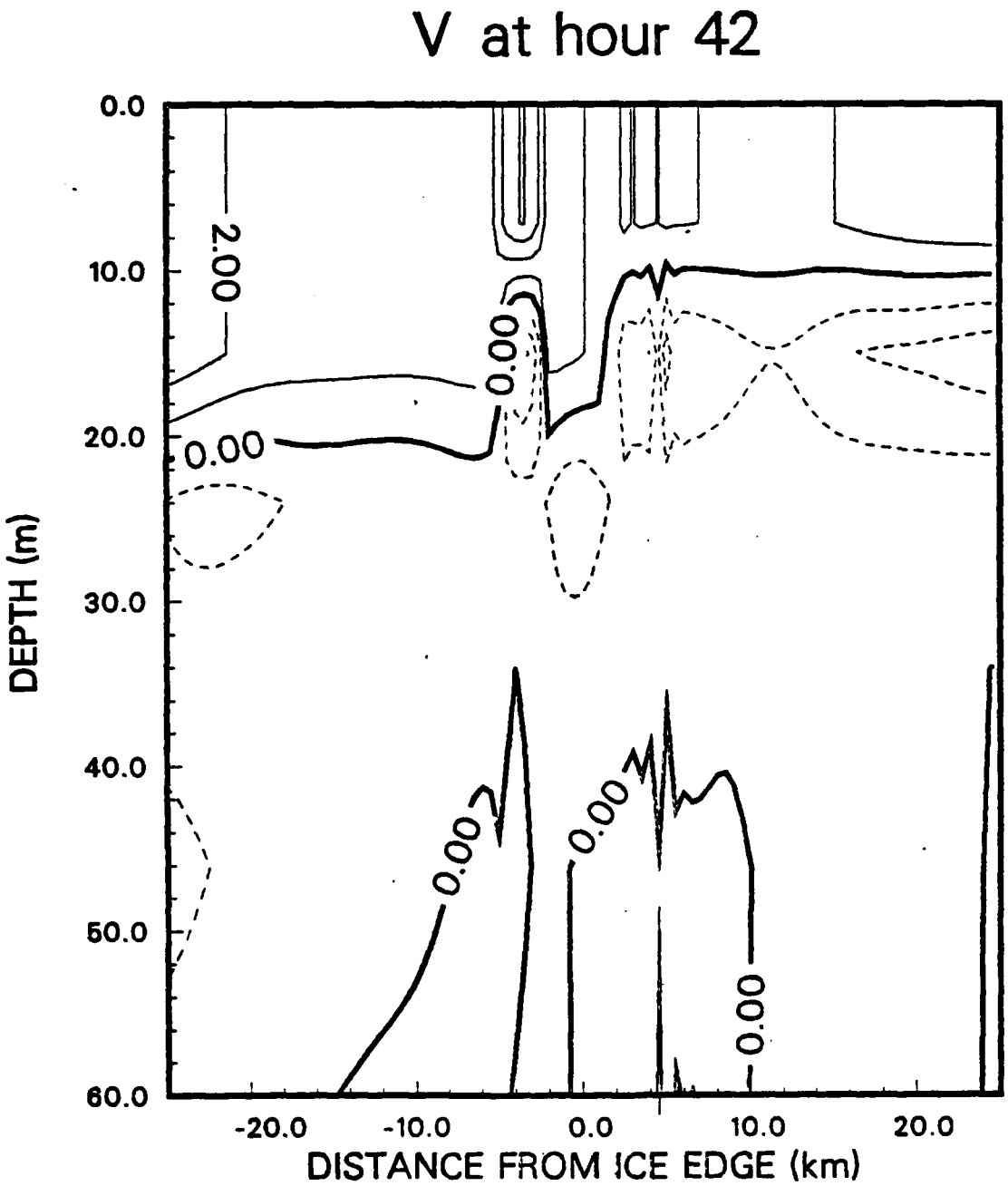


Figure 34. Case IIIC - Across Edge Velocity (V) at Hour 42. The units of velocity are cm/sec and the contouring interval is 1.0 cm/sec.

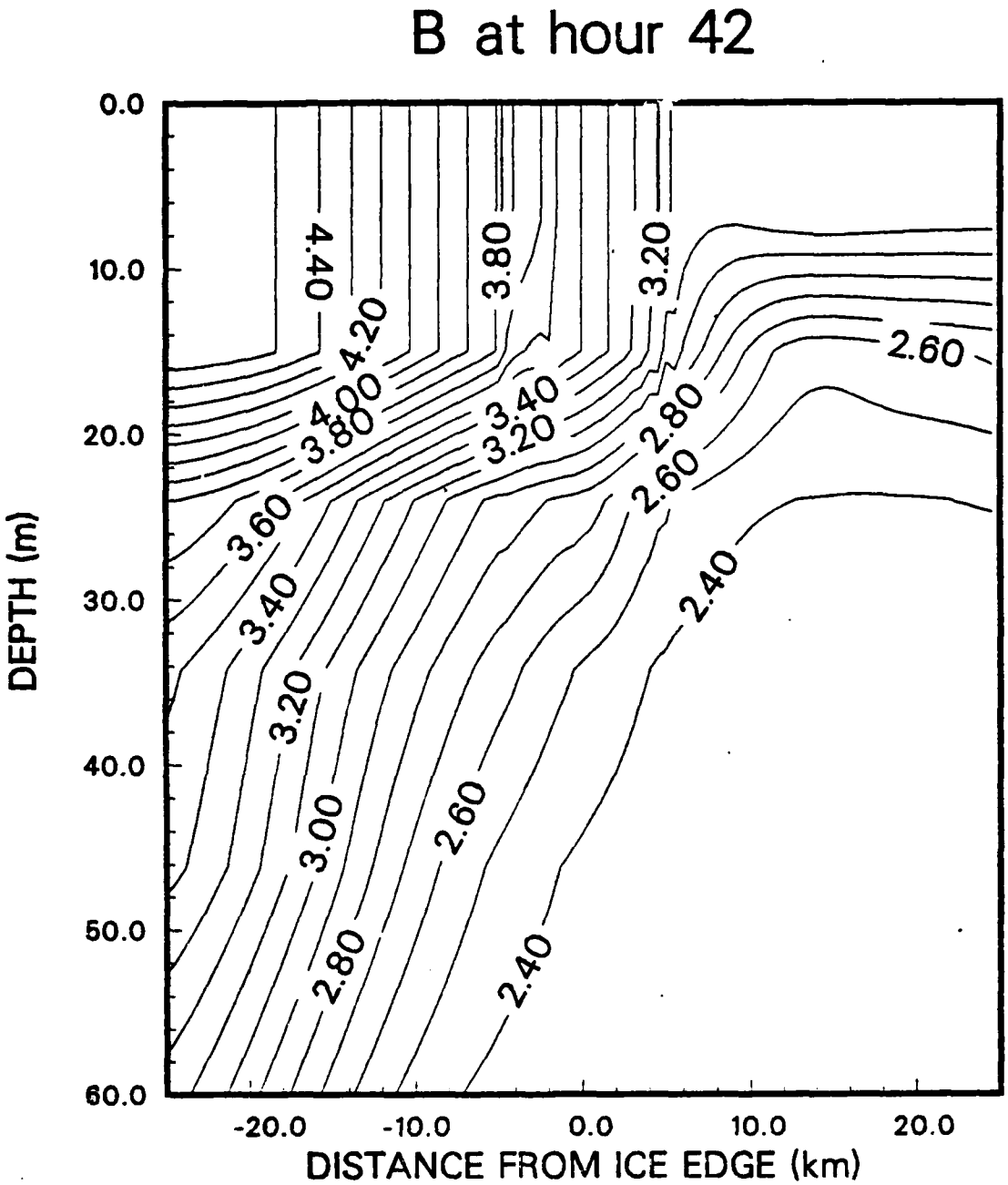


Figure 35. Case IIIC - Buoyancy (B) at Hour 42. The units of buoyancy are cm/sec$^2$ and the contouring interval is 0.1 cm/sec$^2$.

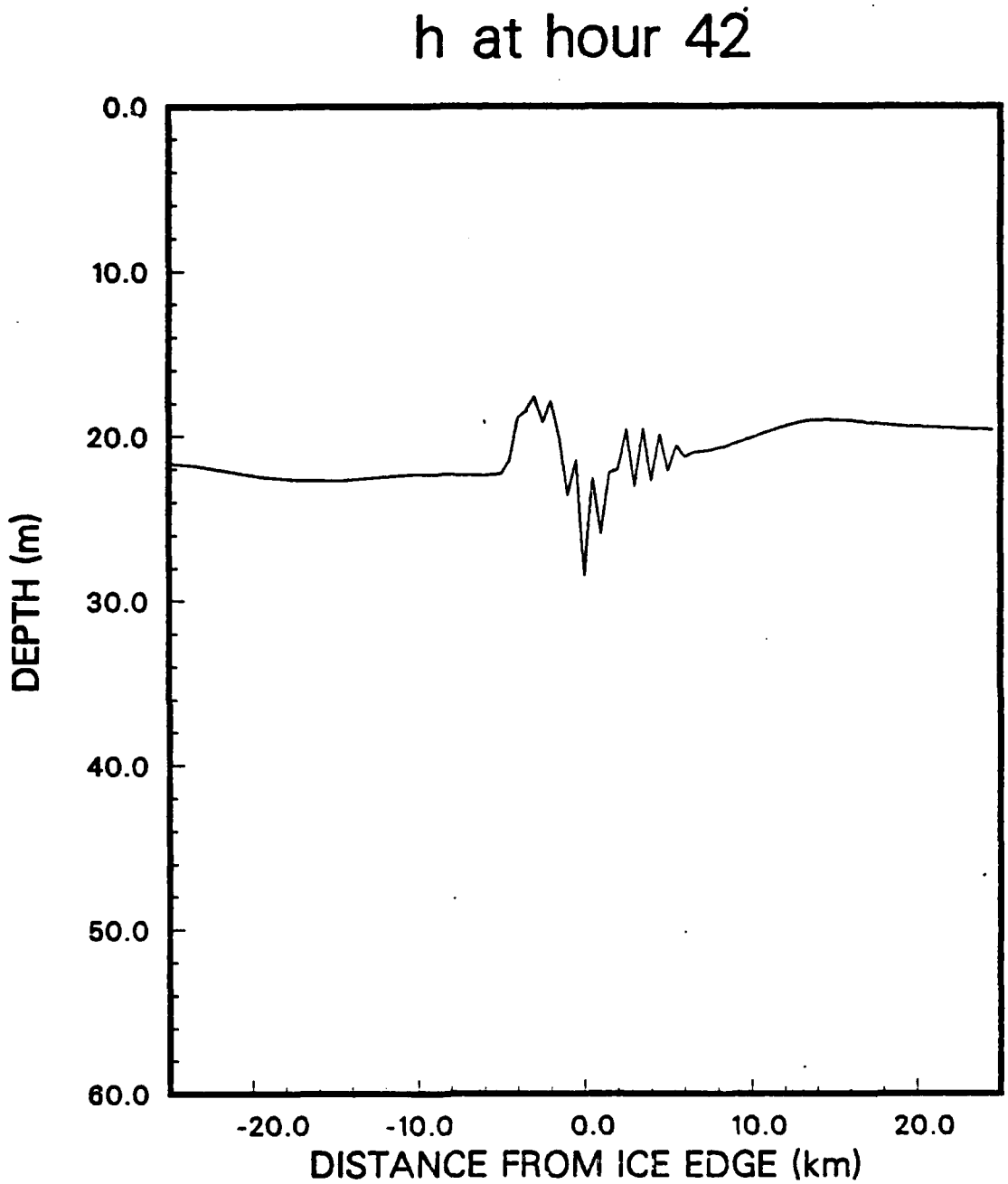


Figure 36. Case IIIC - Mixed Layer Depth (h) at Hour 42.

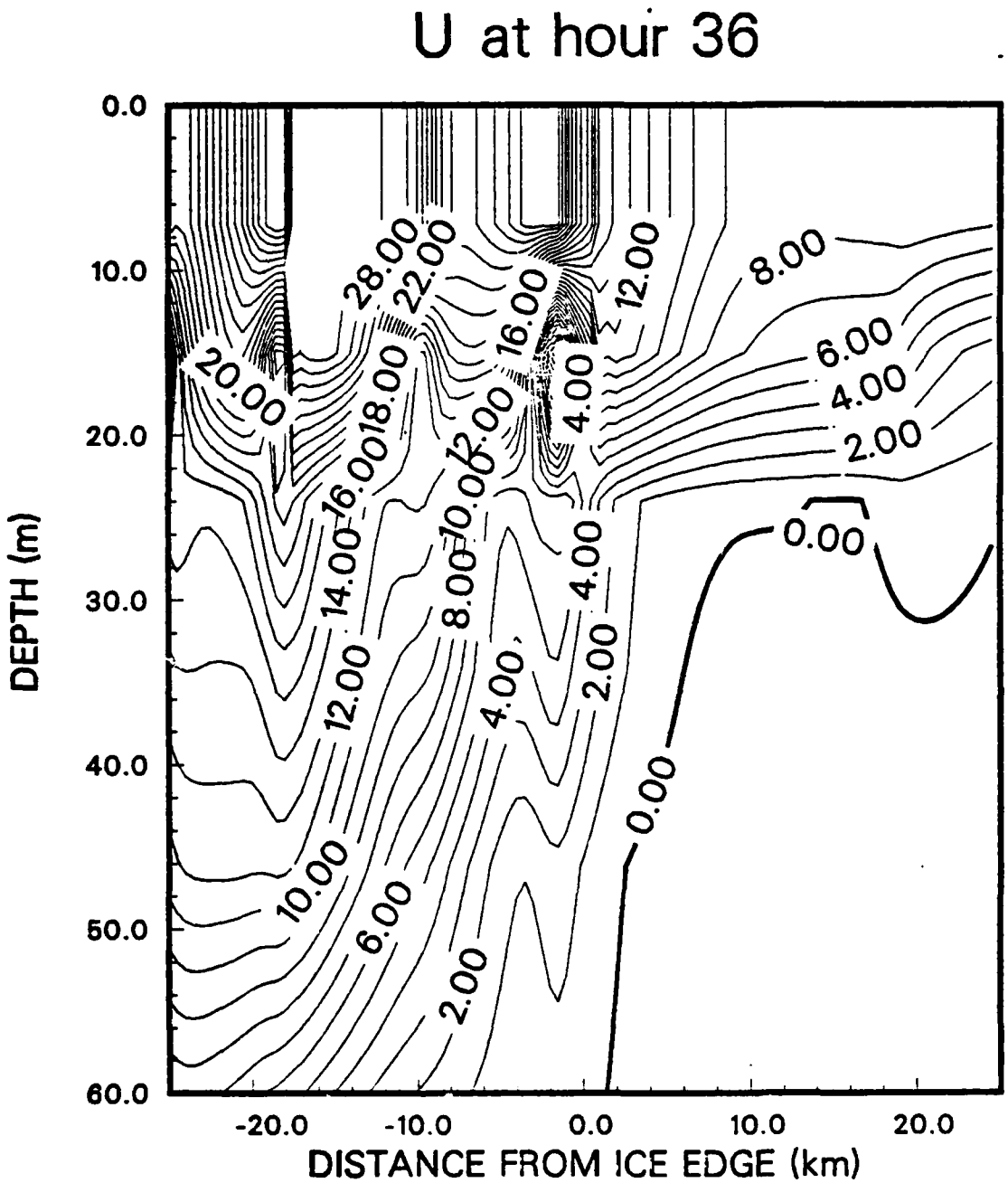


Figure 37. Case IIID - Along Edge Velocity (U) at Hour 36. The units of velocity are cm/sec and the contouring interval is 1.0 cm/sec.

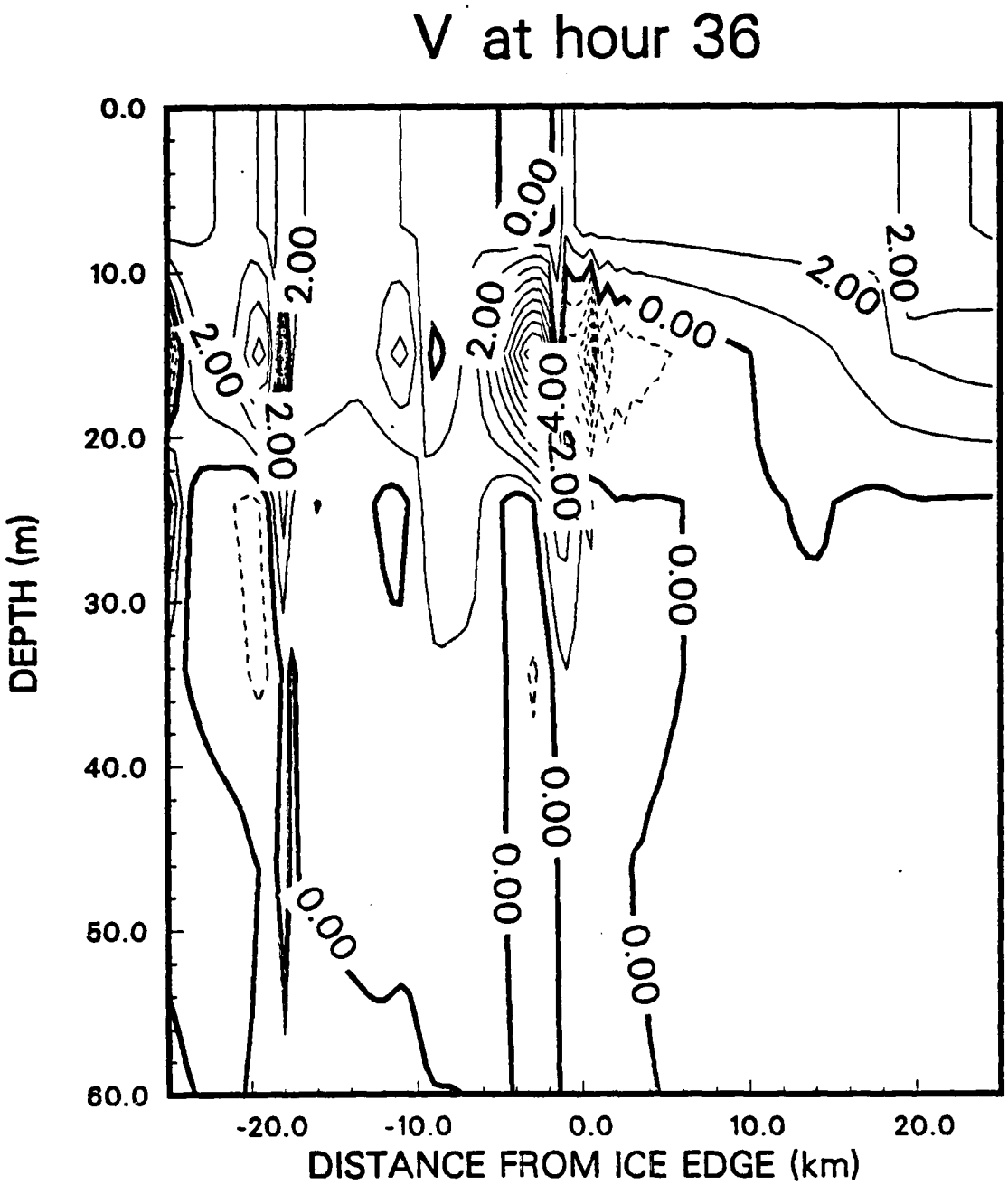


Figure 38. Case IIID - Across Edge Velocity (V) at Hour 36. The units of velocity are cm/sec and the contouring interval is 1.0 cm/sec.

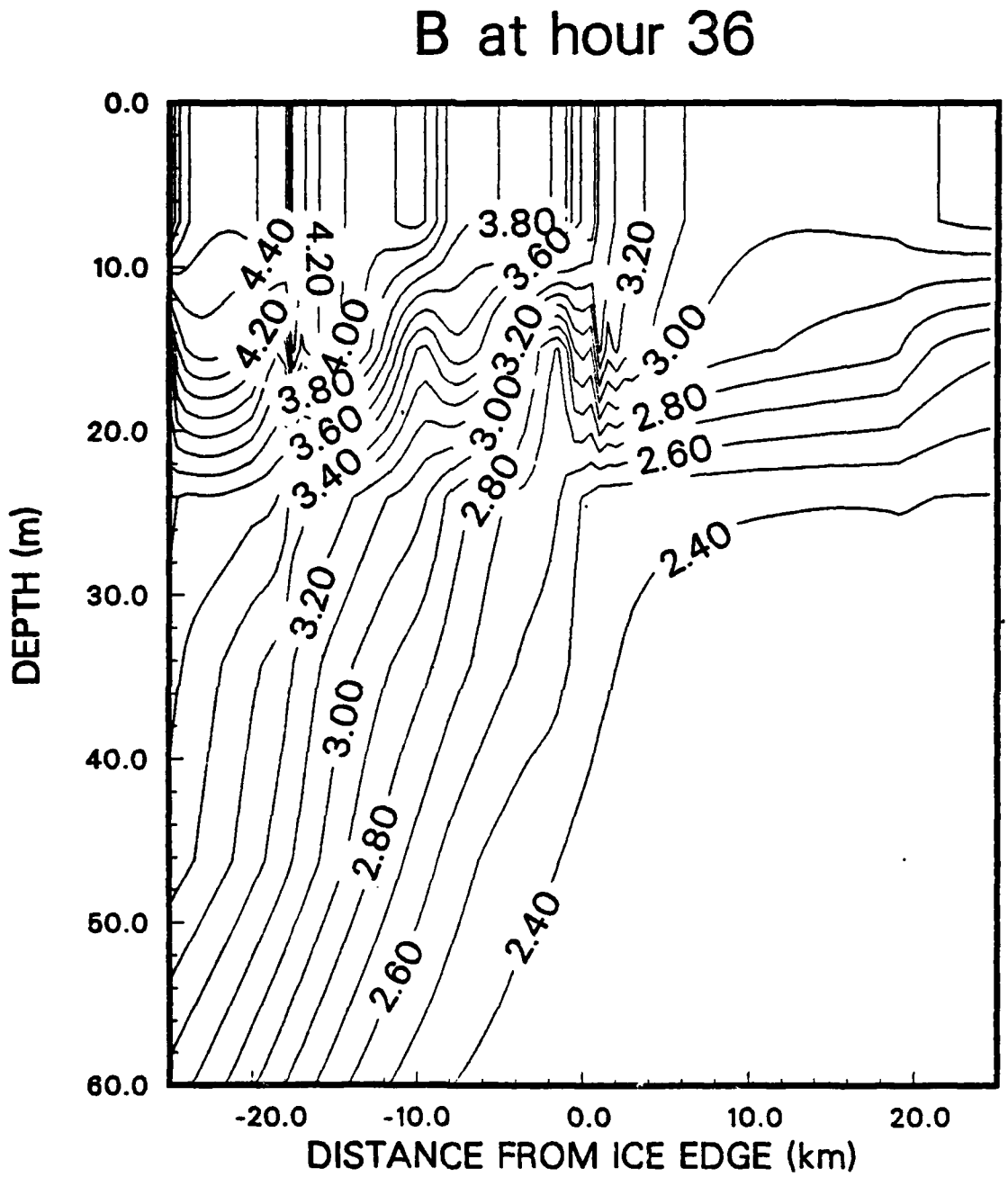


Figure 39. Case IIID - Buoyancy (B) at Hour 36. The units of buoyancy are $cm/sec^2$ and the contouring interval is 0.1 $cm/sec^2$.

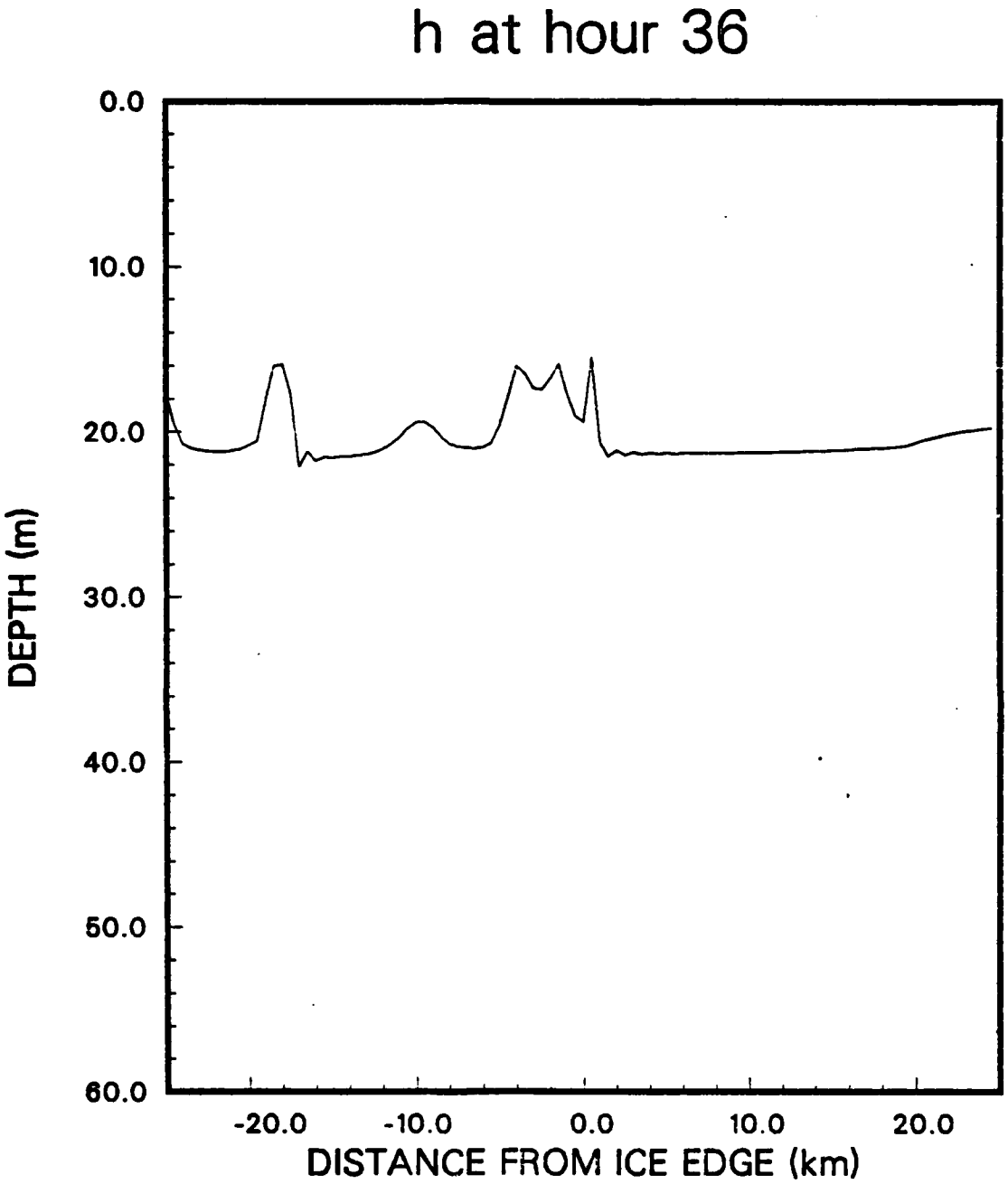


Figure 40. Case IIID - Mixed Layer Depth (h) at Hour 36.

## LIST OF REFERENCES


Adamec, D., R. L. Elsberry, R. W. Garwood, Jr., and R. L. Haney, 1981: An embedded mixed layer--ocean circulation model. Dyn. Atmos. Oceans, 3, 69-96.

Alexander, V., and H. J. Niebauer, 1981: Oceanography of the eastern Bering Sea ice-edge zone in spring. Limnol. Oceanogr., 26, 1111-1125.

Bauer, J., and S. Martin, 1980: Field observations of the Bering Sea ice edge properties during March 1979. Mon. Wea. Rev., 108, 2045-2056.

Buckley, J. R., T. Gammelsrod, J. A. Johannessen, O. M. Johannessen, and L. P. Roed, 1979: Upwelling: Oceanic structure at the edge of the Arctic ice pack in winter. Science, 203, 165-167.

Clarke, A. J., 1978: On wind-driven quasi-geostrophic water movements near fast-ice edges. Deep Sea Res., 25, 41-51.

Crane, R. G., 1983: Atmosphere-sea ice interactions in the Beaufort/ Chukchi Sea and in the european sector of the Arctic. J. Geophys. Res., 88, 4505-4523.

Dey, B., 1980: Variations of August ice cover in the Beaufort Sea and related weather conditions. Bull. Am. Met. Soc., 61, 213-217.

Gammelsrod, T., M. Mork, and L. P. Roed, 1975: Upwelling possibilities at an ice edge. Marine Sci. Comm., 1, 115-145.

Garwood, R. W., Jr., 1977: An oceanic mixed layer model capable of simulating cyclic states. J. Phys. Oceanogr., 7, 455-468.

Haney, R. L., 1980: A numerical study of the formation of upper ocean thermal anomalies during fall and winter of 1976-77. J. Phys. Oceanogr., 10, 541-556.

Joffre, S. M., 1983: Determining the form drag contribution to the total stress of the atmospheric flow over ridged sea ice. J. Geophys. Res., 88, 4524-4530.

Johannessen, O. M., W. D. Hibler, III, P. Wadhams, W. J. Campbell, K. Hasselmann, and I. Dyer (eds.), 1982: MIZEX, a program for meso-scale air-ice-ocean interaction experiments in the Arctic marginal ice zone. II. A plan for a summer marginal ice zone experiment in the Fram Strait/Greenland Sea: 1984. U. S. Army Cold Regions Research and Engineering Laboratory, Hanover, N.H., unpubl. rpt., 41 pp.

Johannessen, O. M., J. A. Johannessen, J. Morison, E. A. Farrelly, and E. A. S. Svensen, 1983: Oceanographic conditions in the marginal ice zone north of Svalbard in early fall 1979 with an emphasis on meso-scale processes. J. Geophys. Res., 88, 2755-2769.

Langleben, M. P., 1982: Water drag coefficient of first-year sea ice. J. Geophys. Res., 87, 573-578.

Macklin, S. A., 1983: Wind drag coefficient over first-year ice in the Bering Sea. J. Geophys. Res., 88, 2845-2852.

McPhee, M. G., 1979: The effect of the oceanic boundary layer on the mean drift of pack ice: Application of a simple model. J. Phys. Oceanogr., 9, 388-400.

McPhee, M. G., 1981: An analytic similarity theory for the planetary boundary layer stabilized by surface buoyancy. Boundary-Layer Met., 21, 325-339.

McPhee, M. G., 1982: Sea ice drag laws and simple boundary layer concepts, including application to rapid melting. U. S. Army Cold Regions Research and Engineering Laboratory, Hanover, N.H., rpt. 82-4, 17 pp.

McPhee, M. G., 1983a: Turbulent heat and momentum transfer in the oceanic boundary layer under melting pack ice. J. Geophys. Res., 88, 2827-2835.

McPhee, M. G., 1983b: Greenland Sea ice-ocean margin. EOS, 64, 82-83.

Niebauer, H. J., 1980: Sea ice and temperature variability in the eastern Bering Sea and the relation to atmospheric fluctuations. J. Geophys. Res., 85, 7507-7515.

Overland, J. E., and C. H. Pease, 1982: Cyclone climatology of the Bering Sea and its relation to sea ice extent. Mon. Wea. Rev., 110, 5-13.

Paquette, R. G., and R. H. Bourke, 1981: Ocean circulation and fronts as related to ice melt-back in the Chukchi Sea. J. Geophys. Res., 86, 4215-4230.

Pease, C. H., S. A. Salo, and J. E. Overland, 1983: Drag measurements for first-year sea ice over a shallow sea. J. Geophys. Res., 88, 2853-2862.

Roed, L. P., and J. J. O'Brien, 1981: Geostrophic adjustment in highly dispersive media: An application to the marginal ice zone. Geophys. Astrophys. Fluid Dynamics, 18, 263-278.

Roed, L. P., and J. J. O'Brien, 1983: A coupled ice-ocean model of upwelling in the marginal ice zone. J. Geophys. Res., 88, 2863-2872.

Roed, L. P., 1982: An analytical coupled ice-ocean model of upwelling in the marginal ice zone. Submitted to J. Geophys. Res., 18 pp.

Saltzman, B., and R. E. Moritz, 1980: A time-dependent climatic feedback system involving sea ice extent, ocean temperature, and $CO_2$. Tellus, 32, 93-118.

Walsh, J. E., and C. M. Johnson, 1979: Interannual atmospheric variability and associated fluctuations in Arctic sea ice extent. J. Geophys. Res., 84, 6915-6928.

Walsh, J. E., and J. E. Sater, 1981: Monthly and seasonal variability in the ocean-ice-atmosphere systems of the North Pacific and the North Atlantic. J. Geophys. Res., 86, 7425-7445.

Walter, B. A., 1980: Wintertime observations of roll clouds over the Bering Sea. Mon. Wea. Rev., 108, 2024-2031.

Untersteiner, N., 1982: Air-sea-ice interaction research programs for the 1980's. Applied Physics Laboratory, Seattle, Washington, unpubl. rpt., 81 pp.

INITIAL DISTRIBUTION LIST

| | | No. Copies |
|---|---|---|
| 1. | Defense Technical Information Center<br>Cameron Station<br>Alexandria, VA 22314 | 2 |
| 2. | Library, Code 0142<br>Naval Postgraduate School<br>Monterey, CA 93940 | 2 |
| 3. | Chairman, Code 68Mr<br>Department of Oceanography<br>Naval Postgraduate School<br>Monterey, CA 93940 | 1 |
| 4. | Chairman, Code 63Rd<br>Department of Meteorology<br>Naval Postgraduate School<br>Monterey, CA 93940 | 1 |
| 5. | Mr. D. A. Adamec, Code 63Ac<br>Department of Meteorology<br>Naval Postgraduate School<br>Monterey, CA 93940 | 1 |
| 6. | Professor R. H. Bourke, Code 68Bf<br>Department of Oceanography<br>Naval Postgraduate School<br>Monterey, CA 93940 | 1 |
| 7. | Professor R. L. Elsberry, Code 63Es<br>Department of Meteorology<br>Naval Postgraduate School<br>Monterey, CA 93940 | 1 |
| 8. | Mr. P. C. Gallacher, Code 63Ga<br>Department of Meteorology<br>Naval Postgraduate School<br>Monterey, CA 93940 | 1 |
| 9. | Professor R. W. Garwood, Code 68Gd<br>Department of Oceanography<br>Naval Postgraduate School<br>Monterey, CA 93940 | 2 |

10. Professor R. L. Haney, Code 63Hy 1
Department of Meteorology
Naval Postgraduate School
Monterey, CA 93940

11. Dr. M. G. McPhee, Code 68 1
Department of Oceanography
Naval Postgraduate School
Monterey, CA 93940

12. Professor R. G. Paquette, Code 68Pa 1
Department of Oceanography
Naval Postgraduate School
Monterey, CA 93940

13. Dr. O. M. Johannessen 1
Geophysical Institute, Division A
University of Bergen
Bergen, Norway

14. Dr. H. J. Niebauer 1
Institute of Marine Science
University of Alaska
Fairbanks, AK 99701

15. Professor J. J. O'Brien 1
Mesoscale Air-Sea Interaction Group
Florida State University
Tallahassee, FL 32306

16. Department of Oceanography 1
University of Hawaii
Attn: Drs. Magaard, Muller, and Wyrtki
1000 Pope Road
Honolulu, HI 96822

17. Commanding Officer 2
Attn: LT David G. Markham
Naval Western Oceanography Center
Pearl Harbor, HI 96860

18. Director 1
Naval Oceanography Command
Naval Observatory
34th and Massachusetts Avenue NW
Washington, D.C. 20390

19. Commander 1
Naval Oceanography Command
NSTL Station
Bay St. Louis, MS 39522

20. Commanding Officer 1
Naval Oceanographic Office
NSTL Station
Bay St. Louis, MS 39522

21. Commanding Officer 1
Fleet Numerical Oceanography Center
Monterey, CA 93940

22. Commanding Officer 1
Naval Ocean Research and Development Activity
NSTL Station
Bay St. Louis, MS 39522

23. Commanding Officer 1
Naval Environmental Prediction Research Facility
Monterey, CA 93940

24. Chairman, Oceanography Department 1
U. S. Naval Academy
Annapolis, MD 21402

25. Chief of Naval Research 1
800 N. Quincy Street
Arlington, VA 22217

26. Office of Naval Research (Code 420) 1
Naval Ocean Research and Development Activity
NSTL Station
Bay St. Louis, MS 39522

27. Scientific Liaison Office 1
Office of Naval Research
Scripps Institution of Oceanography
La Jolla CA 92037

28. Library 1
Department of Oceanography
University of Washington
Seattle, WA 98105

29. Library 1
CICESE
P.O. Box 4803
San Ysidro, CA 92073

30. Library 1
School of Oceanography
Oregon State University
Corvallis, OR 96860

END

DATE
FILMED

10 — 83

DTIC